A STUDY OF MICROWAVE DOWNCONVERTERS OPERATING IN THE K_u BAND

University of South Carolina
College of Engineering
Columbia, S. C. 29208

Final Report

Contract Number NAS8-28660
Control Number PR-R-28660

By: Rufus G. Fellers
Principal Investigator
Ted L. Simpson
Bangjuh Tseng

TABLE OF CONTENTS

LIST OF ILLUSTRATIONS

LIST OF TABLES

CHAPTER I INTRODUCTION

1.1 Background

Microwave parametric amplifiers, the subject of this investigation, are a class of amplifiers which utilize either nonlinear reactances, or reactances which can be varied as a function of time by applying a suitable pump source. The time variation of a reactive parameter can create the equivalent of a negative resistance in a certain frequency range, and this negative resistance can be used to provide amplification. This is the origin of the term negative resistance parametric amplifier, or simply parametric amplifier. There are two distinctive features of parametric amplifiers that are worth mentioning. First, electronic amplifiers use energy from an electrical source to increase the power in a desired signal waveform, for most amplifiers, such as vacuum tube or transistor amplifiers, this electrical source is a direct-current (dc) source, while for parametric amplifiers, it is an alternating-current (ac) source. The second feature of a parametric amplifier is its capability of low noise amplification. A vacuum tube or a transistor is essentially a nonlinear resistor, and it is well known that any resistor at non-zero temperature will generate thermal noise. On the other hand, a parametric amplifier utilizes mainly a nonlinear reactance, and a reactance does not contribute thermal noise. This was first pointed out by van der Ziel in 1948 when he analyzed the mixing properties of nonlinear capacitances [1]. It is this feature that makes parametric amplifiers the most attractive

candidate for low noise front ends in communication systems. When operated cryogenically, the noise figure of a parametric amplifier is comparable to that of a maser, yet its bandwidth and stability are far superior to those of a maser.

Although van der Ziel was the first person to point out the potential use of nonlinear capacitance as low noise amplifier, parametric amplification was theoretically shown to be possible by Faraday in as early as 1831 [2], and later by Lord Raleigh in 1863 [3]. It was, however, one hundred years later, when the parametric effect was experimentally observed in an electro-mechanical nonlinear capacitance device [4]. In 1957, the first realization of a microwave parametric amplifier was finally made by Weiss [5], following the earlier proposal by Suhl [6], suggesting the use of the nonlinear effect in ferrites. This caused widespread interest among microwave engineers, and in the following few years, with high quality semiconductor junction diodes (often referred as varactor diodes, or simply varactors) more readily available, semiconductor parametric amplifiers were soon developed through the efforts of many researchers.

The semiconductor junction diode has a nonlinear capacitance. If a pump source at frequency f_p and a small amplitude signal at frequency f_s are applied simultaneously, the nonlinear capacitance behaves like a time-varying linear capacitance at f_s. The mixing of f_p and f_s will generate a third frequency component, $f_p - f_s$. This frequency is usually called the idler frequency, f_i. The idler frequency is an inevitable by-product of parametric amplification, suppressing it would also suppress the desired

amplification at f_s. It should be pointed out that the closer the signal frequency is to half the pump frequency, the closer the idler frequency is to the signal frequency, and the more difficult it is to separate signal and idler frequencies by filtering. If the signal and idler frequencies are so far apart that the signal circuit does not pass the idler frequency, the amplifier is called a nondegenerate amplifier. On the other hand, if the signal and idler frequencies are very close or if their spectra overlap, the signal circuit can no longer distinguish between them, and the amplifier is then called a degenerate amplifier.

For degenerate amplifiers, the ordinary concepts of noise figure do not apply. Degenerate amplifiers are not amplifiers in the usual sense, because they give output at frequencies not included in the input. While the noise figure of a nondegenerate amplifier is uniquely defined, the noise performance of a degenerate amplifier depends on the type of input signal, the type of detector used, and the interpretation of the detector output. Still, two kinds of noise figure, single-sideband and double-sideband, are often quoted by manufacturers.

The single-sideband noise figure is used in operation where the input signal spectrum is confined to one side of half-pump frequency. Although the signal circuit can not distinguish between the signal and the idler, a sharp filter in a subsequent stage can be used to select f_s. This type of operation is characterized by the reduction of useful amplifier bandwidth and a certain degree of degradation in signal to noise ratio. In operation in which the input spectrum surrounds the half-pump frequency,

the double-sideband noise figure is used. For amplifiers built with diodes of the same quality, the noise figure of a nondegenerate amplifier is higher than the double-sideband noise figure, yet lower than the single-sideband noise figure of a degenerate amplifier. However, it must be kept in mind that a degenerate amplifier and a nondegenerate amplifier can not be compared by their respective noise figures unless the system into which the amplifiers are to be incorporated is first specified.

It should be obvious that in some instances it is possible to realize system sensitivities calculated from the double-sideband noise figure. When this is so, the degenerate amplifier would be no doubt the better choice. Even in applications in which single-sideband noise figure must be used, there may well be practical considerations which would make the degenerate amplifier a better choice. By eliminating the idler circuit, the degenerate amplifier is a much simpler device to build. Its pump frequency is relatively low as compared to that of a nondegenerate amplifier. Also, as a consequence of circuit simplicity, the broadbanding of a degenerate amplifier is easier.

1.2 Statement of Problems

Since its inception, the parametric amplifier has been plagued by the problem of having very narrow bandwidth. Numerous researchers have proposed solutions for this problem [7][8][9][10][11][12]. In most cases, oversimplified assumptions were made and parasitic elements of the diode

together with signal circuit loss were neglected. This caused significant discrepancies in theoretical and actual responses.

Seidel and Herrmann [7] appear to be the first to attempt broadbanding the parametric amplifier by use of a multiple-resonator matching circuit. They gave design criteria for a filter circuit of a degenerate amplifier, using the approach of setting the derivatives of the gain function equal to zero at midband. However, the varactor model is too simple, and loss in signal circuit is not included.

Matthaei [8] subsequently derived the gain expressions suitable for wideband design, using a complete varactor equivalent circuit, and demonstrated that, by using proper filters in signal and idler circuits, fractional bandwidth of 10% (at a gain of 15 dB) can be obtained. However, no direct way of choosing the proper filters is given, and a considerable amount of experimenting is involved.

Kuh and Fukada [9] developed an approximate synthesis technique based on more rigorous network concepts. Starting from Bode's theorem on reflection coefficient limitation, equations for gain-bandwidth product are derived. From a designer's point of view, Kuh and Fukada's technique is more tractable than that of Matthaei, but it also suffers from several deficiencies. Diode parasitics are not included in the equivalent circuit and the circulator is assumed to pass both the signal and the idler frequencies. Ku [10] subsequently derived a more exacting synthesis technique which, although it is more flexible and more elegant, is less tractable than that of Kuh and Fukada, and also suffers from the same deficiencies.

Perhaps the most widely used synthesis technique is that developed by DeJager [11], with extensions by Connors [13] and Porra and Somervuo [14]. However, this technique contains numerous approximations, employs a rather simplified varactor equivalent circuit, and is limited to only double tuned signal circuits. Egami [12] later developed a new design theory based on slope parameter concepts. He has included diode parasitics and signal circuit loss in his derivations. While the technique is more exact, it is also less tractable and is again limited to double tuned signal circuits only.

Many, if not all, of the above mentioned deficiencies can be removed if computer-aided design techniques are fully utilized in parametric amplifier design. With the high speed capability of a digital computer, one can afford to use a more realistic varactor equivalent circuit, to include signal circuit loss in the computation of amplifier performances, and to explore more complicated topologies. In this research report, a computer program will be developed for parametric amplifier design with special emphasis on a degenerate parametric amplifier in the form of a microwave integrated circuit.

Because of their advantages of light weight, low cost and mass producibility, microwave integrated circuits have been increasingly used to replace coaxial cables and waveguides in many microwave instruments. Along with these advantages, microwave integrated circuits also bring to microwave engineers some very challenging design problems. Among these the most serious is perhaps the lack of tunability. To overcome this

difficulty, microwave integrated circuits are sometimes first built and tested with adhesive copper foil on oversized substrate at relatively low frequencies, usually a few hundred megahertz (MHz). Tuning is possible, though very cumbersome, on this low frequency model. Once the circuit is tuned to achieve the desired performance, frequency scaling techniques* are used to bring the operating frequency into the microwave or millimeter-wave frequency range, usually from a few gigahertz to tens of gigahertz (GHz). This technique proves to be very useful for passive network design [15]. However, for active networks, the scaling is far more difficult and less satisfactory because of the difficulty in obtaining two active devices having all their parameters (size, junction and package capacitances, bulk resistance, and lead inductance) related to each other by the same factor. This is particularly true for active networks with low stability and high sensitivity, such as parametric or tunnel diode amplifiers. This may well be the reason that only very few microwave integrated circuit parametric amplifiers are reported in the literature.

1.3 Objectives and Outline of the Present Study

The objective of this study is to develop a computer program for parametric amplifier design with special emphasis on practical design

---

* All circuit dimensions are reduced by a certain factor. Hence, the operating frequency is also increased by the same factor. For more details, see [15].

considerations for microwave integrated circuit degenerate amplifiers. To attain this objective, precision measurement techniques must be developed to obtain a more realistic varactor equivalent circuit, existing theory of parametric amplifier must be modified to include the new equivalent circuit, and microwave integrated circuit properties, such as loss characteristics and circuit discontinuities, must be investigated thoroughly.

In Chapter II the basic theory of semiconductor PN junction is briefly reviewed. Lumped-element equivalent circuits of packaged varactor for various frequency ranges are then proposed following a close examination of the structure of a typical varactor package. Techniques for precision measurement of driving-point impedances are given together with methods for extracting varactor parameters from measured impedance data.

Chapter III is devoted to the analysis of parametric amplifier circuits. The behavior of a varactor under the influence of a pump source is investigated. This is followed by the formulation of the small-signal immittance matrix of a pumped varactor. Gain and noise figure expressions for amplifier circuits employed a complete equivalent circuit are presented in a manner which makes them suitable for implementation in computer-aided design program.

The study of microwave integrated circuit properties is covered in Chapter IV. Computational methods for characteristic impedance, effective dielectric constant, and attenuation constant are given along with numer-

ical results for several frequently used substrates. Circuit discontinuities, such as open circuits and T-junctions, are discussed in detail. Analysis and synthesis methods for one particular circuit component, the parallel-coupled band-pass filter, are presented.

The models and calculation methods developed in Chapter II through Chapter IV are used in Chapter V to design and construct a 5.5 GHz degenerate amplifier. The computer program used for this design is described in detail. Power gain and noise figure of this amplifier are reported.

In Chapter VI the results of this study are summarized and suggestions are given for further research into all aspects of this study.

CHAPTER II CHARACTERIZATION OF MICROWAVE VARACTOR DIODES

2.1 Introduction

The varactor diode is a semiconductor p-n junction which is generally used not for its rectifying properties but rather for its voltage dependent nonlinear capacitance provided primarily by the depletion layer of the junction. By specifying the impurity profile throughout the junction region, the dependence of the depletion width and hence the nonlinear depletion capacitance on applied voltage can be controlled to suit the intended application. As depicted in Fig. 2.1.(a), the p-n junction is formed by diffusing p-type impurity atoms (e. g. boron) into an n-type epitaxial layer which is grown on top of an n^+ substrate. The substrate is purely for mechanical support and is heavily doped (usually with arsenic) to reduce the undesired bulk resistance. An ohmic contact is made to a small circular area on top of the wafer, and most of the epitaxial layer is etched away, except that which is directly underneath the contact. In this way a mesa of desired geometry can be formed. The substrate is then bonded electrically and mechanically to a mounting post, or pedestal which is raised from one of the two conducting end caps of the package as shown in Fig. 2.1(b). The top of the wafer is connected to the other end cap using one or more lead wires or bonding straps. The two end caps are brazed to a ceramic casing to ensure hermetic sealing. While such packages are rugged and convenient for handling, they are also a source of parasitic elements which become significant at microwave frequencies.

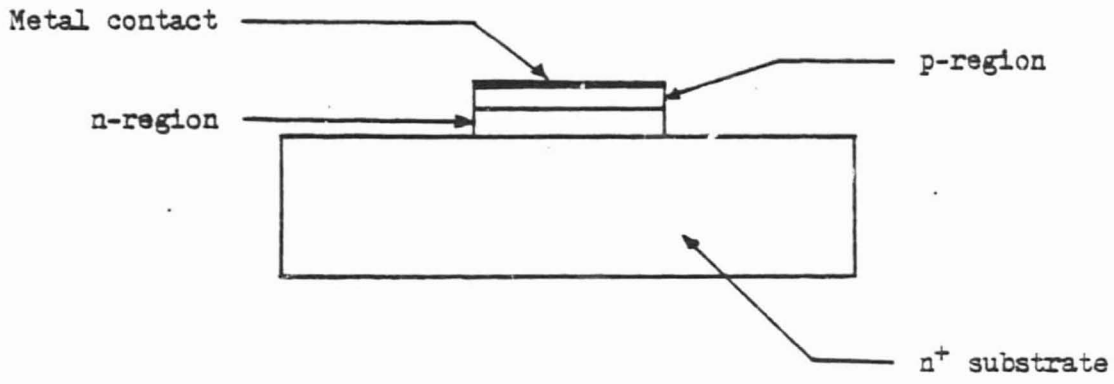

(a)

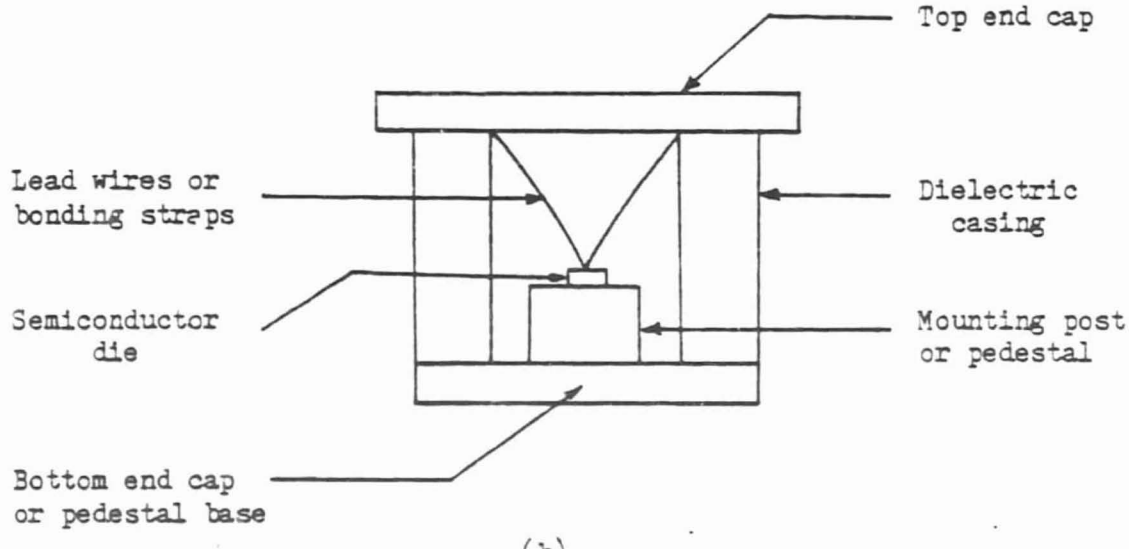

(b)

Fig. 2.1 Typical Varactor Wafer and Package Structure

In this chapter, the electrical characteristics of a varavtor will be dealt with first. By closely examining the varactor properties and the package structure, a realistic equivalent circuit is then proposed. Finally, means for determining the equivalent circuit are discussed. This includes the measurement setup, measurement technique, computational methods, and a computer-aided optimization technique for obtaining numerical values for the equivalent circuit elements from the experimental data.

2.2 Circuit Elements of Packaged Varactor Diodes

2.2.1 Junction Capacitance. Although the formation of a p-n junction is actually done by a diffusion process, let us visualize what would happen if two regions of semiconductor material possessing different type of conductivity, one of p-type and the other of n-type, are brought into contact. Because of the concentration gradient, electrons would diffuse from the n-type region into the p-type region and quickly recombine with holes. Similarly, holes would diffuse from the p-type region into the n-type region and recombine with electrons. This process would leave a net positive charge in the previously neutral n-region near the junction, and a net negative charge in the p-region due to the ionized donor and acceptor atoms respectively. As the diffusion proceeds, an electric field is set up which retards and finally stops the diffusion of majority carriers across the junction. After equilibrium is established, a narrow region called the depletion layer or space-charge layer is left at the

junction, which is swept completely free of charge carriers by the electric field. The potential difference across the depletion layer is called the contact potential or barrier potential.

The width of the depletion layer depends on both the type of semiconductor material and the impurity distribution near the junction. Knowing the impurity distribution, the depletion layer width can be found by solving the one dimensional Poisson's equation for the scalar potential $\psi(x)$

$$\frac{d^2\psi(x)}{dx^2} = -\frac{\rho(x)}{\epsilon} \tag{2.1}$$

with appropriate boundary conditions. Figure 2.2 shows the space-charge distributions of the two most commonly treated junction, namely, the abrupt junction and the linearly-graded junction. For the abrupt junction, the width of the depletion layer is given by*

$$W = \frac{2\epsilon(\phi + V)}{q}\left(\frac{1}{N_a} + \frac{1}{N_d}\right) \tag{2.2}$$

where

q = the electronic charge (1.6×10^{-19} C),

ϕ = the contact potential (volts),

---

* The derivation of Eq. 2.2 is well covered in essentially every semiconductor device theory book. See, for example, Chapter 5 of [16].

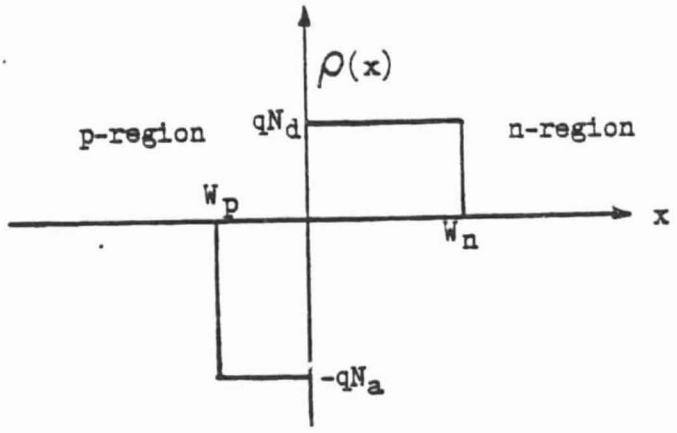

$$\rho(x) = \begin{cases} -qN_a & -W_p \leqslant x \leqslant 0 \\ qN_d & 0 \leqslant x \leqslant W_n \end{cases}$$

(a)

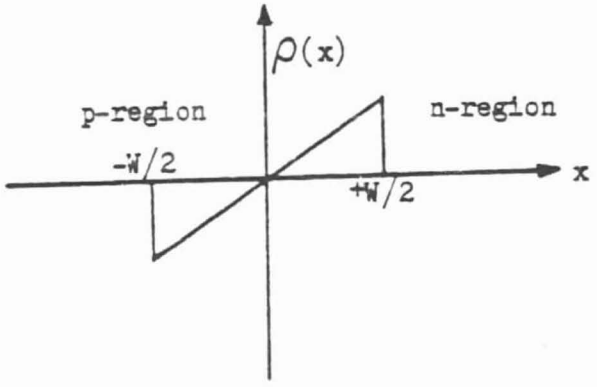

$$\rho(x) = qgx \qquad -W/2 \leqslant x \leqslant W/2$$

(b)

Fig. 2.2 Space-Charge Distributions
(a) abrupt junction
(b) linearly-graded junction

ϵ = the permittivity of the semiconductor material (F/m),

V = the applied voltage (volts),

N_a = the acceptor concentration (m^{-3}),

N_d = the donor concentration (m^{-3}).

Since varactors are usually operated in the reverse bias region, for convenience, a sign convention is adapted such that a reverse bias voltage is positive, while a forward bias voltage is negative. Equation 2.2 can be written as

$$W = W_o(1 + V/\phi)^{1/2} \tag{2.3}$$

where W_o represents the width of the depletion layer at zero bias. The junction capacitance is

$$C_{jV} = \frac{\epsilon A}{W} = \frac{C_{j0}}{(1 + V/\phi)^{1/2}} \tag{2.4}$$

where A is the junction area, and $C_{j0} = A(\epsilon/W_o)$ is the capacitance at zero bias.

Similarly, for linearly-graded junction, the width of the depletion layer at zero bias is

$$W_o = \left(\frac{12\epsilon\phi}{qg}\right)^{1/3} \tag{2.5}$$

where g is the impurity gradient as shown in Fig. 2.2(b). When bias voltage V is applied to the junction, the width of the depletion layer is changed to

$$W = W_o(1 + V/\phi)^{1/3} \tag{2.6}$$

The junction capacitance is then given as

$$C_{jV} = A\frac{\epsilon}{W} = \frac{C_{j0}}{(1 + V/\phi)^{1/3}} \tag{2.7}$$

In practice, the impurity distribution is far more complicated and usually can be approximated by either a gaussian or a complimentary error function, depending on the diffusion process. In this case, the capacitance-voltage relationship must be calculated numerically [17]. However, as a first order approximation, the depletion layer width and the junction capacitance of a real p-n junction can be expressed

$$W = W_o(1 + V/\phi)^{1/n} \tag{2.8}$$

$$C_{jV} = \frac{C_{j0}}{(1 + V/\phi)^{1/n}} \tag{2.9}$$

where the value of n is in the range of 2 to 3.

2.2.2 Series Resistance. The series resistance of a packaged diode consists of two parts: fixed resistance, R_f, and variable resistance, R_v. The fixed resistance includes that of the two end caps, the mounting post, the substrate, and the bonding straps, and is independent of the bias voltage. R_f can be evaluated if the resistivities of the substrate and the conductors are given together with the package configuration. The variable resistance is due to the bulk resistance of the semiconductor

mesa excluding the depletion layer. For the case of an epitaxial diode, this resistance is dominant and is given by

$$R_v = \frac{1}{A} \left[\int \rho_p(x)\, dx + \int \rho_n(x)\, dx \right] \qquad (2.10)$$

where the integration limits for the first term are from the top of the epitaxial layer to the edge of the depletion region in the p-region, and from the epitaxial layer-substrate interface to the edge of the depletion region in the n-region for the second term. The p-type and n-type resistivities are functions of the acceptor and donor impurity concentrations, respectively. R_v is thus a function of depletion width which in turn is a function of the bias voltage. Consequently, the total series resistance R_s is a function of bias voltage. Larger bias voltage causes a wider depletion layer, which lowers the series resistance.

For abrupt junction, Eq. 2.10 can be calculated by making some simplifying approximations. For instance, if the p-region is assumed to be negligibly thick, and $\rho_p \ll \rho_n$, so that $W \approx W_n$, then Eq. 2.10 becomes

$$R_v = \frac{1}{A} \int_W^t \rho_n(x)\, dx \qquad (2.11)$$

where t is the thickness of the epitaxial layer. Since the assumption of an abrupt junction implies a constant donor concentration, $\rho_n(x)$ is constant, and thus

$$R_v = \frac{\rho_n(t - W)}{A} \tag{2.12}$$

Equation 2.12 can be expressed in terms of bias voltage explicitly. Using Eqs. 2.3 and 2.4, the following equation is obtained

$$R_v = \frac{\rho_n t}{A} - \frac{\epsilon \rho_n}{C_{j0}} (1 + V/\phi)^{1/2} \tag{2.13}$$

The total series resistance can now be expressed in the form of

$$R_s = R_1 - R_2(1 + V/\phi)^{1/2} \tag{2.14}$$

where $R_1 = R_f + \rho_n t/A$, and $R_2 = \rho_n \epsilon / C_{j0}$.

For a real varactor, Eq. 2.10 can be evaluated numerically if the diffusion process is known. However, for the purpose of characterization, R_s can be simply expressed as

$$R_s = R_1 - R_2(1 + V/\phi)^{1/n} \tag{2.15}$$

and unknown parameters can be determined experimentally.

2.2.3 Lead Inductance. All the metallic portions of the package contribute parasitic inductance which appears to be in series with the junction capacitance. The most significant contribution undoubtedly comes from the lead wires or bonding straps which connect the semiconductor die to one of the end caps, because of their very small cross-sectional dimensions. Typically, the connection consists of a single piece of gold wire with a diameter of 25 micrometers (μm), or an ortho-

gonal pair of 25 μm thick by 75 μm wide gold straps, with the center attached to the semiconductor die and both dens to the end cap (refer to Fig. 2.1 a).

The inductance of a round wire with length ℓ and diameter d is given as [18]

$$L = 2\ell\left[\ln\frac{4\ell}{d} - 0.75\right] \tag{2.16}$$

where L is in nanohernies (nH), and ℓ and d are in centimeters. The low frequency inductance of a straight rectangular bar with length ℓ, width w, and thickness t is [18]

$$L = 2\ell\left[\ln\frac{2\ell}{w + t} + 0.5 + 0.2235\,\frac{w + t}{\ell}\right] \tag{2.17}$$

where L is again in nH, and all dimension are in centimeters. The inductance values at microwave frequencies are affected by skin effect, but are lower than those given by the low frequency formula by less than 6 per cent [19].

The value of lead inductance associated with a particular type of package can be obtained from the manufacturer. However, the lead wires or bonding straps are almost universally installed by hand, thus the lead inductance usually varies from unit to unit. Therefore the data supplied by the minufacturer must be verified experimentally.

2.2.4 Package Capacitance. In general, capacitance exists between any two separated conductors. Therefore, the package capacitance of a varactor diode comes from many sources; between the two end caps, between the bonding straps and the bottom end cap, between the bonding straps and

the mounting post, and between the top end cap and the mounting post. Even if the fringing field effect and discontinuities are neglected, evaluation of the package capacitance is still a formidable, if not impossible, task [20]. However, the value of the package capacitance can be easily obtained by measuring the capacitance of a dummy package at low frequencies.

2.3 Lumped-Element Equivalent Circuits

As depicted in Fig. 2.3(a), the parasitic capacitance and inductance are in fact distributed elements. Thus, the general approach to the package representation would seem to be either a three-port transformation matrix [21], or a distributed-element circuit, as illustrated in Figs. 2.3(b) and 2.3(c), respectively. However, the transformation matrix suffers from two major drawbacks: one, that the matrix elements may not have any physical meaning and two, that each matrix evaluation is only valid at one frequency. While the distributed-element circuit does relate its elements to the physical parameters of the package structure, it also makes the analysis of the circuit much more difficult, and thus renders itselt undesirable. However, if the package dimensions are much smaller than one wavelength at the frequency of interest, these dificiencies can be readily removed by employing a lumped-element equivalent circuit.

To see how the equivalent circuit in Fig. 2.4(a) is conceived, a closer look at the distributed-element circuit in Fig. 2.3(c) is in order.

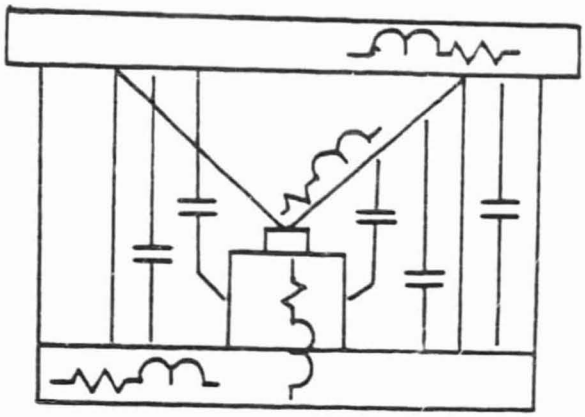

(a)

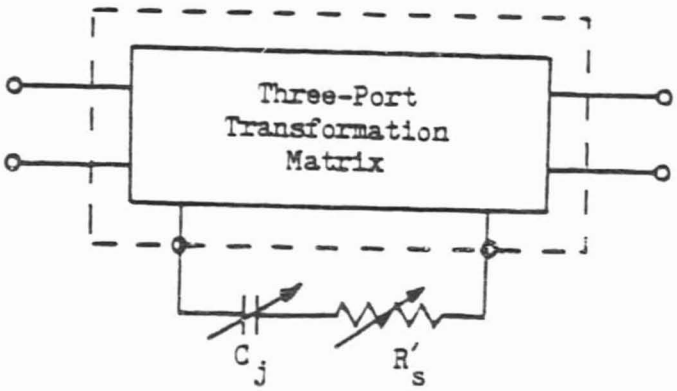

(b)

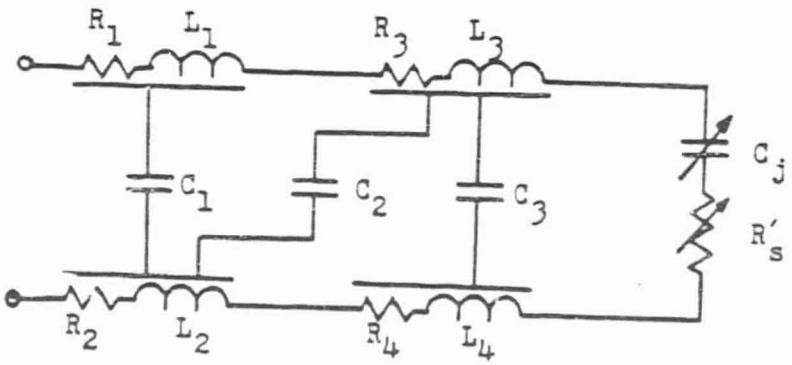

(c)

Fig. 2.3 Packaged Varactor Representation
(a) parasitics associated with package
(b) basic three-port representation
(c) distributed-element equivalent circuit

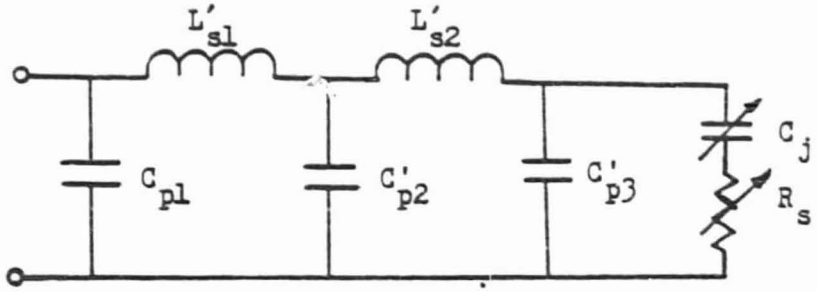

(a)

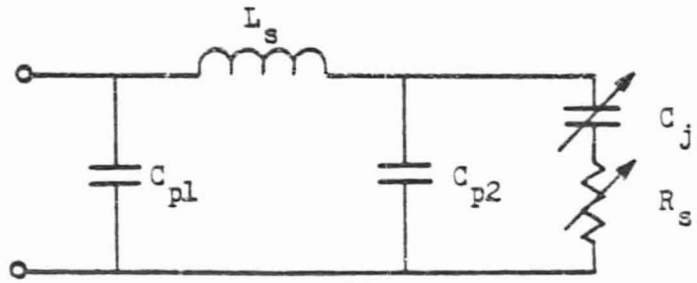

$C_{p2} = C'_{p2} + C'_{p3}$

(b)

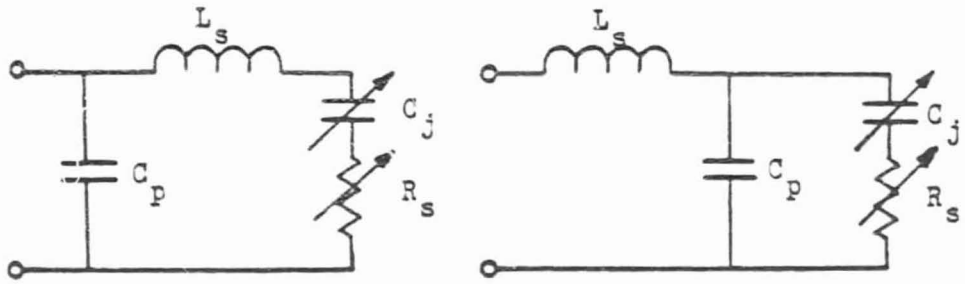

$C_p = C_{p1} + C_{p2}$

(c) (d)

Fig. 2.4 Lumped-Element Equivalent Circuits of Varactor Diodes

The elements C_j and R_s' represent the junction capacitance and the bulk resistance of the semiconductor material (i. e., the substrate and the undepleted epitaxial layer). The resistance and inductances with subscript 1 through 4 are those contributed from the top end cap, the bottom end cap, the bonding straps, and the mounting post, in that order. C_1 is attributed to the capacitance between the two end caps, while C_2 is that between the bonding straps and the bottom end cap, with C_3 being that between the bonding straps and the mounting post.

In Fig. 2.4(a), it is obvious that C_j remains unchanged while R_s becomes the sum of R_s' and all distributed resistive elements. The capacitance between the straps and the post in the immediate vicinity of the semiconductor wafer forms the first shunt element, C_{p3}', with portion of the strap inductance and all the post inductance appearing immediately in series with the semiconductor elements past the initial shunt capacitance as represented by L_{s2}'. The second shunt element, C_{p2}', represents the other part of the capacitance between the straps and the post, together with portion of the capacitance between the two end caps in the air volume. L_{s1}', the second series element, consists of the other part of the strap inductance and all the end cap inductance. Finally, C_{p1} represents the capacitance between the end caps in the ceramic casing.

This equivalent circuit does, to some extent, actually relate the circuit elements to the physical parameters to the package structure, and therefore is relatively invariant over a wide frequency range. Thus, in many applications it is useful over several octaves for frequencies as

high as that in the lower end of the millimeter-wave range. For lower frequencies, this equivalent circuit can be reduced to that of Fig. 2.4(b). This is done by observing that if two adjacent circuit elements, a series inductance and a shunt capacitance, having small immittances, but not small enough to be neglected outright, they may often be interchanged in position. This will allow them to be combined with elements of the same type and thus reduce the number of loops in the circuit by one. Considering the L-section containing L'_{s2} and C'_{p2}, the ABCD matrix (see Appendix A) which represents this section is

$$\begin{bmatrix} 1 & 0 \\ j\omega C'_{p2} & 1 \end{bmatrix} \begin{bmatrix} 1 & j\omega L'_{s2} \\ 0 & 1 \end{bmatrix} = \begin{bmatrix} 1 & j\omega L'_{s2} \\ j\omega C'_{p2} & 1 - \omega^2 L'_{s2} C'_{p2} \end{bmatrix} \tag{2.18}$$

If the positions of L'_{s2} and C'_{p2} are interchanged, then the ABCD matrix becomes

$$\begin{bmatrix} 1 & j\omega L'_{s2} \\ 0 & 1 \end{bmatrix} \begin{bmatrix} 1 & 0 \\ j\omega C'_{p2} & 1 \end{bmatrix} = \begin{bmatrix} 1 - \omega^2 L'_{s2} C'_{p2} & j\omega L'_{s2} \\ j\omega C'_{p2} & 1 \end{bmatrix} \tag{2.19}$$

Equations 2.18 and 2.19 indicate that the positions of L'_{s2} and C'_{p2} may be interchanged without introducing significant error for frequencies satisfying the condition

$$\omega^2 L'_{s2} C'_{p2} \ll 1 \tag{2.20}$$

For most standard packages, the criterion of Eq. 2.20 can be easily met for frequencies in the X-band (8-12.4 GHz) or lower. The equivalent circuit can be further simplified to those in Figs. 2.4(c) and (d).

Because of their simplicities, these two circuits, in one form or the other, have been used by numerous authors. However, they are only valid at ultra-high frequencies or lower microwave frequencies, and any attempt to use them at high frequencies might cause significant discrepancies between theoretical and actual responses.

2.4 Measurement of Packaged Varactor Diodes

The measurement techniques of microwave varactor diodes can be broadly characterized into two catagories: the "transmission loss versus frequency" method due to DeLoach [22], with extensions by Roberts and Wilson [23], and the "impedance versus bias" method due to Houlding [24], with extensions by Harrison [25]. Diode parameters, namely C_j and R_s, are calculated from the measured data and expressed in terms of Q factor [26], from which amplifier performances can be roughly predicted. Parasitic elements are not of great importance, and thus are not accurately determined, since they can be easily tuned out in waveguide or coaxial line circuits. Unfortunately, for the current study, this is not the case because of the lack of tunability in microwave integrated circuits.

In the following sections, a measurement technique is described which will enable the determination of the diode equivalent circuit more accurately. The diodes used in this study are Microwave Associates' MA 4850E gallium-arsenide (GaAs) varactor diodes, commonly employed in microwave parametric amplifiers. Figure 2.5 shows its dimensions. Diode parameters at two reverse bias voltages, 0 and 6 volts, were supplied by the manu-

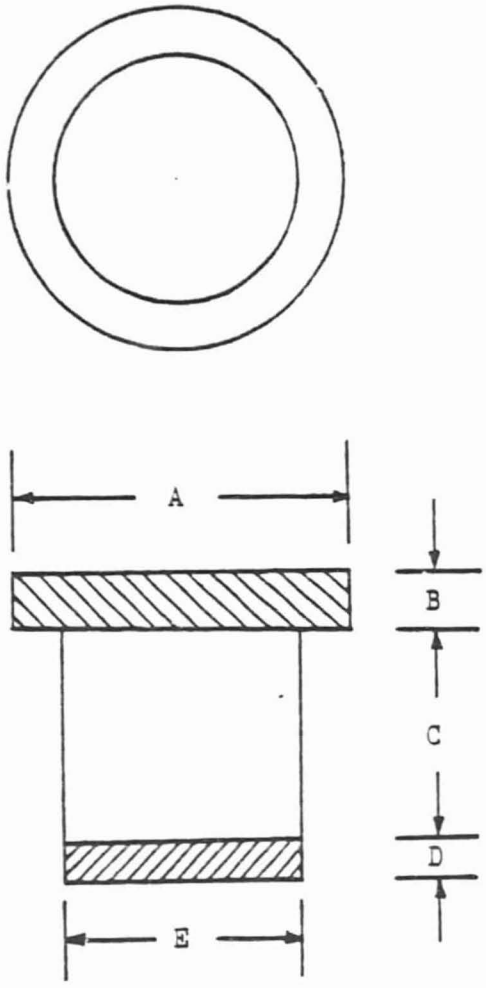

A = 3.04 mm

B = 0.58 mm

C = 0.71 mm

D = 0.25 mm

E = 2.03 mm

Fig. 2.5 Dimensions of MA 48509E Varactor Diode

facturer, and are listed in Table 2.1.

Table 2.1 Manufacturer Supplied Data for MA 48509E Varactor Diode

Parameter	Diode #1	Diode #2	Diode #3
C_{j0} (pF)	0.578	0.552	0.594
C_{j6} (pF)	0.271	0.252	0.280
L_s (nH)	0.3	0.3	0.3
C_p (pF)	0.292	0.292	0.292
f_{co}* (GHz)	292	294	267
V_B (volts)	13	18	18

* $f_{co} = \frac{1}{2\pi C_j R_s}$ at 0 volt.

2.4.1 Measurement Setup. Since parametric amplifiers are generally used for low-level reception with signal level usually below -70 dBm (10^{-7} mW), the measurement must be carried out with power level compatible to the low-level condition. Preliminary investigations indicated that the diode parameters are affected by power levels when the incident power is above -15 dBm. As a result, the power level under which the diodes are to be measured was then decided to be about -20 dBm. This requires a measurement system with very high sensitivity, and consequently

the superheterodyne system shown in Fig. 2.6 was chosen.

A brief description of the system follows. To eliminate the pulling effect, a circulator with one port terminated in a 50-ohm load is inserted between the signal generator and the rest of the system. Frequency is measured by a precision frequency meter. Power level is continuously monitored through a directional coupler. Bias voltage is applied via a coaxial bias-tee. The recision slotted-line is a 50-ohm HP type 816A with APC-7 connectors. Signal picked up by the untuned RF probe is fed to the low-noise mixer. The IF output from the mixer is then displayed by a precisely calibrated, 30 MHz amplifier (GR type 1236).

The diode test mount deserves a more detailed description since it plays the most important role in the whole system, and is not commercially available. To be compatible with the slotted-line, the diode test mount was designed around an APC-7 air line connector. Every part was machined in brass and then gold plated to minimize ohmic loss. The diode is held between the inner conductor and a cylindrical slug with the center of one end slightly recessed to ensure that the diode will be properly centered. A fine thread screw is used to keep the slug, and thus the diode, firmly in position. Figure 2.7 is a photograph of the completely disassembled diode mount. Some critical dimensions are indicated in Fig. 2.8.

2.4.2 System Calibration. Before the diode measurement can be made, two important parameters of the system must be determined: the attenuation constant of the slotted-line, and the position of the reference plane consistent with the scale on the slotted-line. Losses on a slotted-line

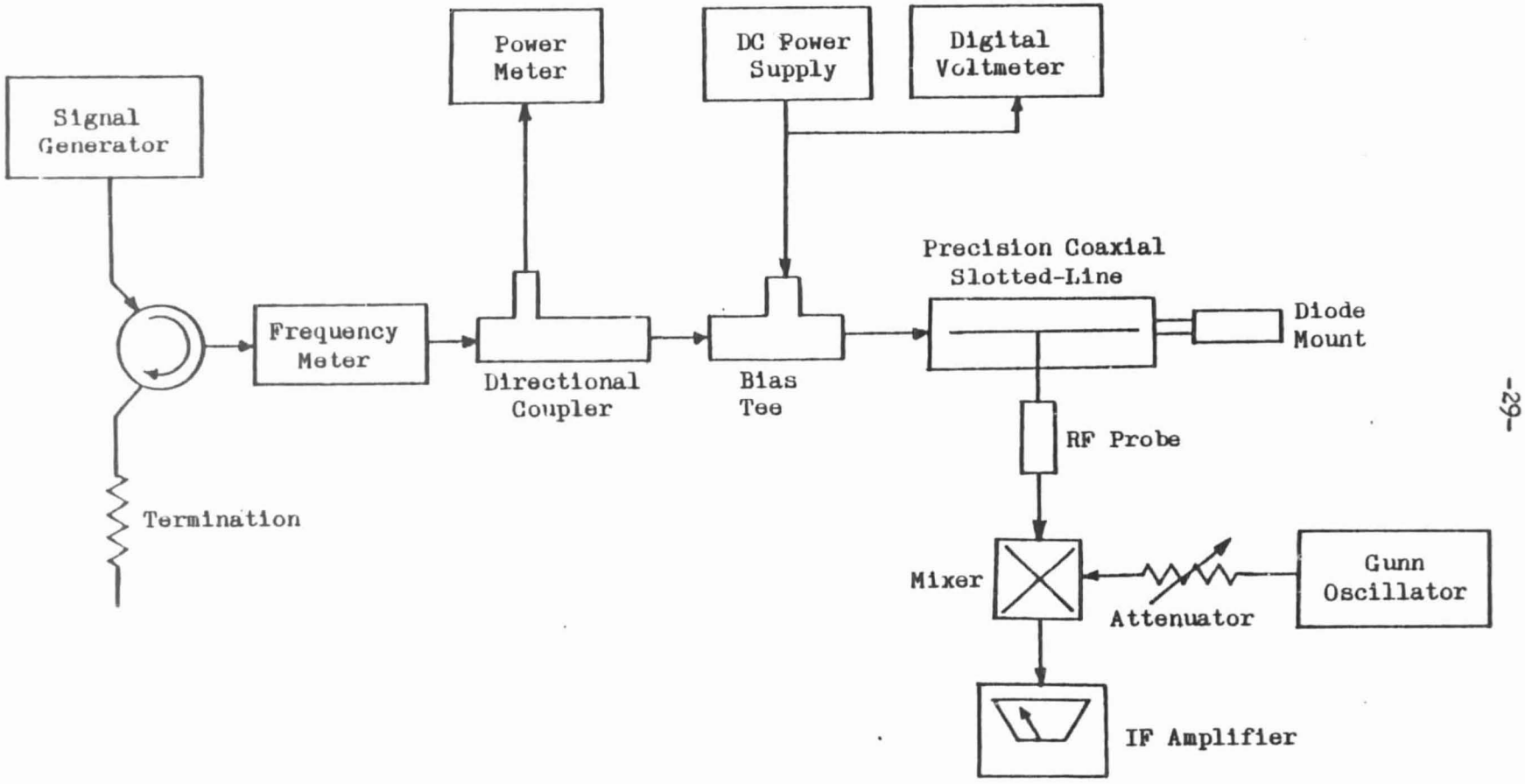

Fig. 2.6 Superheterodyne Measurement System

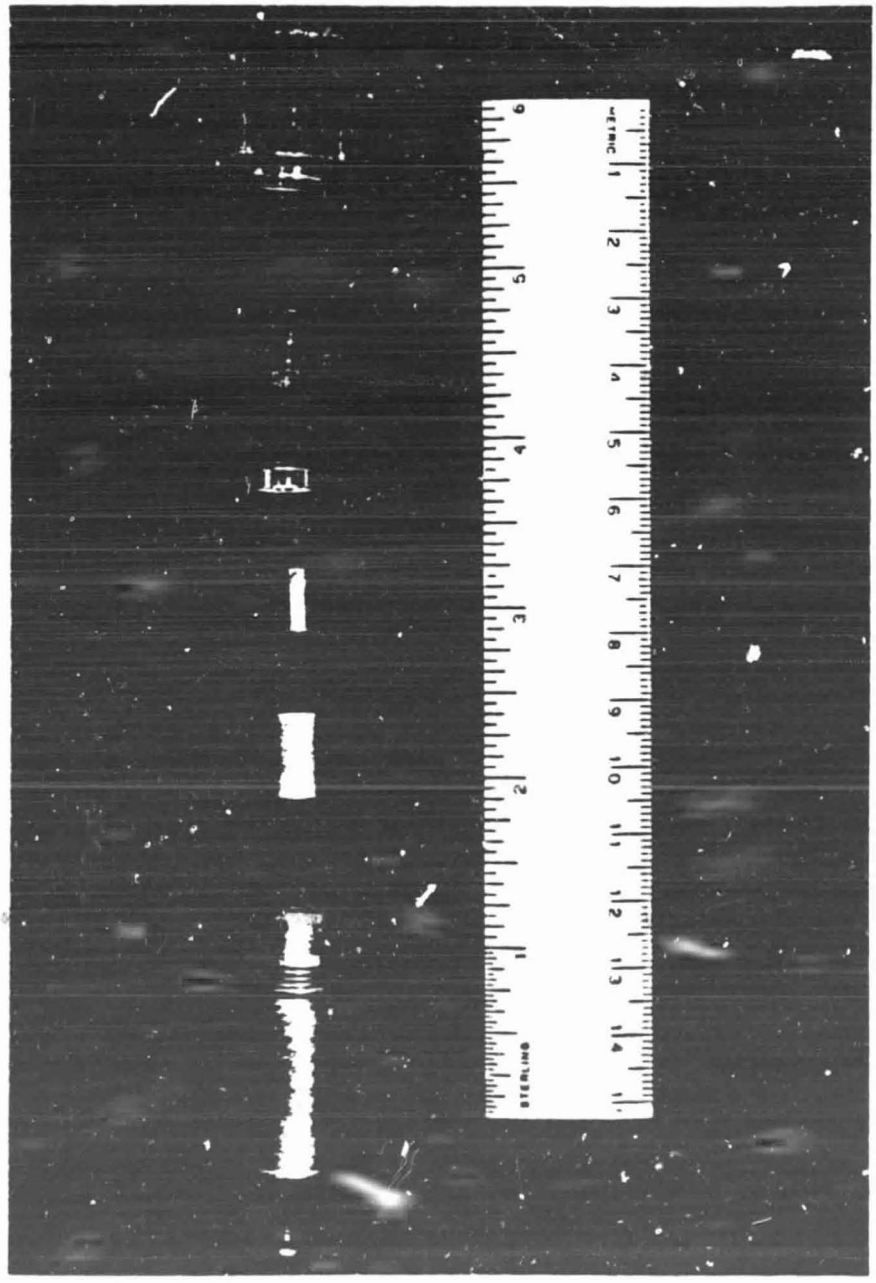

Fig. 2.7 Photograph of the Disassembled Diode Test Mount

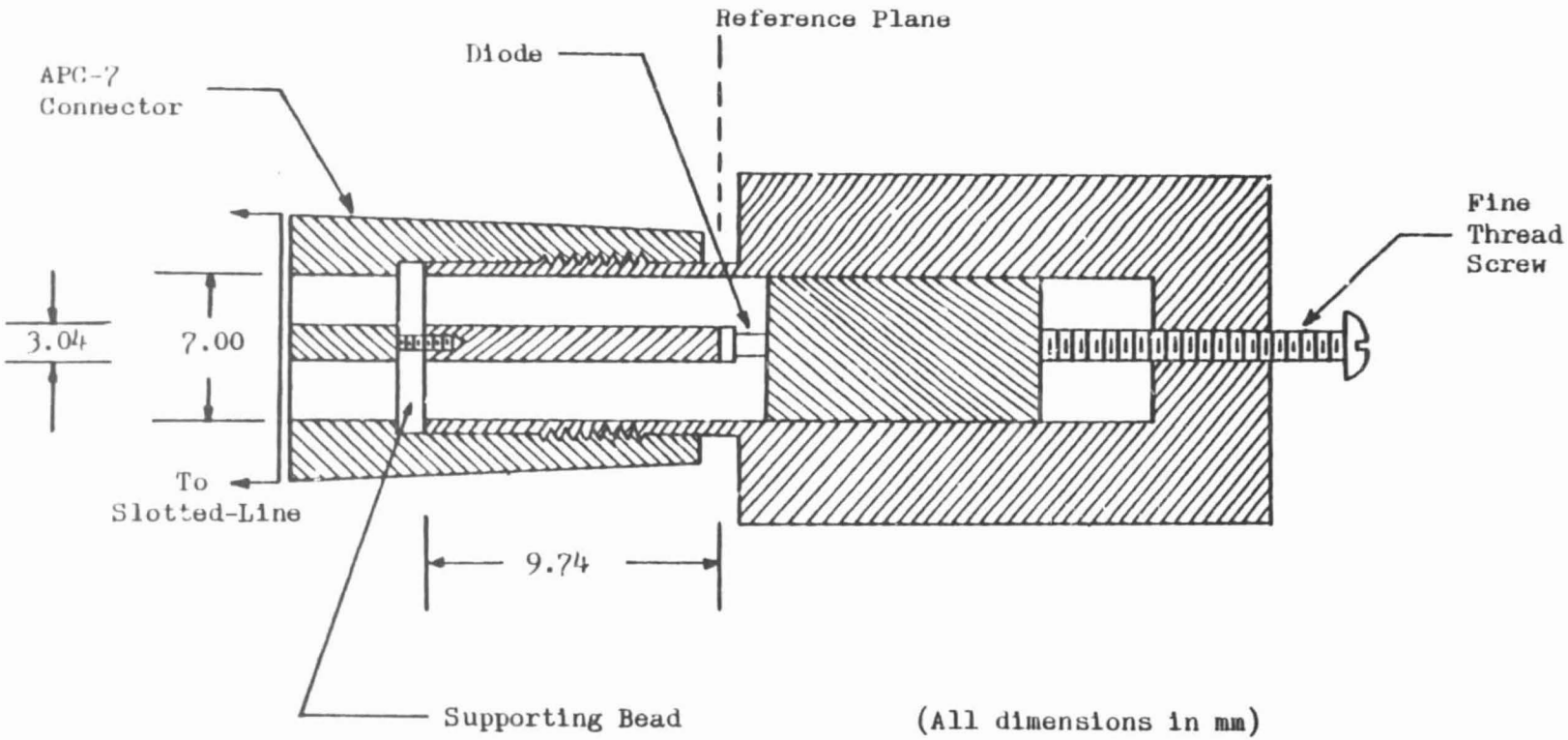

Fig. 2.8 Diode Test Mount

are usually very small, and can be neglected in most cases. However, in this case, the diodes have a very small resistance, and hence the voltage standing-wave ratio (VSWR) is very high. As a result, neglecting the line loss can affect the measured data drastically. Bandler [27] has shown that the attenuation constant, α, of a slotted-line is related to the short-circuited VSWR, S_o, by

$$\alpha = \frac{1}{S_o \ell} \qquad \text{nepers/cm} \qquad (2.21)$$

where ℓ is the distance between the position of the probe and the reference plane in centimeters. The attenuation constant measured by this method has a value of 0.00046 nepers/cm at 5 GHz and 0.00056 nepers/cm at 6 GHz.

To establish the load reference plane, the center-recessed slug was replaced by another slug with identical dimensions, yet an even and smooth surface, which made firm contact with the inner conductor. The positions of standing-wave minima were recorded at intervals of approximately 1 GHz from 1 to 18 GHz. These positions were numerically extrapolated by integer numbers of half-wavelength until they coincided, and this, of course, was the load reference plane. The value cocsistent with the slotted-line scale was determined to be -1.383 cm. The scatter through the whole frequency range was rather small and could well be attributed to experimental errors, thus the system was believed to be substantially free from major defects.

For the diode measured in this report, the diameter of the larger end cap is 3.05 mm, which is identical to the diameter of the inner

conductor. Thus, the load reference plane can be further moved to the end cap-dielectric casing interface. As will be seen later in this chapter, this makes the data reduction procedure much simpler. Since the thickness of the end cap is 0.058 cm, the new load reference plane was then moved to -1.441 cm.

2.4.3 Measurement Technique. Due to the combination of low power and high VSWR, the accuracy of measurement by the "double-minimum" method [28] is rather poor because of the difficulty in precisely measuring the power level at locations of standing-wave minima. To overcome this problem, the "four-point" method [29] was employed. Referring to Fig. 2.9, this method requires the measurements of four positions (x_1, x_2, x_3, and x_4) and the difference between two power levels (P dB) which was usually taken to be about 10 dB. Measurements were made at intervals of about 200 MHz from 4.8 GHz to 6.2 GHz, and again from 10 to 12 GHz. At each frequency, measurements were made at six different bias voltages: 0, 0.5, 1.0, 2.0, 4.0, and 6.0 volts. At each bias voltage, the probe moved from one end of the slotted-line to the other covering all standing-wave minima. Usually several hundred sets of data were taken for each diode.

The calculation of standing-wave ratio, S, is quite straightforward. Let d_1 be the distance between x_1 and x_2, and d_2 between x_3 and x_4, then

$$S = \left[1 + \frac{\exp(0.23026P) - 1}{\sin^2\left(\frac{\pi d_2}{\lambda_g}\right) - \exp(0.23026P)\sin^2\left(\frac{\pi d_1}{\lambda_g}\right)} \right]^{1/2} \tag{2.22}$$

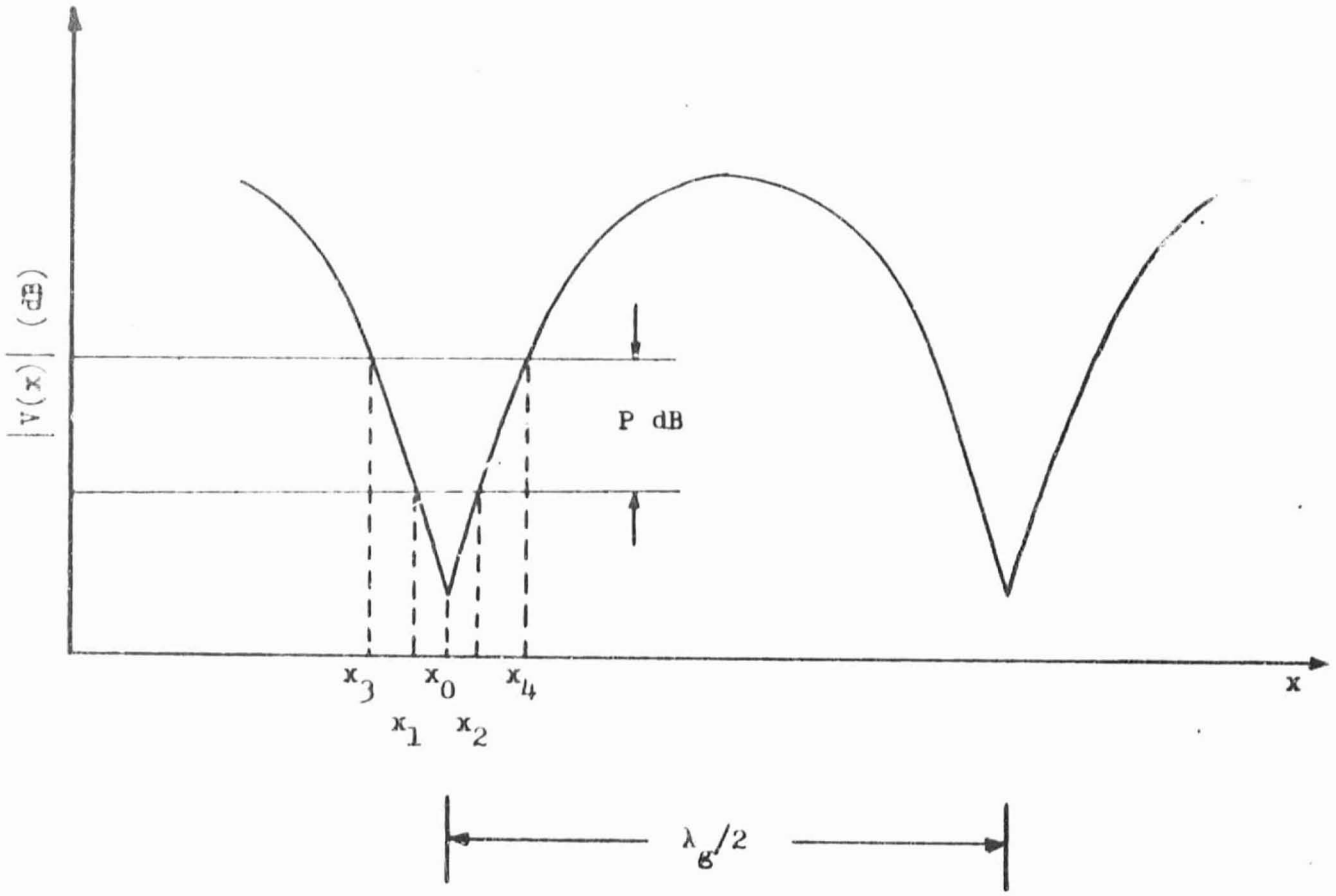

Fig. 2.9 Standing-Wave Pattern on a Slotted-Line

where λ_g is the wavelength and P is the difference in dB between the two power levels where the four positions were measured. However, Eq. 2.22 gives VSWR at the position of minimum (x_0). For lossy slotted-line, the value at the load reference plane is [28][30]

$$S_\ell = \coth[\operatorname{arctanh}(1/S) - \alpha\ell] \tag{2.23}$$

where ℓ is the distance between x_0 and the load reference plane. If $S \gg 1$, and $\alpha\ell \ll 1$, Eq. 2.23 becomes

$$S = \frac{1}{1/S - \alpha\ell} \tag{2.24}$$

and the load impedance at the reference plane is

$$Z_\ell = Z_o \frac{1 - jS_\ell \tan\theta}{S_\ell - j\tan\theta} \tag{2.25}$$

where Z_o is the characteristic impedance of the slotted-line and θ is the electric angle between x_0 and the load reference plane, and is given as

$$\theta = \frac{2\pi\ell}{\lambda_g} \tag{2.26}$$

A computer program was written to process the measured data according to Eqs. 2.22, 2.23, and 2.25. During the initial run, all data points were processed individually, and an "average impedance" was calculated at each bias. The computer printout was carefully examined and data point with value greatly different from the average value was considered

to be "bad point" due to experimental errors, and thus was discarded. After the cleanup, the data were reprocessed. Figure 2.10 shows one page of the computer printout on the initial run.

2.5 Determination of Equivalent Circuit Parameters

2.5.1 Diode Test Mount Equivalent Circuit. As has been discussed in great detail by Getsinger [31], the impedance calculated from Eq. 2.25 is in fact the impedance of both the diode mount and the diode itself. Figure 2.11(b) shows the diode mount equivalent circuit proposed by Getsinger. Circuit elements will now be briefly described.

The first element from the left, C_f, is the fringing capacitance between the end cap and the outer conductor. The series inductance, L_c, is the coaxial inductance caused by magnetic fields in the volume bounded by the outer conductor as indicated in Fig. 2.11(a). The pi-network formed by C_{r1}, L_r, and C_{r2}, is the equivalent network for the radial line [32] with length h, extending from the diode to the diameter D_i of the inner conductor.

Based on the dimensions of the diode and the diode mount, these parameters were calculated to be (see Appendix B)

$$C_f = 0.062 \quad pF$$

$$L_c = 0.118 \quad nH$$

$$C_{r1} = C_{r2} = 0.025 \quad pF$$

$$L_r = 0.058 \quad nH$$

To test its validity, the impedance calculated from this equivalent

FREQUENCY (GHZ)	BIAS (VOLT)	VSWR	IMPEDANCE REAL	IMAG
4.94100				
	0.00			
		80.117	0.766	-23.835
		87.918	0.699	-23.917
		79.456	0.815	-23.997
		69.937	0.881	-24.078
	*** AVERAGE IMPEDANCE ***		0.790	-23.957
	-0.50			
		91.540	0.711	-27.432
		104.865	0.621	-27.519
		96.042	0.679	-27.605
		74.458	0.878	-27.688
	*** AVERAGE IMPEDANCE ***		0.722	-27.561
	-1.00			
		95.549	0.714	-30.191
		119.315	0.573	-30.283
		115.547	0.592	-30.373
		90.851	0.755	-30.461
	*** AVERAGE IMPEDANCE ***		0.658	-30.327
	-2.00			
		135.914	0.544	-34.603
		151.803	0.488	-34.702
		140.044	0.530	-34.800
		94.404	0.788	-34.895
	*** AVERAGE IMPEDANCE ***		0.587	-34.750
	-4.00			
		142.257	0.570	-39.411
		169.205	0.429	-39.520
		158.573	0.513	-39.627
		185.439	0.439	-39.627
		104.213	0.783	-39.731
	*** AVERAGE IMPEDANCE ***		0.547	-39.583

Fig. 2.10 Computer Printout of Measured Impedances

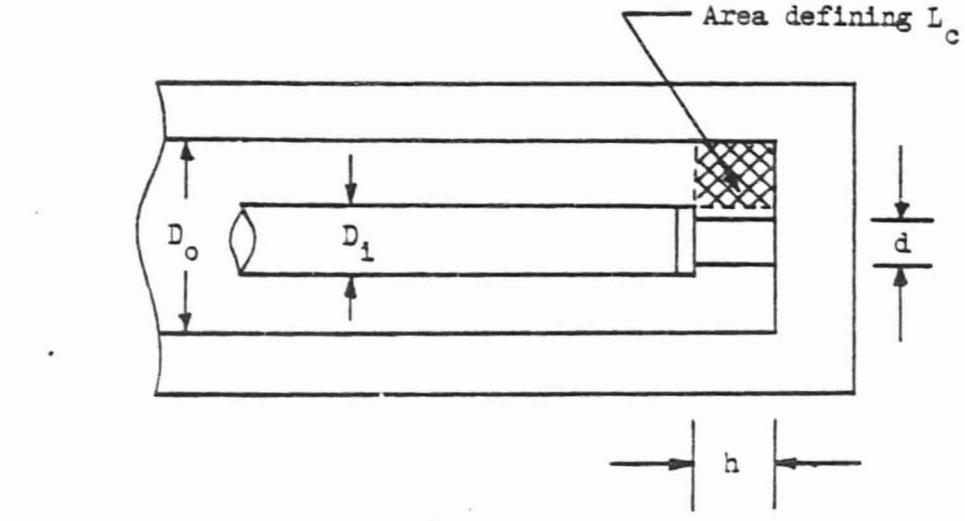

(a)

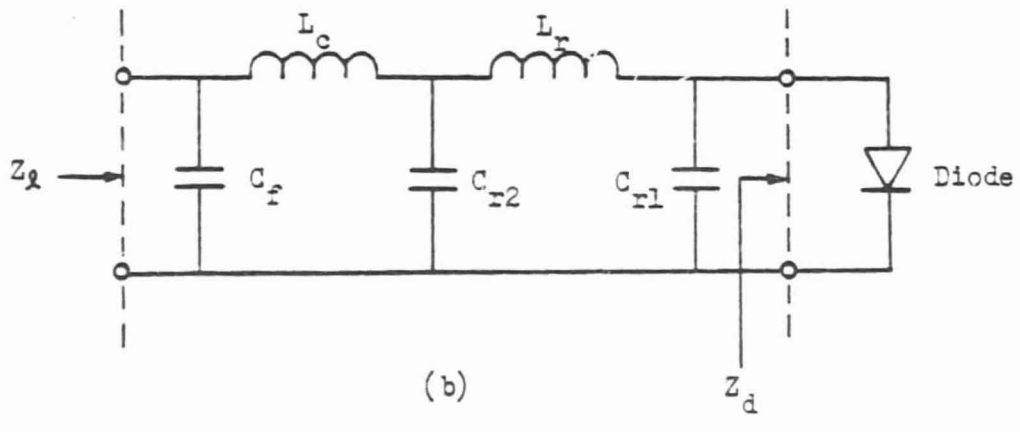

(b)

Fig. 2.11 Diode Mount Representation
(a) diode terminating coaxial line
(b) diode mount equivalent circuit

circuit together with the diode parameters in Table 2.1 are compared with the measured impedances. Figure 2.12 shows excellent agreement between the calculated and measured reactances, and thus substantially confirms the validity of the equivalent circuit.

Once the equivalent circuit of the diode mount is determined, the diode impedance, Z_d, can be easily obtained from the measured impedance, Z_ℓ. The diode reactances at two bias voltages are also plotted in Fig. 2.12.

2.5.2 Computer-Aided Optimization of Diode Parameters and Equivalent Circuit Elements. The problem of obtaining numerical values for the equivalent circuit elements from the measured impedance data is usually solved by the least-square polynomial approximation method [33]. Conceptually, it is very straightforward. A polynomial function which fits the measured data is compared with a second polynomial function which represents the impedance of the equivalent circuit. Numerical values of the circuit elements are solved from a set of simultaneous equations formed by equating the coefficients of like terms from these two polynomial functions. In practice, this method is very tedious and involves enormous amount of computational efforts. Worse yet, the equivalent circuit thus determined is only valid at one bias voltage.

What is really desired is to determine not just the equivalent circuit at any particular bias voltage. Instead, it is more desirable to determine the values of the parasitic elements and the diode parameters, namely, n, Φ, C_{j0}, R_1, and R_2 as in Eqs. 2.9 and 2.15. Knowing these

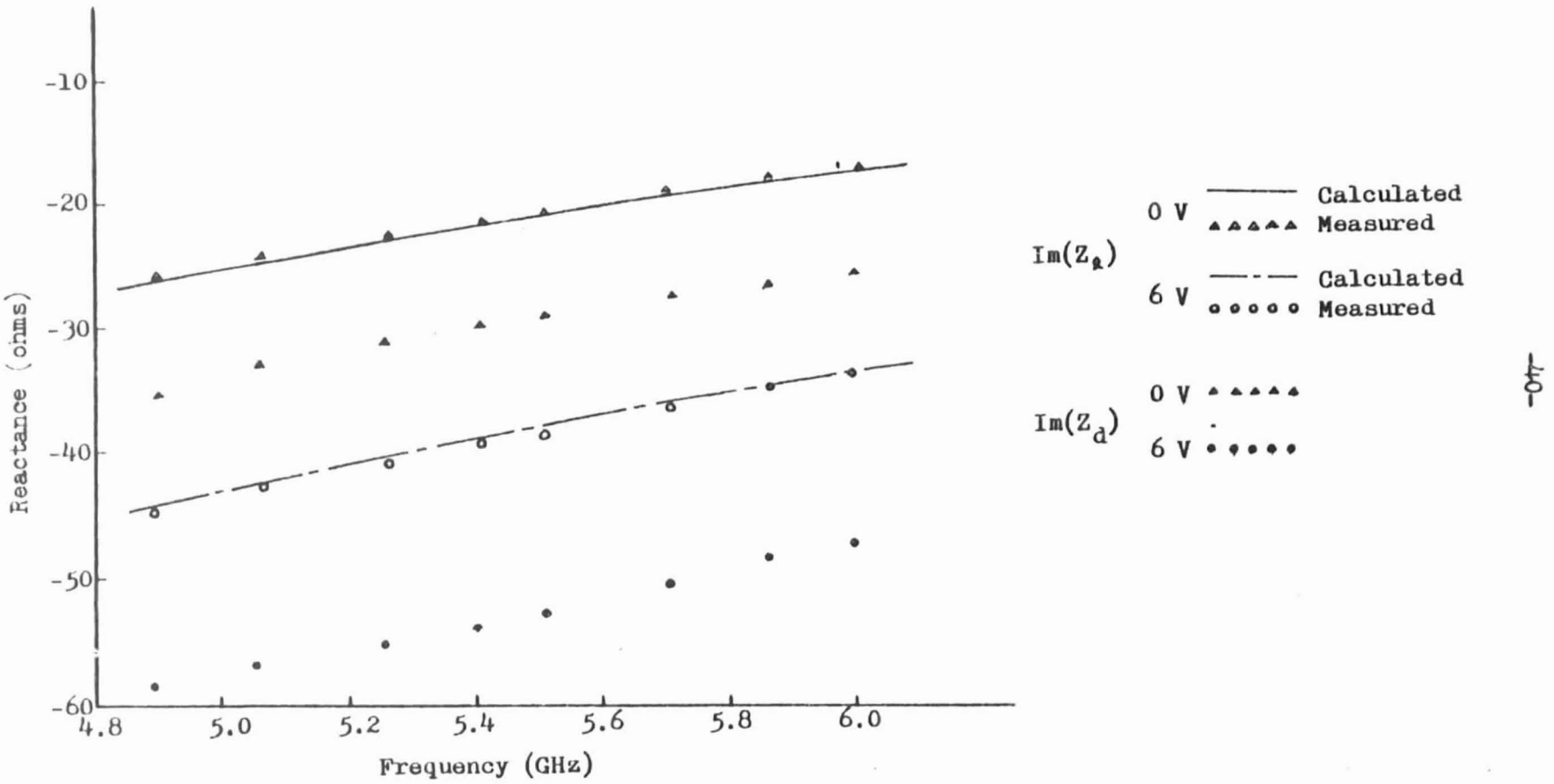

Fig. 2.12 Comparison of Calculated and Measured Reactances

parameters, the equivalent circuit at any given bias voltage can be contructed. Furthermore, these parameters also permit the more accurate calculation of pump power level and amplifier performance.

To determine these parameters, a computer-aided optimization technique was employed. This technique can be simply explained as follows. Initial parameter values are obtained by "educated guess" or any other judicial means. Following a certain strategy, or optimization method, each parameter is then adjusted (within certain constraints) so as to minimize the error between the measured impedance and those calculated. By doing this successively, the error is finally minimized, and thus the "optimum" parameter values are obtained. This is obviously not a systematic method, and a certain amount of experience and intuition is required. In fact, many factors such as initial parameter values, step sizes, optimization method, and error difinition, can all affect the final outcome.

A computer program employing a modified "direct search" method [34] was written for this study*. The error function is defined as

$$\text{ERROR} = \sum \left\{ w_1 [\text{Re}(Z_{d,\text{cal.}}) - \text{Re}(Z_{d,\text{mea.}})]^2 + w_2 [\text{Im}(Z_{d,\text{cal.}}) - \text{Im}(Z_{d,\text{mea.}})]^2 \right\} \qquad (2.27)$$

---

* Two subroutine similar to "DIRECT" and "EXPLOR" in Appendix C were used in this program to perform the "direct search". This method will be covered in more detail in Chapter V.

where w_1 and w_2 are weighting coefficients, and the summation is over all frequencies of interest. As is evident from Fig. 2.10, the real part of the measured impedances is less repeatable, and thus less reliable, than the imaginary part. Therefore a value of 0.2 or less was assigned to the ratio of w_1/w_2. Measured data of each diode were usually optimized more than ten times, each with slightly different initial value and step size, for the equivalent circuit shown in Fig. 2.4(b). The results were then compared and the one with the smallest error was retained. Table 2.2 shows the optimum parameter values for the three diodes listed in Table 2.1.

Table 2.2 Optimum Parameter Values for MA 48509E Varactor Diodes

Parameter	Diode #1	Diode #2	Diode #3
n	2.332	2.154	2.218
Φ (volts)	1.214	1.147	1.126
C_{j0} (pF)	0.581	0.552	0.596
R_1 (ohms)	1.04	1.03	1.11
R_2 (ohms)	0.12	0.14	0.15
L_s (nH)	0.317	0.324	0.325
C_{p1} (pF)	0.251	0.251	0.247
C_{p2} (pF)	0.043	0.046	0.051

where w_1 and w_2 are weighting coefficients, and the summation is over all frequencies of interest. As is evident from Fig. 2.10, the real part of the measured impedances is less repeatable, and thus less reliable, than the imaginary part. Therefore a value of 0.2 or less was assigned to the ratio of w_1/w_2. Measured data of each diode were usually optimized more than ten times, each with slightly different initial value and step size, for the equivalent circuit shown in Fig. 2.4(b). The results were then compared and the one with the smallest error was retained. Table 2.2 shows the optimum parameter values for the three diodes listed in Table 2.1.

Table 2.2 Optimum Parameter Values for MA 48509E Varactor Diodes

Parameter	Diode #1	Diode #2	Diode #3
n	2.332	2.154	2.218
Φ (volts)	1.214	1.147	1.126
C_{j0} (pF)	0.581	0.552	0.596
R_1 (ohms)	1.04	1.03	1.11
R_2 (ohms)	0.12	0.14	0.15
L_s (nH)	0.317	0.324	0.325
C_{p1} (pF)	0.251	0.251	0.247
C_{p2} (pF)	0.043	0.046	0.051

CHAPTER III THEORY OF NEGATIVE RESISTANCE PARAMETRIC AMPLIFIERS

3.1 Introduction

In the analysis of parametric amplifiers and converters, a set of power relations originally developed by Manley and Rowe [35] provedes a fundamental basis. It is convenient for the purpose of illustration to consider the general situation as represented by the circuit of Fig. 3.1. Two voltage generators at frequencies f_1 and f_2 together with associated series resistances and ideal band-pass filters are placed across a loss-less nonlinear reactance. Each filter presents a short-circuit to the desired frequency, and an open-circuit to all other frequencies. In addition to the two voltage generators, an infinite array of ideal band-pass filters and load resistances are also connected to the nonlinear reactance. These filters are tuned to the various sum and difference frequencies which will arise because of the nonlinear reactance. The equations that relates the power flowing into (positive power) and out of (negetive power) the nonlinear reactance are shown by Manley and Rowe to be

$$\sum_{m=0}^{\infty} \sum_{n=-\infty}^{\infty} \frac{mP_{m,n}}{mf_1 + nf_2} = 0 \qquad (3.1)$$

$$\sum_{n=0}^{\infty} \sum_{m=-\infty}^{\infty} \frac{nP_{m,n}}{mf_1 + nf_2} = 0 \qquad (3.2)$$

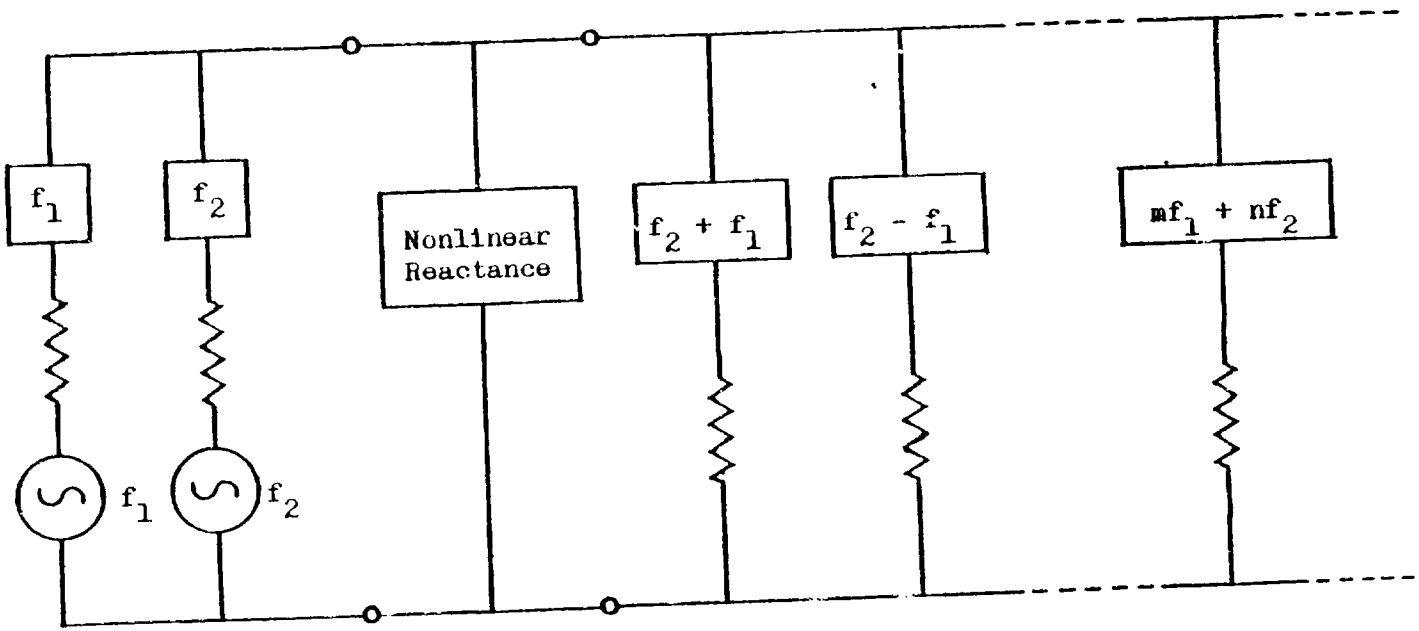

Fig. 3.1 Circuit Illustrating Use of Manley-Rowe Relations

where $P_{m,n}$ is the average power flowing into the nonlinear reactance at the frequency $mf_1 + nf_2$. Equations 3.1 and 3.2 are often referred as the Manley-Rowe relations. These relations are independent of the shape of reactance characteristics and of the driving power level.

To illustrate the applications of the Manley-Rowe relations, a particular case will now be examined in which power is permitted to flow at only three frequencies. If the nonlinear reactance is excited at f_1 and f_2, it will generate a third frequency f_3. The circuit is assumed to present an open-circuit to all other frequencies. It is further assumed that the power from the voltage generator at f_1 is much smaller than that from the voltage generator at f_2 which is responsible for driving the nonlinear reactance, and which is usually called the pump source. If f_3 is the defference frequency, i. e., $f_3 = f_2 - f_1$, Eqs. 3.1 and 3.2 become

$$\frac{P_1}{f_1} - \frac{P_3}{f_3} = 0 \qquad (3.3)$$

$$\frac{P_2}{f_2} + \frac{P_3}{f_3} = 0 \qquad (3.4)$$

Since pump power P_2 is supplied to the nonlinear reactance and is positive, it follows that P_1 and P_3 are negative. This means that the nonlinear reactance is <u>supplying</u> power to the voltage generator at f_1 rather than <u>absorbing</u> power from it. Since this power is independent of that supplied by the generator itself, it follows that infinite power gain is possible at f_1. This is the case of the so-called negetive

resistance parametric amplifiers, and f_1 and f_3 are the signal and the idler frequency, respectively.

The nonlinear reactance can be either inductive or capacitive. In this study, the treatment is limited to the latter case in which the nonlinear depletion capacitance of a varactor described in last chapter is employed. More precisely, a varactor has not only a nonlinear capacitance, but also a nonlinear resistance. Engelbrecht [36] has studied circuits containing both nonlinear capacitance and resistance for frequency converters. The time-varying capacitive and resistive elements were assumed to be 90° out of phase, i. e., they are pumped in time-quadreture. This arrangement allows the circuit to exhibit non-reciprocal features not found in single nonlinear element circuits. Other have also studied the cases in which the two nonlinear elements are pumped in arbitrary phase relationship [37][38]. However, for high quality varactors, the nonlinear effect in series resistance is insignificantly small, and may thus be neglected. Throughout the remainder of this report, the series resistance of a varactor will be treated as a variable (i. e., dependent upon bias voltage) but linear element.

In the subsequent sections, the behavior of a varactor under the influence of a large-amplitude pump voltage will be investigated. This is followed by the formulation of the small-signal immittance matrix of a pumped varactor. The analysis of parametric amplifiers employing a simplified equivalent circuit, i. e., a nonlinear capacitance and a linear resistance, has been covered in a number of well-known books [37]

[38][39][40][41], and numerous journal articles [42][43]. No attempt to review the vast literature will be made here. Instead, generalized expressions for power gain and noise figure will be derived for amplifiers employing a more realistic equivalent circuit.

3.2 Pumping of Varactor Diodes

In a parametric amplifier, let a large-amplitude pumping voltage of frequency f_p be applied across the varactor. By Fourier series expansion, the nonlinear capacitance can then be replaced by a time-varying linear capacitance,

$$C(t) = \sum_{k=-\infty}^{\infty} C_k \, e^{jk\omega_p t} \tag{3.5}$$

The purpose of this section is to calculate the Fourier coefficients C_k, and the required pumping power. The discussion is limited to the case of voltage pumping, in which the voltage across the nonlinear capacitance is assumed to be sinusoidal. The calculation methods for the case of current pumping, in which the current through the nonlinear capacitance is assumed to be sinusoidal, are similar to that of voltage pumping, and are given elsewhere [38][41].

The range of the pumping voltage, $v_p(t)$, across the nonlinear capacitance is limited by the contact potential, ϕ, in the forward bias region, and by the breakdown voltage, V_B, in the reverse bias region. The pumping is said to be full if $v_p(t)$ varies from $-\phi$ to V_B. In this case, the bias voltage is chosen to be

$$V_o = \frac{V_B + \phi}{2} \tag{3.6}$$

If the pumping power is limited, then the field of variation of $v_p(t)$ is narrower, and the pumping is said to be partial. In this case, the bias voltage should be chosen such that the following condition is met at any instant,

$$-\phi \leq v_p(t) \leq V_B \tag{3.7}$$

Since the voltage across the nonlinear capacitance is sinusoidal in voltage pumping, $v_p(t)$ can be expressed as

$$v_p(t) = V_o + V_p \cos\omega_p t \tag{3.8}$$

where, without loss of generality, the time origin is chosen in such a way that the pumping phase is zero. From Eq. 2.9, the time-varying capacitance may be written as

$$C(t) = \frac{C_{j0}}{[1 + (V_o + V_p \cos\omega_p t)/\phi]^{1/n}} \tag{3.9}$$

Letting $a = V_p/(V_o + \phi)$, Eq. 3.9 becomes

$$C(t) = \frac{C_{jV_o}}{(1 + a\cos\omega_p t)^{1/n}} \tag{3.10}$$

where $C_{jV_o} = C_{j0}/(1 + V_o/\phi)^{1/n}$. The Fourier coefficients, C_k, are then given as

$$C_k = \frac{1}{T} \int_0^T C(t) \cdot e^{-jk\omega_p t} \, dt \tag{3.11}$$

Since C(t) is an even function, it follows that

$$2|C_k| = |C_k + C_{-k}| = \left| \frac{2}{T} \int_0^T C(t) \cos(k\omega_p t) \, dt \right| \tag{3.12}$$

Equations 3.10 and 3.12 yield

$$|C_k| = \left| \frac{C_j V_o}{T} \int_0^T \frac{\cos(k\omega_p t)}{(1 + a \cos\omega_p t)^{1/n}} \, dt \right|$$

$$= \left| \frac{C_j V_o}{2\pi} \int_0^{2\pi} \frac{\cos kx}{(1 + a \cos x)^{1/n}} \, dx \right|$$

Equation 3.13 can be evaluated by either expansion in terms of hypergeometric functions [44][45], or numerical integration. Tables 3.1 to 3.4 give the results of the computation of the first four Fourier coefficients for several different values of n in the range from 2 to 3.

The maximum gain-bandwidth product of a negative resistance parametric amplifier as derived by Kuh and Fukada [9] is given by

$$b(10 \log G_t + 6) \leq 13.64 \sqrt{f_i/f_s} \, (C_1/C_0) \tag{3.14}$$

where b is the fractional bandwidth, and G_t is the transducer gain. From

Table 3.1 Ratio of First Fourier Coefficient to DC Capacitance as a Function of a

$C_0/C_1(V)$

a	n = 2.0	n = 2.2	n = 2.4	n = 2.6	n = 2.8	n = 3.0
0.00	1.0000	1.0000	1.0000	1.0000	1.0000	1.0000
0.05	1.0005	1.0004	1.0004	1.0003	1.0003	1.0003
0.10	1.0019	1.0017	1.0015	1.0013	1.0012	1.0011
0.15	1.0043	1.0038	1.0034	1.0030	1.0028	1.0025
0.20	1.0077	1.0068	1.0060	1.0054	1.0049	1.0045
0.25	1.0121	1.0107	1.0095	1.0086	1.0078	1.0072
0.30	1.0178	1.0156	1.0139	1.0126	1.0114	1.0105
0.35	1.0246	1.0217	1.0193	1.0174	1.0158	1.0145
0.40	1.0329	1.0290	1.0258	1.0232	1.0211	1.0193
0.45	1.0429	1.0376	1.0335	1.0301	1.0274	1.0250
0.50	1.0546	1.0479	1.0426	1.0383	1.0348	1.0318
0.55	1.0686	1.0601	1.0534	1.0480	1.0435	1.0398
0.60	1.0854	1.0747	1.0662	1.0594	1.0539	1.0492
0.65	1.1055	1.0921	1.0816	1.0731	1.0662	1.0604
0.70	1.1300	1.1133	1.1001	1.0896	1.0810	1.0739
0.75	1.1605	1.1395	1.1231	1.1099	1.0992	1.0903
0.80	1.1998	1.1730	1.1522	1.1357	1.1222	1.1111
0.85	1.2531	1.2181	1.1911	1.1698	1.1525	1.1383
0.90	1.3318	1.2839	1.2474	1.2187	1.1957	1.1769
0.95	1.4737	1.4001	1.3450	1.3025	1.2687	1.2414

Table 3.2 Normalized Second Fourier Coefficient as a Function of a

$|C_1/C_0|$

a	n = 2.0	n = 2.2	n = 2.4	n = 2.6	n = 2.8	n = 3.0
0.00	0.0000	0.0000	0.0000	0.0000	0.0000	0.0000
0.05	0.0125	0.0114	0.0104	0.0096	0.0089	0.0083
0.10	0.0251	0.0228	0.0209	0.0193	0.0179	0.0167
0.15	0.0377	0.0343	0.0314	0.0290	0.0270	0.0252
0.20	0.0506	0.0460	0.0421	0.0389	0.0361	0.0337
0.25	0.0636	0.0579	0.0530	0.0489	0.0454	0.0424
0.30	0.0770	0.0700	0.0642	0.0592	0.0550	0.0513
0.35	0.0907	0.0825	0.0756	0.0698	0.0648	0.0605
0.40	0.1049	0.0954	0.0874	0.0807	0.0749	0.0699
0.45	0.1197	0.1088	0.0997	0.0921	0.0855	0.0797
0.50	0.1352	0.1229	0.1127	0.1040	0.0965	0.0901
0.55	0.1516	0.1378	0.1263	0.1166	0.1082	0.1009
0.60	0.1691	0.1537	0.1409	0.1300	0.1207	0.1126
0.65	0.1880	0.1709	0.1566	0.1445	0.1341	0.1251
0.70	0.2088	0.1898	0.1739	0.1604	0.1489	0.1389
0.75	0.2321	0.2110	0.1933	0.1783	0.1654	0.1543
0.80	0.2590	0.2354	0.2156	0.1988	0.1844	0.1720
0.85	0.2912	0.2647	0.2424	0.2235	0.2072	0.1932
0.90	0.3329	0.3025	0.2769	0.2552	0.2365	0.2204
0.95	0.3953	0.3591	0.3286	0.3026	0.2802	0.2608

Table 3.3 Normalized Third Fourier Coefficient as a Function of a

$|C_2/C_0|$

a	n = 2.0	n = 2.2	n = 2.4	n = 2.6	n = 2.8	n = 3.0
0.00	0.0000	0.0000	0.0000	0.0000	0.0000	0.0000
0.05	0.0002	0.0002	0.0002	0.0002	0.0002	0.0001
0.10	0.0009	0.0008	0.0007	0.0007	0.0006	0.0006
0.15	0.0021	0.0019	0.0017	0.0015	0.0014	0.0013
0.20	0.0038	0.0034	0.0030	0.0027	0.0025	0.0023
0.25	0.0061	0.0053	0.0048	0.0043	0.0039	0.0036
0.30	0.0089	0.0078	0.0070	0.0063	0.0057	0.0053
0.35	0.0123	0.0109	0.0097	0.0087	0.0080	0.0073
0.40	0.0165	0.0145	0.0129	0.0117	0.0106	0.0097
0.45	0.0214	0.0189	0.0168	0.0152	0.0138	0.0127
0.50	0.0273	0.0240	0.0214	0.0193	0.0176	0.0161
0.55	0.0342	0.0302	0.0269	0.0243	0.0221	0.0202
0.60	0.0425	0.0374	0.0334	0.0301	0.0274	0.0251
0.65	0.0524	0.0462	0.0412	0.0372	0.0338	0.0310
0.70	0.0645	0.0568	0.0507	0.0457	0.0415	0.0381
0.75	0.0793	0.0699	0.0624	0.0562	0.0511	0.0468
0.80	0.0983	0.0866	0.0773	0.0696	0.0633	0.0579
0.85	0.1235	0.1088	0.0970	0.0874	0.0794	0.0727
0.90	0.1598	0.1408	0.1255	0.1130	0.1026	0.0938
0.95	0.2215	0.1951	0.1737	0.1562	0.1417	0.1294

Table 3.4 Normalized Fourth Fourier Coefficient as a Function of a

$|C_3/C_0|$

a	n = 2.0	n = 2.2	n = 2.4	n = 2.6	n = 2.8	n = 3.0
0.00	0.0000	0.0000	0.0000	0.0000	0.0000	0.0000
0.05	0.0000	0.0000	0.0000	0.0000	0.0000	0.0000
0.10	0.0000	0.0000	0.0000	0.0000	0.0000	0.0000
0.15	0.0001	0.0001	0.0001	0.0001	0.0001	0.0001
0.20	0.0003	0.0003	0.0002	0.0002	0.0002	0.0002
0.25	0.0006	0.0006	0.0005	0.0004	0.0004	0.0004
0.30	0.0011	0.0010	0.0009	0.0008	0.0007	0.0006
0.35	0.0019	0.0016	0.0014	0.0013	0.0011	0.0010
0.40	0.0029	0.0025	0.0022	0.0019	0.0017	0.0016
0.45	0.0042	0.0037	0.0032	0.0029	0.0026	0.0023
0.50	0.0061	0.0053	0.0046	0.0041	0.0037	0.0034
0.55	0.0086	0.0074	0.0065	0.0058	0.0052	0.0047
0.60	0.0118	0.0102	0.0090	0.0080	0.0072	0.0065
0.65	0.0162	0.0140	0.0123	0.0109	0.0098	0.0089
0.70	0.0220	0.0191	0.0167	0.0149	0.0134	0.0121
0.75	0.0300	0.0260	0.0228	0.0203	0.0182	0.0165
0.80	0.0412	0.0357	0.0313	0.0278	0.0250	0.0227
0.85	0.0578	0.0500	0.0439	0.0390	0.0350	0.0317
0.90	0.0844	0.0730	0.0640	0.0569	0.0510	0.0462
0.95	0.1359	0.1175	0.1030	0.0913	0.0818	0.0740

Eq. 3.14, it is obvious that a large C_1/C_0 ratio is highly desirable. C_1/C_0 increases, as is evident from Table 3.2, with (1) decreasing n, and (2) increasing a. The first condition dictates the choice of a varactor with junction being as nearly abrupt as possible. The second condition indicates the varactor should be pumped as hard as possible. However, this raises an important question: How hard can a varactor be pumped? In other words, what is the reasonable value for a? Obviously the ac voltage swing can not be allowed to carry all the way to the contact potential because of the onset of forward conduction. Such a condition introduces shot noise, and thus must be avoided. At the present time, there is no theoretical analysis on maximum allowable a. Experimentally, this parameter appears to be from 0.85 to 0.95, depending on the type of semiconductor materials and reverse breakdown voltages. For design purposes, a value of 0.90 will be assumed. With this assumption, it can be observed from these tables that C(t) can be well approximated by only the first three terms of the Fourier series.

The current flowing through the nonlinear capacitance is [41],

$$i(t) = C(t) \frac{dv_p(t)}{dt}$$

$$= \frac{C_{jV_0}}{(1 + a \cos\omega_p t)^{1/n}} V_p(-\omega_p)\sin\omega_p t \qquad (3.15)$$

The pumping power then can be calculated from

$$P_p = \frac{1}{T} \int_0^T R_s[i(t)]^2 \, dt$$

$$= \frac{R_s}{2} C_{jV_o}^2 \omega_p^2 V_p^2 \int_0^{2\pi} \frac{(\sin x)^2}{(1 + a \cos x)^{2/n}} \, dx \quad (3.16)$$

If the cutoff frequency at a specified bias V_o is defined as

$$\omega_c = \frac{1}{R_s C_{jV_o}} \quad (3.17)$$

and the normalization pumping power at a specified bias V_o is defined as

$$P_n = \frac{(V_o + \phi)^2}{R_s} \quad (3.18)$$

then Eq. 3.16 can be written as

$$P_p = \frac{1}{2\pi} \left(\frac{\omega_p}{\omega_c}\right)^2 P_n \int_0^{2\pi} \frac{(a \sin x)^2}{(1 + a \cos x)^{2/n}} \, dx \quad (3.19)$$

$$\frac{P_p}{P_n(\omega_p/\omega_c)^2} = \frac{1}{2\pi} \int_0^{2\pi} \frac{(a \sin x)^2}{(1 + a \cos x)^{2/n}} \, dx \quad (3.20)$$

The integral in Eq. 3.20 can be evaluated by numerical integration, and results are given in Table 3.5.

3.3 Small Signal Representation of a Nonlinear Capacitance

The relationships between the current flowing through a nonlinear

Table 3.5 Normalized Pumping Power as a Function of a

$P_p/P_n(\omega_p/\omega_c)^2$

a	n = 2.0	n = 2.2	n = 2.4	n = 2.6	n = 2.8	n = 3.0
0.00	0.0000	0.0000	0.0000	0.0000	0.0000	0.0000
0.05	0.0013	0.0013	0.0013	0.0013	0.0013	0.0013
0.10	0.0050	0.0050	0.0050	0.0050	0.0050	0.0050
0.15	0.0113	0.0113	0.0113	0.0113	0.0113	0.0113
0.20	0.0202	0.0202	0.0202	0.0201	0.0201	0.0201
0.25	0.0318	0.0317	0.0316	0.0316	0.0316	0.0315
0.30	0.0461	0.0459	0.0458	0.0457	0.0456	0.0456
0.35	0.0633	0.0630	0.0628	0.0626	0.0625	0.0623
0.40	0.0835	0.0830	0.0826	0.0823	0.0821	0.0819
0.45	0.1070	0.1062	0.1056	0.1051	0.1047	0.1044
0.50	0.1340	0.1327	0.1318	0.1310	0.1304	0.1299
0.55	0.1648	0.1629	0.1615	0.1603	0.1593	0.1585
0.60	0.2000	0.1972	0.1950	0.1932	0.1918	0.1907
0.65	0.2401	0.2359	0.2327	0.2302	0.2281	0.2265
0.70	0.2859	0.2798	0.2752	0.2716	0.2687	0.2663
0.75	0.3386	0.3299	0.3233	0.3182	0.3141	0.3108
0.80	0.4000	0.3876	0.3782	0.3710	0.3652	0.3605
0.85	0.4732	0.4552	0.4418	0.4314	0.4232	0.4166
0.90	0.5641	0.5372	0.5175	0.5024	0.4906	0.4812
0.95	0.6877	0.6446	0.6136	0.5905	0.5727	0.5585

capacitance and the signal voltage across its terminals will now be developed. The amplitude of the signal voltage is assumed to be much smaller than that of the pumping voltage. The treatment is limited to the case of negative resistance parametric amplifiers, i. e., besides the pumping voltage, voltages at only two other frequencies are assumed to be of significant magnitude. These frequencies are the signal frequency f_s, and the idler frequency f_i. The respective voltages and currents at these frequencies are

$$v_s(t) = \frac{1}{2}\left[V_s e^{j\omega_s t} + V_s^* e^{-j\omega_s t} \right] \tag{3.21a}$$

$$v_i(t) = \frac{1}{2}\left[V_i e^{j\omega_i t} + V_i^* e^{-j\omega_i t} \right] \tag{3.21b}$$

$$i_s(t) = \frac{1}{2}\left[I_s e^{j\omega_s t} + I_s^* e^{-j\omega_s t} \right] \tag{3.21c}$$

$$i_i(t) = \frac{1}{2}\left[I_i e^{j\omega_i t} + I_i^* e^{-j\omega_i t} \right] \tag{3.21d}$$

where the asterisk denotes the complex conjugate. If it is assumed that only the first two terms in the Fourier series are significant, then C(t) can be expressed as

$$C(t) = C_0 + C_1\left(e^{j\omega_p t} + e^{-j\omega_p t} \right)$$

$$= C_0\left[1 + \gamma_1\left(e^{j\omega_p t} + e^{-j\omega_p t} \right)\right] \tag{3.22}$$

where $\gamma_1 = C_1/C_0$. The voltage across a nonlinear capacitance and the current flowing through it are related by

$$i(t) = \frac{d}{dt}\left[C(t)v(t)\right] \tag{3.23}$$

or

$$i_s + i_i = \frac{d}{dt}\left[C(t)(v_s + v_i)\right] \tag{3.24}$$

Substituting Eqs. 3.21 and 3.22 into Eq. 3.24, and equating the coefficients on the left- and right-hand sides at f_s and f_i, the following equation is obtained,

$$\begin{bmatrix} I_s \\ I_i^* \end{bmatrix} = \begin{bmatrix} j\omega_s C_0 & j\omega_s \gamma_1 C_0 \\ -j\omega_i \gamma_1 C_0 & -j\omega_i C_0 \end{bmatrix} \cdot \begin{bmatrix} V_s \\ V_i^* \end{bmatrix} \tag{3.25}$$

In deriving the small-signal admittance matrix of Eq. 3.25, it is implied that all unwanted harmonics are short-circuited. In practice, a perfect short-circuit can never be obtained because of the inevitable series resistance. A different set of relationships which correspond to a condition of open-circuited harmonics can also be derived by taking several additional frequencies into consideration. These additional frequencies are $\omega_3 = \omega_p + \omega_s$, $\omega_4 = 2\omega_p - \omega_s$, and $\omega_5 = 2\omega_p + \omega_s$. To account for the ω_4 and ω_5 terms, the second harmonic component must be included in the expression of $C(t)$. Thus

$$C(t) = C_0[1 + \gamma_1(e^{j\omega_p t} + e^{-j\omega_p t}) + \gamma_2(e^{j2\omega_p t} + e^{-j2\omega_p t})] \qquad (3.26)$$

where $\gamma_2 = C_2/C_0$. Following the same procedure as in the derivation of Eq. 3.25, the small-signal admittance matrix for the case of open-circuited harmonics is obtained as follows:

$$\begin{bmatrix} I_s \\ I_i^* \\ I_3 \\ I_4^* \\ I_5 \end{bmatrix} = \begin{bmatrix} j\omega_s C_0 & j\omega_s \gamma_1 C_0 & j\omega_s \gamma_1 C_0 & j\omega_s \gamma_2 C_0 & j\omega_s \gamma_2 C_0 \\ -j\omega_i \gamma_1 C_0 & -j\omega_i C_0 & -j\omega_i \gamma_2 C_0 & -j\omega_i \gamma_1 C_0 & 0 \\ j\omega_3 \gamma_1 C_0 & j\omega_3 \gamma_2 C_0 & j\omega_3 C_0 & 0 & j\omega_3 \gamma_1 C_0 \\ -j\omega_4 \gamma_2 C_0 & -j\omega_4 \gamma_1 C_0 & 0 & -j\omega_4 C_0 & 0 \\ j\omega_5 \gamma_2 C_0 & 0 & j\omega_5 \gamma_1 C_0 & 0 & j\omega_5 C_0 \end{bmatrix} \cdot \begin{bmatrix} V_s \\ V_i^* \\ V_3 \\ V_4^* \\ V_5 \end{bmatrix} \qquad (3.27)$$

I_s and I_i^* can be solved from Eq. 3.27 by the Perturbation method [37], and are given as follows:

$$\begin{bmatrix} I_s \\ I_i^* \end{bmatrix} = \begin{bmatrix} j\omega_s C_0(1 - \gamma_1^2) & j\omega_s C_0 \gamma_1 (1 - \gamma_2) \\ -j\omega_i C_0 \gamma_1 (1 - \gamma_2) & -j\omega_i C_0 (1 - \gamma_1^2) \end{bmatrix} \cdot \begin{bmatrix} V_s \\ V_i^* \end{bmatrix} \qquad (3.28)$$

The small-signal admittance matrix of either Eq. 3.25 or Eq. 3.28 can be used for the analysis of negative resistance parametric amplifiers, depending upon whether the unwanted harmonics are more nearly short-circuited or open-circuited. In practice, it is difficult to control

this condition, and thus it can not be siad a priori that one is more accurate than the other. The difference in amplifier performance calculated for both cases will be shown in Chapter V.

To include the effects of the series resistance and the parasitics, the admittance matrices must be inverted into impedance matrices. For either case the resulting matrix is

$$\begin{bmatrix} V_s \\ V_i^* \end{bmatrix} = \begin{bmatrix} \frac{1}{j\omega_s C} & \frac{\gamma}{j\omega_i C} \\ \frac{-\gamma}{j\omega_s C} & \frac{-1}{j\omega_i C} \end{bmatrix} \cdot \begin{bmatrix} I_s \\ I_i^* \end{bmatrix} \quad . \tag{3.29}$$

where

$$\gamma = \gamma_1$$
$$C = C_0(1 - \gamma_1^2) \tag{3.30}$$

for the case of short-circuited harmonics, and

$$\gamma = \gamma_1(1 + \gamma_1^2)(1 - \gamma_2)$$
$$C = C_0(1 - 2\gamma_1^2) \tag{3.31}$$

for the case of open-circuited harmonics.

3.4 Circuit Analysis of Basic Amplifier Configuration

Figure 3.2 shows a practical configuration of a negative resistance parametric amplifier. A circulator is used to separate the input from the output since a negative resistance amplifier is in essence a one-port

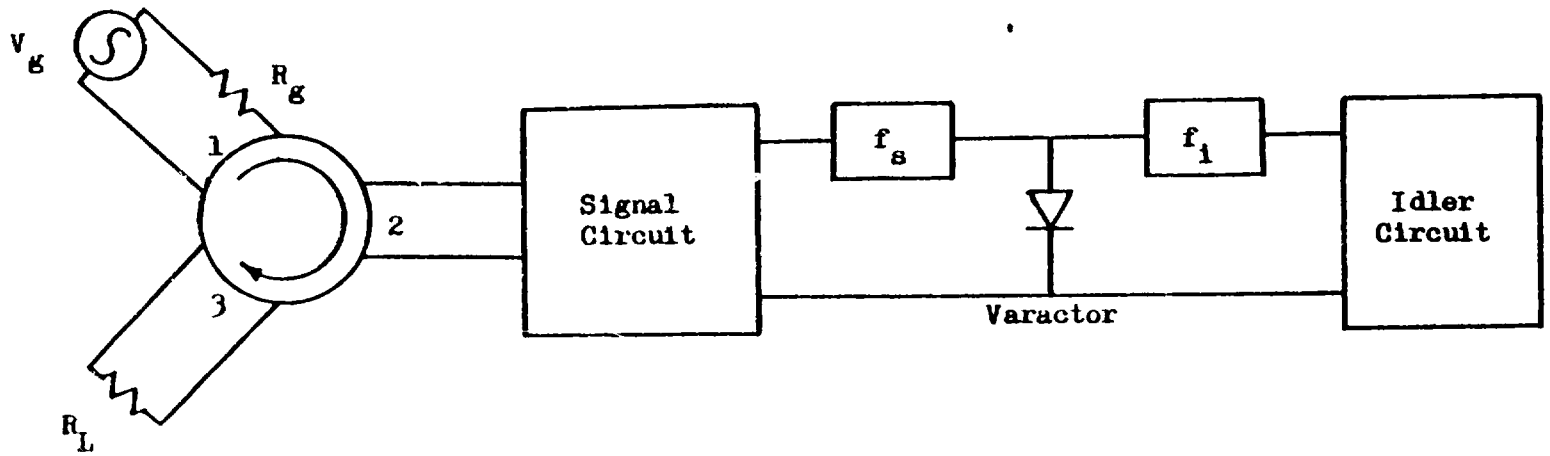

Fig. 3.2 Negative Resistance Parametric Amplifier Configuration

amplifier, i. e., the input and output signals are of the same frequency and at the same port. A circulator is a non-reciprocal device which transfers power from port 1 to port 2, from port 2 to port 3, and from port 3 to port 1, but not vice versa. Of course, it is possible to extract the output power from a load connected in series with the generator and the amplifier. This is not desirable, however, since some of the output power is lost in the generator resistance. The gain and noise figure of such a configuration are much inferior to those of an amplifier making use of a circulator [41].

The boxes labeled f_s and f_i are band-pass filters centered around the signal and the idler frequency bands, respectively. Pump and bias circuits are not shown in Fig. 3.2, since they are assumed to be perfectly isolated , and thus need not be included in the analysis. Expressions for transducer gain* and noise figure will now be derived. It should be pointed out that these expressions are intended for computer-aided design implementation, thus the step-by-step derivation is presented in such a way as to facilitate computer programming.

3.4.1 Transducer Gain. In practice, the generator resistance R_g, and the load resistance R_L, are always equal to Z_c, the characteristic impedance of the circulator. Hence, the transducer gain of the amplifier is given by

---

* Transducer gain is defined as the ratio of the power delivered to the load, to the available power of the source.

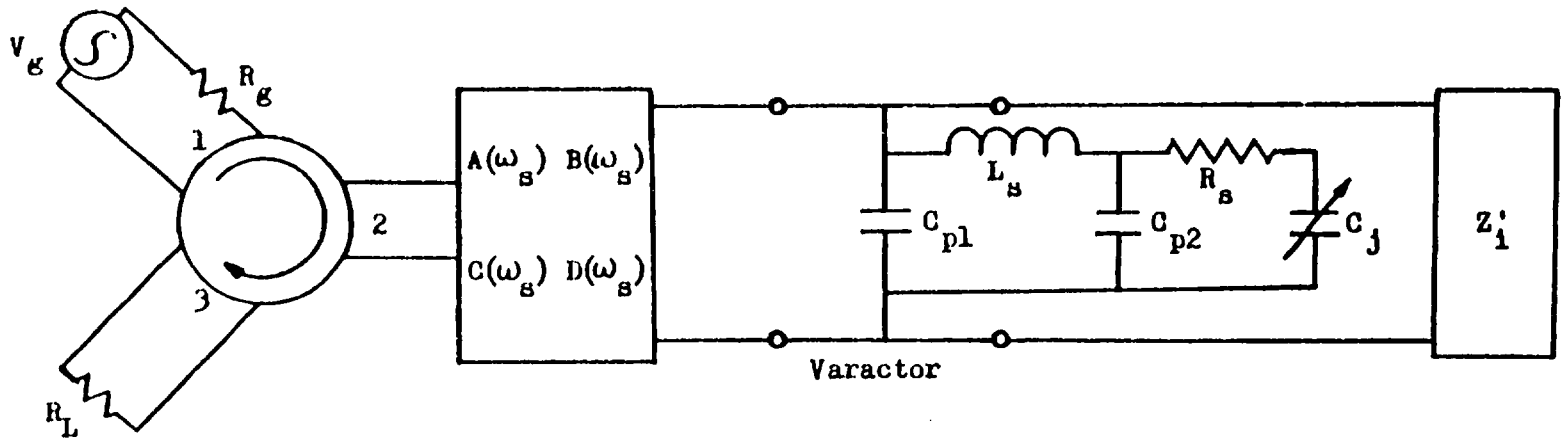

Fig. 3.3 Equivalent Circuit of a Negative Resistance Parametric Amplifier

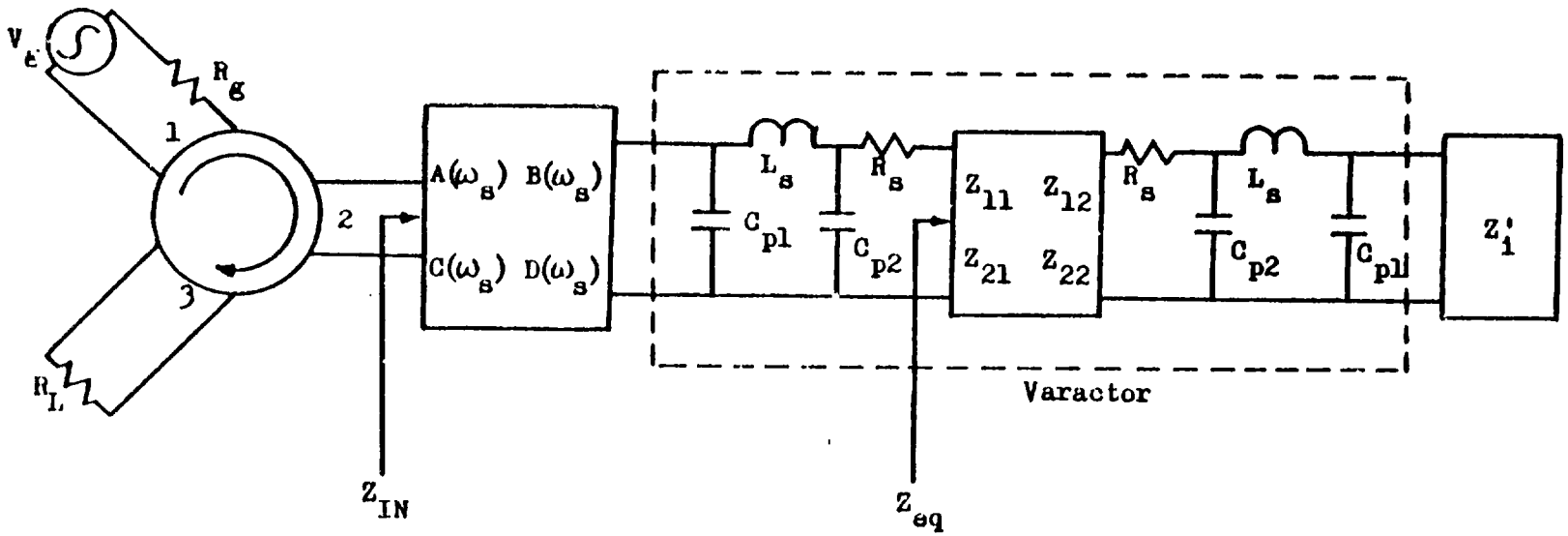

Fig. 3.4 Revised Equivalent Circuit

$$G_t = \left| \frac{Z_{IN} + Z_c}{Z_{IN} + Z_c} \right|^2 \qquad (3.32)$$

where Z_{IN} is the input impedance looking into the amplifier from port 2 of the circulator. Obviously, for the transducer gain to be computed, the input impedance, Z_{IN}, must first be determined. To accomplish this, consider the circuit in Fig.3.3, in which the diode is replaced by its equivalent circuit of Fig. 2.4(b). Z_i' represents the impedance of the idler circuit together with the idler band-pass filter, while the signal circuit and the signal band-pass filter are represented by an ABCD matrix with elements $A(\omega_s)$, $B(\omega_s)$, $C(\omega_s)$, and $D(\omega_s)$. To facilitate the analysis, the nonlinear capacitance is replaced by the small-signal impedance matrix of Eq. 3.29 with elements denoted as Z_{11}, Z_{12}, Z_{21}, and Z_{22}, as shown in Fig. 3.4.

If Z_i represents the impedance of the circuit to the right of the matrix as indicated in Fig. 3.4, then

$$Z_i = R_i + jX_i$$

$$= R_s + \left(\frac{1}{j\omega_i C_{p2}}\right) || \left[j\omega_i L_s + \left(\frac{1}{j\omega_i C_{p1}}\right) || (Z_i') \right] \qquad (3.33)$$

where the symbol "||" is used to designate two impedances connected in parallel. The impedance of the nonlinear capacitance loaded by the idler circuit as seen from the signal circuit is

$$Z_{eq} = Z_{11} - \frac{Z_{12}Z_{21}}{Z_{22} + Z_i^*}$$

$$= \frac{1}{j\omega_s C} - \frac{\gamma^2}{\omega_s \omega_i C^2 (Z_i^* - \frac{1}{j\omega_i C})} \qquad (3.34)$$

where the asterisk denotes the complex conjugate. At this point, it is perhaps worthwhile to digress from the derivation and show why this type of amplifier is called a negative resistance amplifier, and how the amplication is achieved.

Substituting $Z_i^* = R_i - jX_i$, Eq. 3.34 becomes

$$Z_{eq} = \frac{1}{j\omega_s C} - \frac{\gamma^2}{\omega_s \omega_i C^2 [R_i - j(X_i - 1/\omega_i C)]}$$

$$= \frac{1}{j\omega_s C} - \frac{\gamma^2}{\omega_s \omega_i C^2 [R_i^2 + (X_i - 1/\omega_i C)^2]}$$

$$= \frac{1}{j\omega_s C} - \frac{\gamma^2 R_i}{\omega_s \omega_i C^2 [R_i^2 + (X_i - 1/\omega_i C)^2]}$$

$$- \frac{j\gamma^2 (X_i - 1/\omega_i C)}{\omega_s \omega_i C^2 [R_i^2 + (X_i - 1/\omega_i C)^2]} \qquad (3.35)$$

The second term on the right-hand side of Eq. 3.35 obviously represents

a negative resistance

$$-R_N = -\frac{\gamma^2 R_i}{\omega_s \omega_i C^2 [R_i^2 + (X_i - 1/\omega_i C)^2]} \tag{3.36}$$

If the signal circuit is assumed to be lossless and all reactances are tuned out, the impedance looking into the signal circuit from port 2 is then a pure negative resistance (not necessarily equal to that of Eq. 3.36 since the signal circuit may contain impedance transformers), thus

$$Z_{IN} = -R_N' \tag{3.37}$$

From Eq. 3.32, the transducer gain of the amplifier is

$$G_t = \left| \frac{Z_{IN} - Z_c}{Z_{IN} + Z_c} \right|^2 = \left| \frac{Z_c - R_N'}{Z_c - R_N'} \right|^2 \tag{3.38}$$

From Eq. 3.38, it is evident that amplification is achieved. When R_N' is made to equal to Z_c, the transducer gain becomes infinite.

Returning to the derivation of the transducer gain, the impedance at the varactor terminals seen from the signal circuit is

$$Z_s = \left(\frac{1}{j\omega_s C_{p2}}\right) || [j\omega_s L_s + \left(\frac{1}{j\omega_s C_{p1}}\right) || (R_s + Z_{eq})] \tag{3.39}$$

If the elements of the ABCD matrix of the signal circuit are $A(\omega_s)$,

$B(\omega_s)$, $C(\omega_s)$, and $D(\omega_s)$, the input impedance is then

$$Z_{IN} = \frac{A(\omega_s)Z_s + B(\omega_s)}{C(\omega_s)Z_s + D(\omega_s)} \tag{3.40}$$

The transducer gain can now be calculated from Eq. 3.32.

The preceeding formulation is applicable to both nondegenerate and degenerate amplifiers. For nondegenerate amplifiers, Z_i is the impedance of an external idler circuit which is completely unrelated to the signal circuit. However, for degenerate amplifiers, Z_i is the impedance looking into the signal circuit from the terminals of the varactor. Therefore

$$Z_i = \frac{D(\omega_i)Z_c + B(\omega_i)}{C(\omega_i)Z_c + A(\omega_i)} \tag{3.41}$$

where $A(\omega_i)$, $B(\omega_i)$, $C(\omega_i)$, and $D(\omega_i)$ are the ABCD matrix elements of the signal circuit calculated at the idler frequency.

3.4.2 Noise Figure. The fundamental noise in a parametric amplifier is due mainly to the thermal noise generated by the signal circuit, the idler circuit, and the diode series resistance. Although numerous authors have provided approximate expressions for predicting parametric amplifier noise performance [37][38][41][46][47], for computer-aided design, a more general expression for the circuit in Fig. 3.2 must be developed.

Thermal noise of a resistor results from the random motion of free electrons within the resistor. This random motion causes a small fluctuating voltage, or noise voltage, to exist at the terminals of the resistor. Nyquist [48] was able to show, based on fundamental thermo-

dynamic considerations, that the mean square noise voltage in the frequency interval Δf generated by a resistor R at an absolute temperature T is

$$\overline{e_n^2} = 4kTR\Delta f \tag{3.42}$$

where k is Boltzmann's constant (1.38×10^{-23} J/°K). For analytical purpose, a noisy resistor can be replaced by either a noise voltage source in series with a noiseless resistor, or a noise current source in parallel with a noiseless resistor, as shown in Fig. 3.5.

The equivalent circuit in Fig. 3.4 is redrawn in Fig. 3.6 for purpose of noise analysis. As indicated in the figure, Z_{Ts} and Z_{Ti} are the impedances looking from R_s into the signal circuit and the idler circuit, respectively.

$$Z_{Ts} = R_{Ts} + jX_{Ti}$$

$$= \left(\frac{1}{j\omega_s C_{p2}}\right) \| \left[j\omega_s L_s + \left(\frac{1}{j\omega_s C_{p1}}\right) \| (Z_{sm})\right] \tag{3.43}$$

where

$$Z_{sm} = \frac{D(\omega_s)Z_c + B(\omega_s)}{C(\omega_s)Z_c + A(\omega_s)} \tag{3.44}$$

and

$$Z_{Ti} = R_{Ti} + jX_{Ti}$$

$$= \left(\frac{1}{j\omega_i C_{p2}}\right) \| \left[j\omega_i L_s + \left(\frac{1}{j\omega_i C_{p1}}\right) \| (Z_i')\right] \tag{3.45}$$

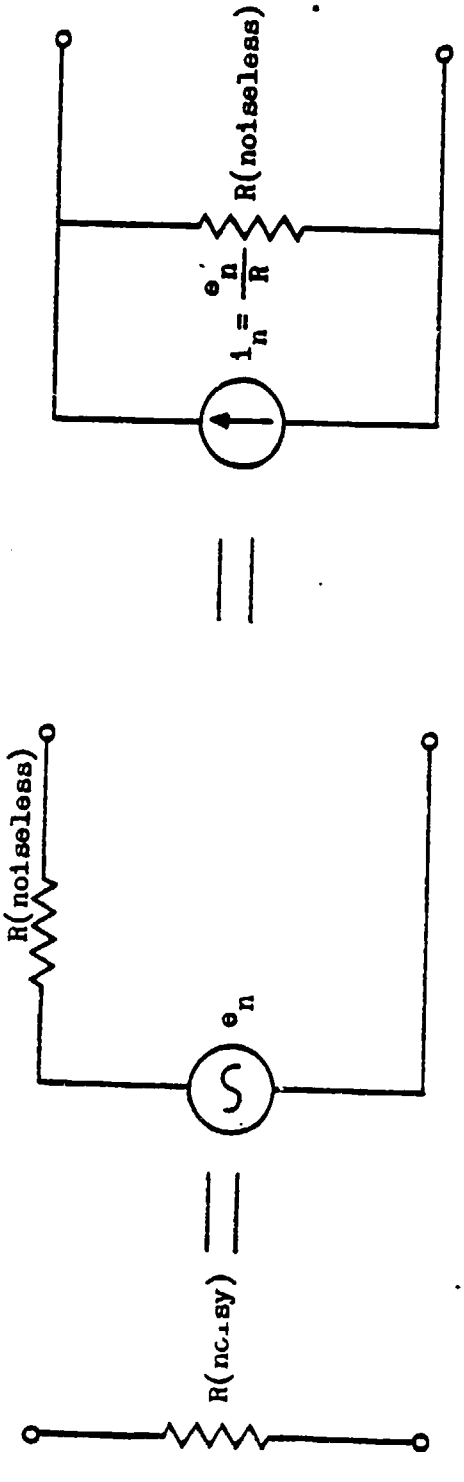

Fig. 3.5 Resistor Noise Source Representation

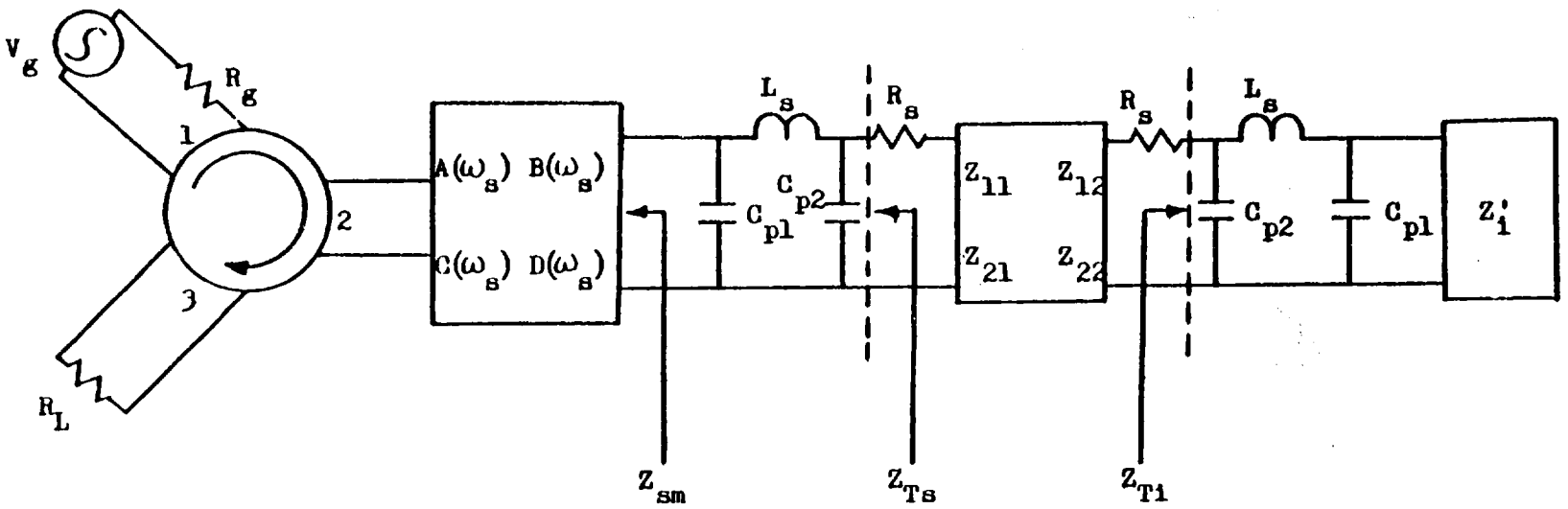

Fig. 3.6 Equivalent Circuit of a Negative Resistance Parametric Amplifier

As shown in Fig. 3.7, the thermal noise generated by resistances, R_{Ts}, R_{Ti}, and R_s, can now be represented by noise voltage sources, e_{ns}, e_{ni}, and e_{nd}, respectively. These noise sources are uncorrelated and, in addition, components of e_{nd} at ω_s which excites the signal circuit are uncorrelated to the components of e_{nd} at ω_i which excites the idler circuit.

The matrix equation for the circuit in Fig. 3.7 is

$$\begin{bmatrix} e_{nd} + e_{ns} \\ e_{nd}^* + e_{ni}^* \end{bmatrix} = \begin{bmatrix} Z_{11} + R_s + Z_{Ts} & Z_{12} \\ Z_{21} & Z_{22} + R_s + Z_{Ti}^* \end{bmatrix} \begin{bmatrix} I_{ns} \\ I_{ni}^* \end{bmatrix} \tag{3.46}$$

The noise current in the signal circuit due to the noise sources at ω_s, i. e., $e_{nd} + e_{ns}$, is

$$I_{nss} = \frac{(e_{nd} + e_{ns})(Z_{22} + R_s + Z_{Ti}^*)}{(Z_{11} + R_s + Z_{Ts})(Z_{22} + R_s + Z_{Ti}^*) - Z_{12} Z_{21}} \tag{3.47}$$

Thus, the output noise power at ω_s is

$$\begin{aligned} N_s &= \left|I_{nss}\right|^2 Z_c \\ &= \frac{(e_{nd} + e_{ns})^2 \left|Z_{22} + R_s + Z_{Ti}^*\right|^2 Z_c}{\left|(Z_{11} + R_s + Z_{Ts})(Z_{22} + R_s + Z_{Ti}^*) - Z_{12} Z_{21}\right|^2} \end{aligned} \tag{3.48}$$

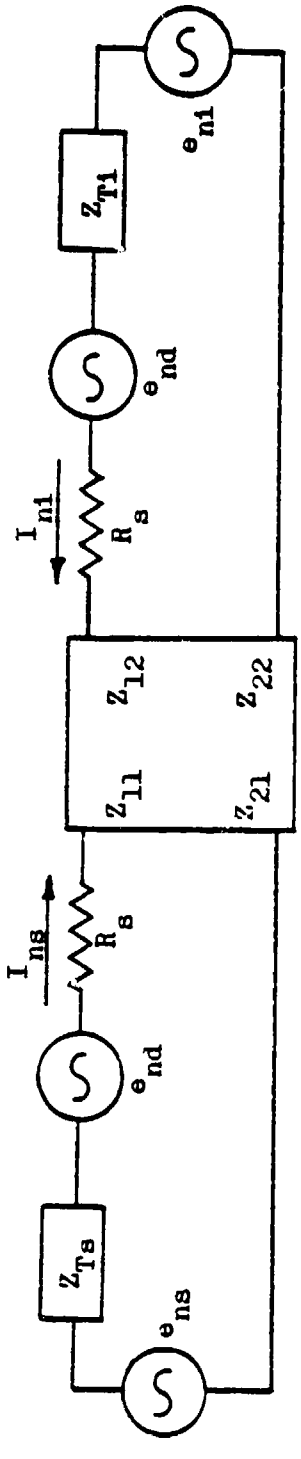

Fig. 3.7 Equivalent Circuit with Noise Sources

Since e_{nd} and e_{ns} are uncorrelated, it follows that

$$(e_{nd} + e_{ns})^2 = 4kB(T_s R_{Ts} + T_d R_s) \tag{3.49}$$

where

B = effective amplifier bandwidth (Hz),

T_s = signal circuit temperature (^oK),

T_d = diode temperature (^oK).

Equation 3.48 then becomes

$$N_s = \frac{4kB(T_s R_{Ts} + T_d R_s)\left|Z_{22} + R_s + Z_{Ti}^*\right|^2 Z_c}{\left|(Z_{11} + R_s + Z_{Ts})(Z_{22} + R_s + Z_{Ti}^*) - Z_{12}\, Z_{21}\right|^2} \tag{3.50}$$

Similarly, the output noise power at ω_i is

$$N_i = \frac{4kB(T_i R_{Ti} + T_d R_s)\left|Z_{12}\right|^2 Z_c}{\left|(Z_{11} + R_s + Z_{Ts})(Z_{22} + R_s + Z_{Ti}^*) - Z_{12}\, Z_{21}\right|^2}$$

where T_i is the idler circuit temperature.

The noise figure of the amplifier is given by [37],

$$F = \frac{N_s + N_i}{G_t k T_o B} \tag{3.52}$$

where $T_o = 290\ ^oK$ is the standard noise temperature.

The preceeding formulation is again applicable to both nondegenerate and degenerate amplifiers. However, as discussed in Chapter I, degenerate amplifiers possess the distinction of having two noise figures, namely,

the single-sideband and the double-sideband noise figures. The single-sideband noise figure can be calculated directly from Eq. 3.52, while the double-sideband noise figure is one-half of that calculated from Eq. 3.52.

CHAPTER IV PROPERTIES OF MICROSTRIP TRANSMISSION LINES

4.1 Introduction

In the process of technological evolution, continuous interaction exists between techniques of different fields. Often techniques developed for one field stimulate and promote the development and progress in others. Such is the case of the microwave integrated circuit (MIC).

Prior to the early sixties, nearly all microwave systems utilized waveguides and coaxial lines. Semiconductor devices such as varactors, tunnel diodes, and point-contact diodes were used in receivers. Varactor harmonic generators were used in a few systems as low power sources. But, for the most part, tubes were still the principal microwave power sources. Hence, although the MIC was introduced in the fifties [49], progress, both theoretical and experimental, was very slow in the decade following its inception.

In the mid-sixties, with rapid improvements in the low-frequency integrated circuit (IC) techniques such as epitaxial growth, passivation, photolithography, and metal deposition by evaporation or sputtering, microwave transistors as well as transferred electron devices and avalanche diodes were developed for solid-state microwave power sources. Schottky-barrier diodes and PIN diodes were also developed for receivers and control circuits. With all these solid-state devices available, it was only natural that attempts toward circuit miniaturization should be made. To achieve miniaturization, the MIC was of course one of the

choices considered. Not only did advances in low-frequency IC techniques make these solid-state devices possible, they also made the fabrication of microwave integrated circuits more precise and more reproducible. Out went the old and crude techniques of glue and razor blades, along came the more sophisticated and more reliable techniques of metal deposition and photolithography. In the years following 1965, several semiconductor manufacturers, radar system manufacturers, and government laboratory started programs to develop miniaturized microwave circuits for applications in phased-array radar systems. This early work was culminated in the construction of a feasibility radar system by Texas Instruments in 1968 [50]. This radar system uses more than six hundred transmit-receive (T/R) modules fabricated by MIC techniques. Each module contains a power amplifier, an IF amplifier, a varactor frequency multiplier, a balanced Schottky-barrier diode mixer, PIN diode switches, PIN diode phase shifters, and associated phase shift logic circuits. The module is about 1.8cm by 6.4 cm, and delivered 0.5 W at 9 GHz.

With the feasibility demonstrated, nearly all manufacturers of microwave equipment entered the MIC field. Today, MICs are well accepted and are employed in essentially all the low- and medium-power microwave applications.

Microwave integrated circuits can be broadly divided into two catagories: monolithic and hybrid. A monolithic MIC is one in which all components, active and passive, are formed simultaneously on a single piece of semiconductor material. Due to the large variety of active devices,

it is extremely difficult, if not impossible, to specify a diffusion process that simultaneously optimizes the performance of every active device. Furthermore, the interconnections between active devices have relatively large dimensions, especially when distributed elements are used. This requires large substrate areas which are very expensive in the case of monolithic technology.

A hybrid MIC is one in which circuit interconnections are formed by metal lines on a dielectric substrate and active devices are attached to the substrate. Depending upon the techniques by which the metallization is formed, the hybrid technology itself can be divided into two classes: thin- and thick-film. In thin-film technology, the conductor films are deposited in vacuum by evaporation or sputtering, followed by electroplating to increase the film thickness, if necessary. The desired pattern is defined by photolithographic techniques. In thick-film technology, the metallization is usually formed by silk-screening, in which the desired pattern is incorporated into the screen.

Hybrid MICs can also be classified according to the types of circuit elements employed, namely, lumped and distributed. Lumped-element circuits for applications at frequencies in the X-band have been reported [51][52]. The limitation on the use of lumped-element circuits comes from the excessive circuit losses at higher frequencies.

For the distributed-element circuits, various types of circuit configurations are currently in use. Figure 4.1 shows the configurations of several commonly used circuits; stripline [53], microstrip [49], slot

line [54][55], and coplanar waveguide [56]. Among these, microstrip is certainly the most popular configuration, and is most frequently identified with the term "microwave integrated circuit".

In the subsequent sections, electrical characteristics of microstrip lines relevant to this study will be investigated. These include characteristic impedance, effective dielectric constant, conductor and dielectric losses, and frequency dispersion effects. Discontinuities in circuit structure, such as open circuits and T-junction, will be examined in detail. Finally, analysis and synthesis methods for one circuit component, parallel-coupled microstrip band-pass filters, will be developed.

In dealing with various techniques in each area, the emphasis is placed upon those that are applicable to computer-aided design. In other words, closed form expressions which, in most cases they are derived empirically, are preferred over the more rigorous and more time-consuming analytical techniques. However, major works in each area will still be referenced, and interested readers are urged to consult the original publications.

Material selections and fabrication techniques, two important aspects in MIC technology, will not be covered here; they can be found in books dealing with low-frequency ICs or MICs [57][58][59].

4.2 Electrical Characteristics of Microstrip Lines

4.2.1 Characteristic Impedance and Effective Dielectric Constant.

The difficulty in microstrip analysis stems from the fact that electro-

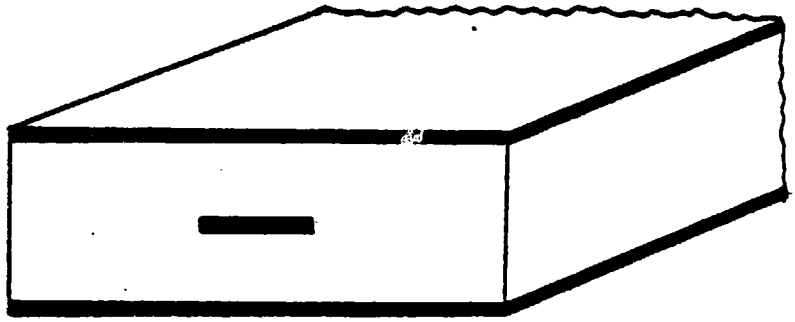

(a)

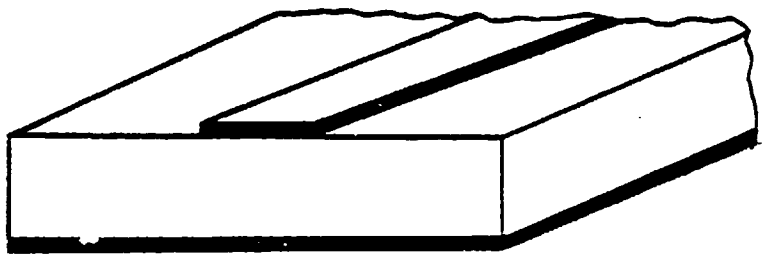

(b)

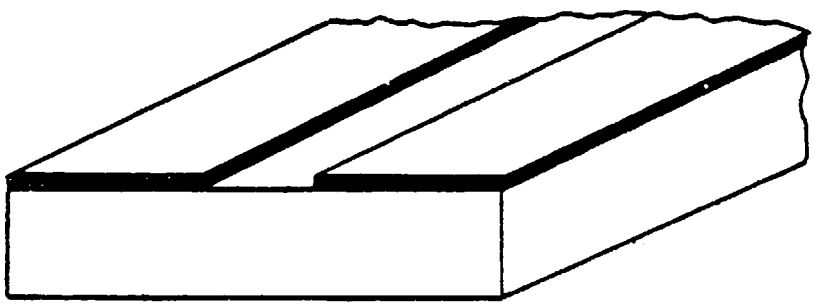

(c)

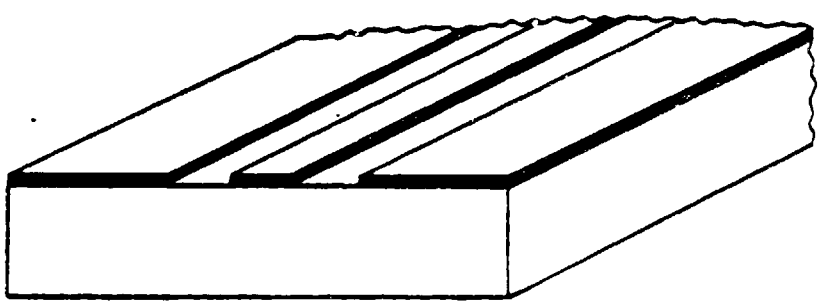

(d)

Fig. 4.1 Various Types of Microwave Integrated Circuits, (a) Stripline, (b) Microstrip, (c) Slot Line, (d) Coplanar Waveguide.

magnetic waves propagete along the line in two regions with different dielectric constant, i. e., in the substrate with a dielectric constant equal to ϵ_r, and in the air with a dielectric constant equal to 1. In such a composite structure, the concept of effective dielectric constant is quite useful. The effective dielectric constant is a weighted mean of the dielectric constants of the two regions, and has a value in the range from ϵ_r to 1. If the substrate and the air are both replaced by a material with a dielectric constant equal to the effective dielectric constant, the capacitance between the center strip and the ground plane remains unchanged.

From basic electromagnetic theory, it is obvious that a transverse electromagnetic (TEM) wave can not exist in this structure since the wave velocity in the substrate is different from that in the air. In fact, one can show that not even the pure transverse electric (TE) or transverse magnetic (TM) waves can exist alone in the structure, but that it can only support a hybrid mode in which both the longitudinal electric and magnetic components are non-zero [60]. The effective dielectric constant therefore is dispersive, or frequency-dependent.

In microstrip analysis, two different approaches are usually taken. In the "quasi-TEM" analysis, the structure is assumed to support a TEM wave. The problem then is reduced to one of determining the electrostatic potential from a two-dimensional Laplace's equation with proper boundary conditions. Various techniques have been used to solve this problem. These include the conformal mapping method by Wheeler [61], the finite-

element method (relaxation method) by Stinehelfer [62], the moment method by Adams [63], and the variational method by Yamasita and Mittra [64]. Dispersion effects are accounted by separate equations, often obtained empirically. In the "wave theory" analysis, the dispersion effects are calculated directly from a hybrid mode analysis of the structure. Various analytical techniques have also been used in this problem [65][66][67].

Most of the analytical techniques mentioned above require lengthy computation that is generally reserved for a digital computer. No attempt to review these techniques will be made here. Instead, analytical and synthetic equations by Wheeler [61] and Schneider [68], with extension by Hammerstad [69], will be introduced. These equations are in closed forms, and thus are suitable for computer-aided designs.

The effective dielectric constant, ϵ_{eff}, of a microstrip with width W, and substrate thickness H, is given by

$$\epsilon_{eff} = 0.5(\epsilon_r + 1) + 0.5(\epsilon_r - 1)/(1 + 12H/W)^{1/2} \qquad (4.1)$$

for the case of $W/H \geq 1$, and

$$\epsilon_{eff} = 0.5(\epsilon_r + 1) + 0.5(\epsilon_r - 1)[(1 + 12H/W)^{-1/2} + 0.04(1 - W/H)^2] \qquad (4.2)$$

for the case of $W/H \leq 1$. The characteristic impedance Z_o is given as

$$Z_o = \frac{60}{\sqrt{\epsilon_{eff}}} \ln(8H/W + W/4H) \qquad (4.3)$$

for $W/H \leq 1$, and

$$Z_o = \frac{376.73}{\sqrt{\epsilon_{eff}}}[W/H + 1.393 + 0.667 \ln(W/H + 1.444)]^{-1} \qquad (4.4)$$

for $W/H \geq 1$.

For the purposes of synthesis, W/H can be expressed in terms of desired characteristic impedace Z_o. For $W/H \leq 2$,

$$W/H = \frac{8}{\exp(A) - 2\exp(-A)} \qquad (4.5)$$

and for $W/H \geq 2$,

$$W/H = \frac{2}{\pi}\{B - 1 - \ln(2B - 1) + \frac{\epsilon_r - 1}{2\epsilon_r}[\ln(B - 1) + 0.39 - 0.61/\epsilon_r]\} \qquad (4.6)$$

where

$$A = \frac{Z_o}{120}\sqrt{2(\epsilon_r + 1)} + \frac{\epsilon_r - 1}{\epsilon_r + 1}(0.23 + 0.11/\epsilon_r) \qquad (4.7)$$

and

$$B = \frac{591.766}{\sqrt{\epsilon_r}\, Z_o} \qquad (4.8)$$

Values of characteristic impedance and effective dielectric constant calculated from Eqs.4.1-4.4 are plotted in Fig. 4.2 for several dielectric materials, namely, Duroid 5880* ($\epsilon_r = 2.22$), fused quartz ($\epsilon_r = 3.82$), and alumina ($\epsilon_r = 9.0$).

---

* Trade name for a non-woven glass microfiber-reinforced polytetrafluoroethylene (PTFE) structure made by Rogers Corp., Chandler, Arizona.

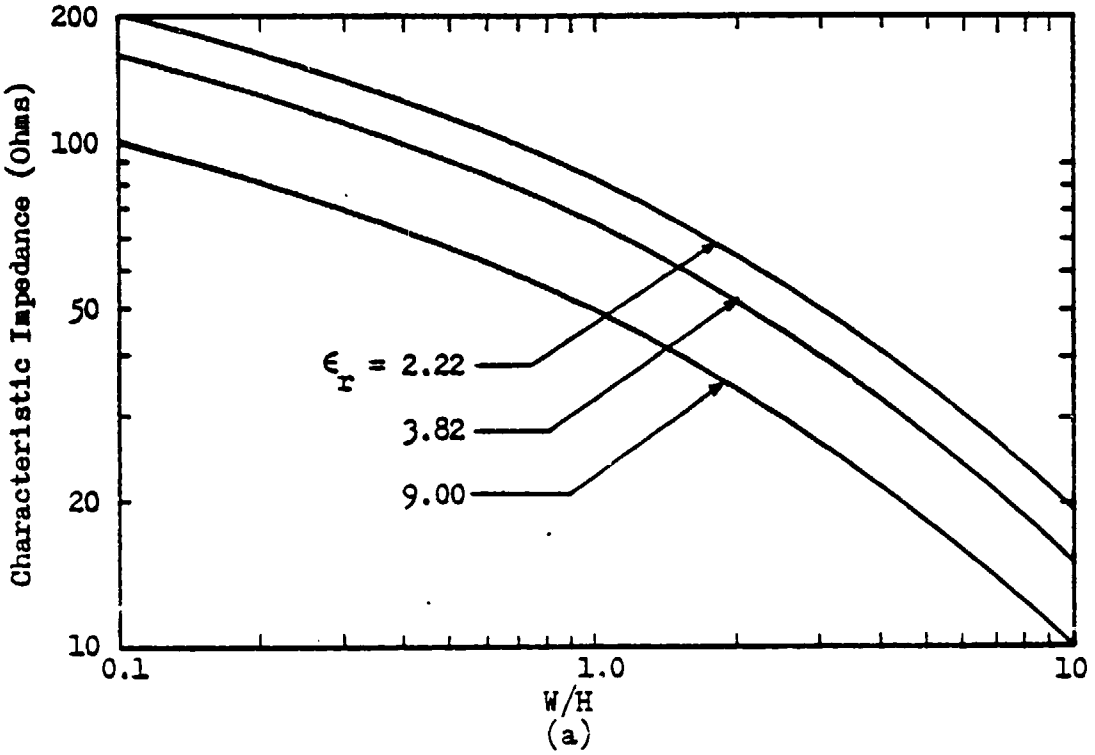
200
100
50
20
10
Characteristic Impedance (Ohms)
ϵ_r = 2.22
3.82
9.00
0.1
1.0
10
W/H

(a)

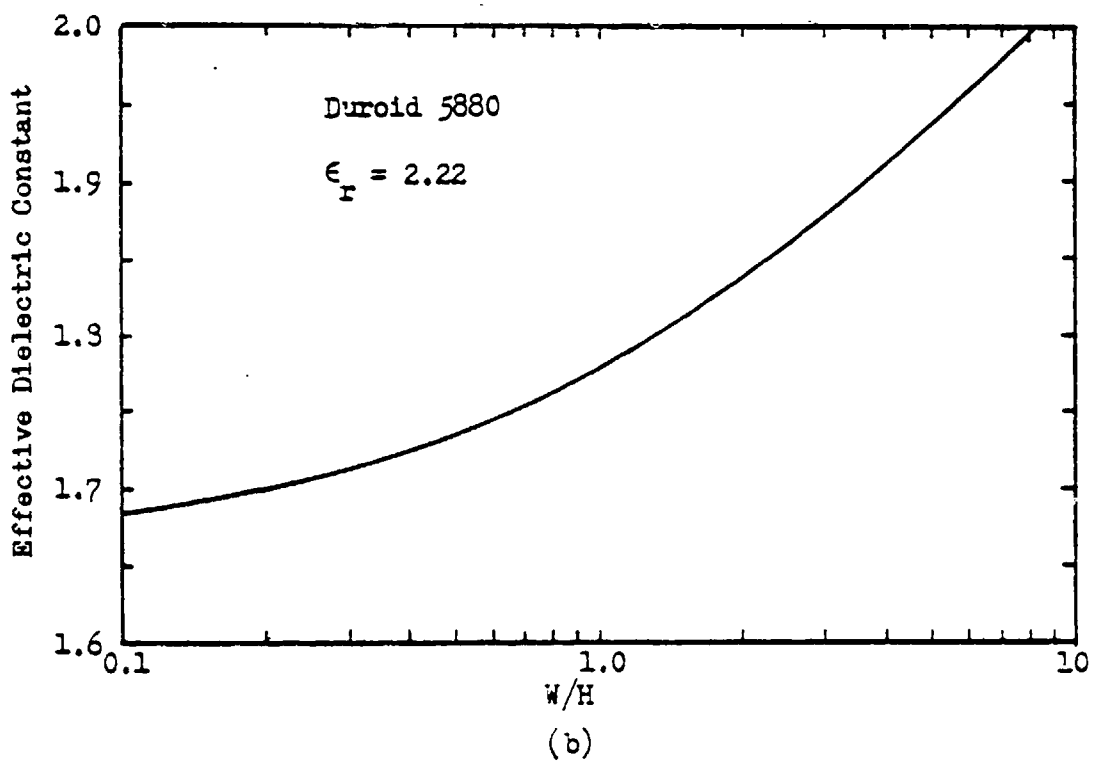
2.0
1.9
1.8
1.7
1.6
Effective Dielectric Constant
Duroid 5880
ϵ_r = 2.22
0.1
1.0
10
W/H

(b)

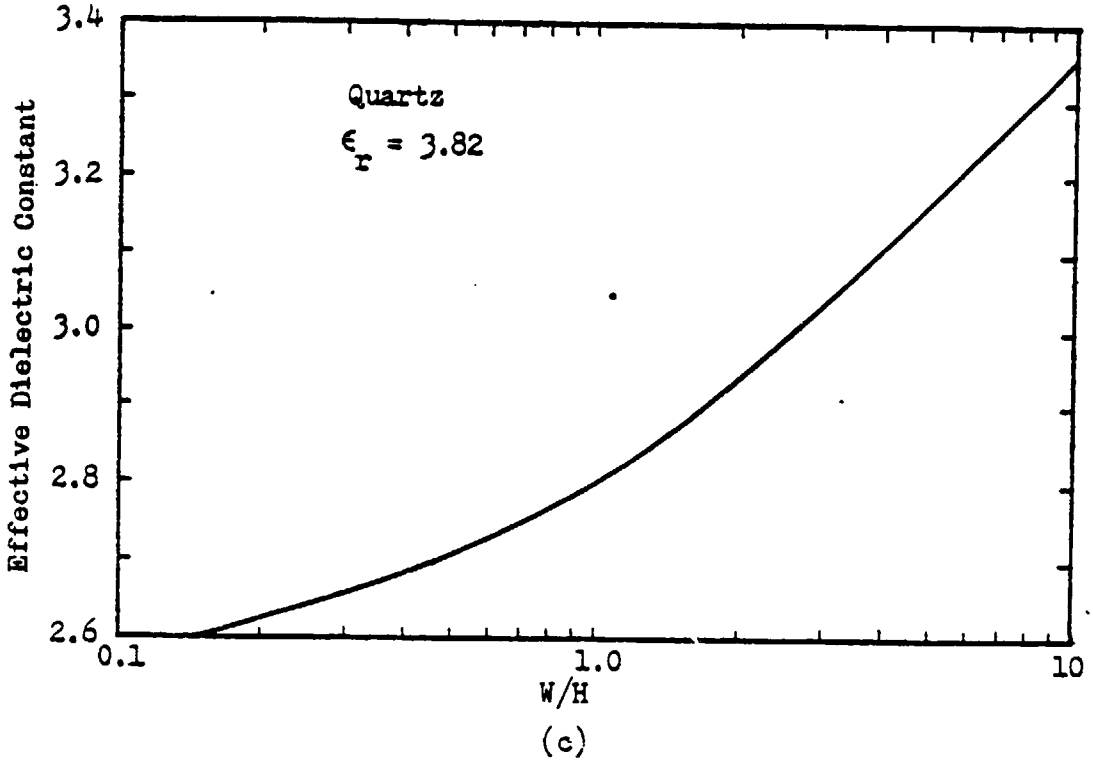

(c)

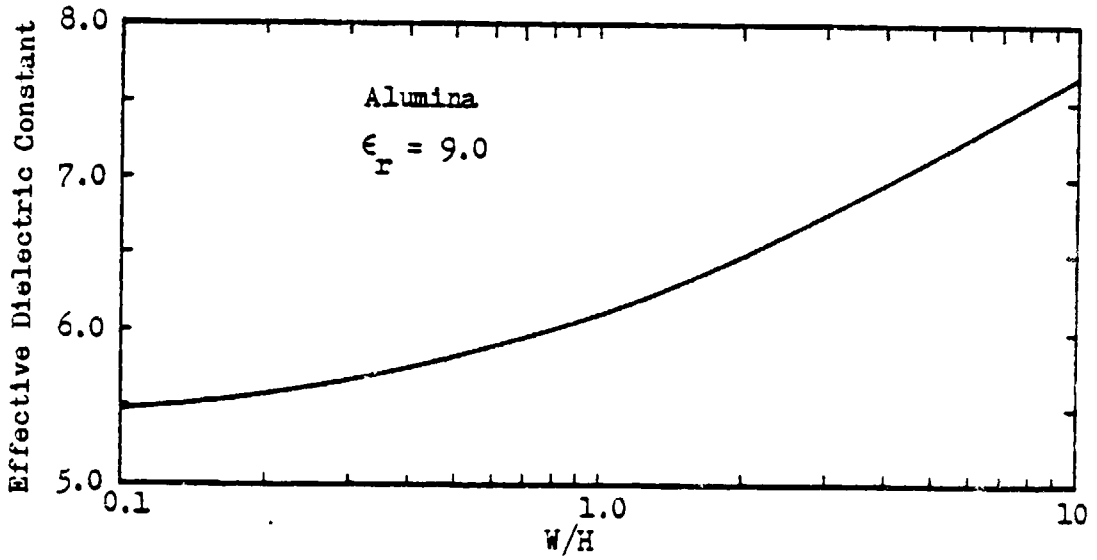

(d)

Fig. 4.2 Characteristic Impedance(a), and Effective Dielectric Constant(b),(c), and (d) as a Function of W/H.

An ingenious empirical equation has been developed by Schneider [70] to describe the dispersion effects. The normalized phase velocity is expressed as

$$v_p = \frac{\lambda_g}{\lambda_o} = \frac{1}{\sqrt{\epsilon_r \epsilon_{eff}}} \frac{\sqrt{\epsilon_{eff}}\, f_n^2 + \sqrt{\epsilon_r}}{f_n^2 + 1} \tag{4.9}$$

where

$$f_n = \frac{4H\sqrt{\epsilon_r - 1}}{\lambda_o} \tag{4.10}$$

and λ_g and λ_o are the microstrip and the free-space wavelengths, respectively. Graphical plots for the normalized phase velocity are shown in Fig. 4.3. It is evident that, for the same W/H ratio, the dispersion effect is more profound for a substrate with a higher dielectric constant.

4.2.2 Conductor and Dielectric Losses. The losses in microstrip lines are due to the finite resistivity of the center and ground conductors as well as the dissipation in the dielectric substrate. The attenuation constant α can be expressed as [72],

$$\alpha = \frac{P_c + P_d}{2P} \tag{4.11}$$

where P_c and P_d are the powers dissipated in the conductors and the dielectric substrate, respectively, and P is the power transmitted along the line. Letting $\alpha = \alpha_c + \alpha_d$, then

$$\alpha_c = \frac{P_c}{2P} \tag{4.12}$$

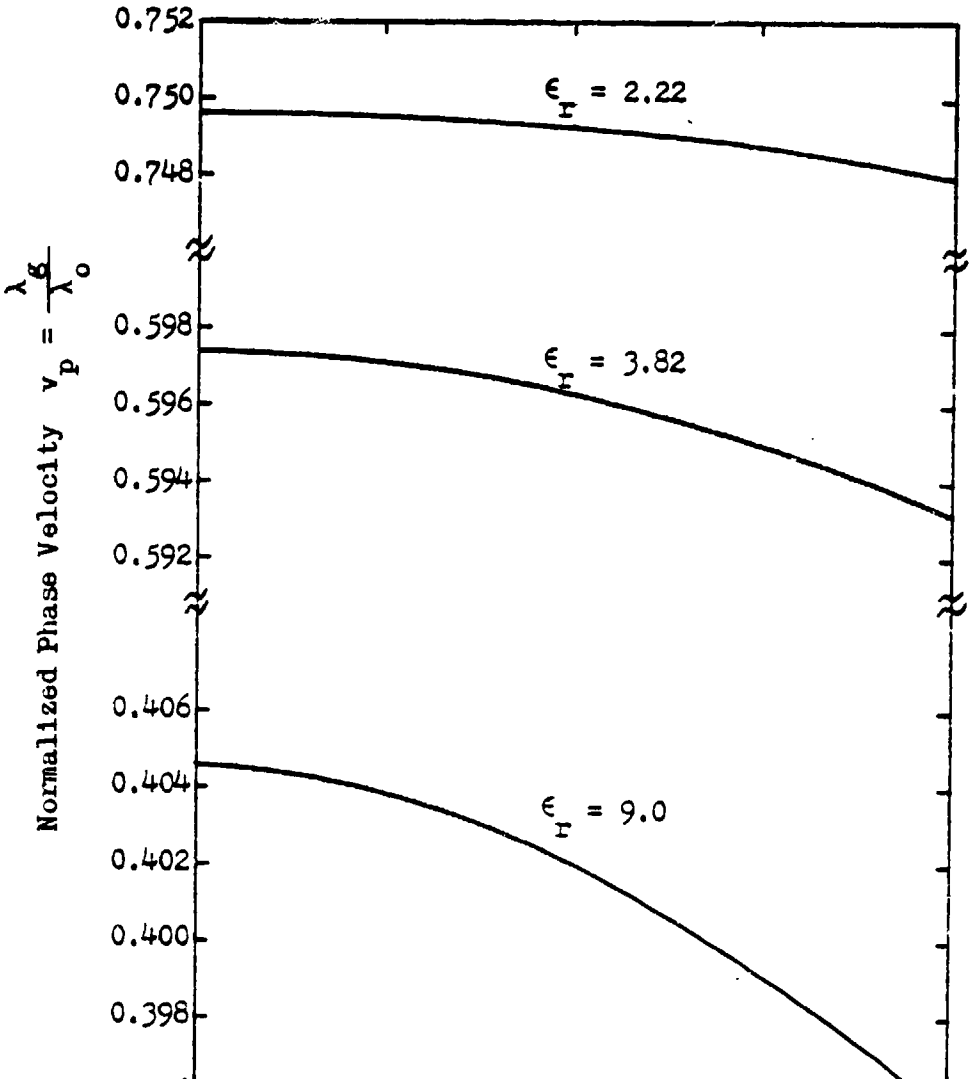

Fig. 4.3 Microstrip Dispersion Effect, H = 0.508 mm, W/H = 1.

and

$$\alpha_d = \frac{P_d}{2P} \tag{4.13}$$

If the surface current density distributions on the strip conductor and the ground plane are known, Eq. 4.12 can be written as

$$\alpha_c = \frac{R_{s1}}{2Z_o} \int \frac{|J_1(x)|^2}{|I|^2}\, dx + \frac{R_{s2}}{2Z_o} \int \frac{|J_2(x)|^2}{|I|^2}\, dx \tag{4.14}$$

where $R_{s1} = (\pi f \mu_1 \rho_1)^{1/2}$ and $R_{s2} = (\pi f \mu_2 \rho_2)^{1/2}$ denote the surface skin resistivity in ohms per sqaure for the strip conductor and the ground plane, respectively, $J_1(x)$ and $J_2(x)$ the corresponding surface current densities, and I the total current per conductor. The quantities μ_1, μ_2 and ρ_1, ρ_2 represent the permeability and bulk resistivity of center and ground conductors, respectively, and f denotes the operating frequency. The first integral is around the periphery of the center conductor, and the second integral is over the entire ground plane. Using a technique based on the so-called "incremental inductance rule" [71], Pucel et al. [72] were able to derive a set of approximate equations for various linewidths. Assuming $R_{s1} = R_{s2}$, the normalized conductor attenuation constant is, for $W/H \leq 1/2\pi$,

$$\frac{\alpha_c Z_o H}{R_{s1}} = \frac{8.686}{2\pi}\left[1 - (W'/4H)^2\right]\left[1 + H/W' + \frac{H}{W'}\left(\ln\frac{4W}{t} + \frac{t}{W}\right)\right] \tag{4.15a}$$

for $1/2\pi \leq W/H \leq 2$,

$$\frac{\alpha_c Z_o H}{R_{sl}} = \frac{8.686}{2\pi}[1 - (W'/4H)^2]\,[1 + H/W' + \frac{H}{W'}(\ln\frac{2H}{t} - \frac{t}{H})] \qquad (4.15b)$$

and for $W/H \geq 2$,

$$\frac{\alpha_c Z_o H}{R_{sl}} = \frac{8.686}{\{W'/H + 0.637\ln[2\pi e(W'/2H + 0.94)]\}^2}[\frac{W'}{H} + \frac{W'/H}{W'/2H + 0.94}]$$

$$[1 + \frac{H}{W'} + \frac{H}{W'}(\ln\frac{2H}{t} + \frac{t}{H})] \qquad (4.15c)$$

where $e = 2.71828....$ is the base of natural, or Naperian logarithm, and t denotes the thickness of the strip conductor. The attenuation constant α_c is in dB/cm. The effective linewidth W' is given by [61],

$$W' = W + \frac{t}{\pi}(\ln\frac{4\pi W}{t} + 1) \qquad (4.16a)$$

for $W/H \leq 1/2\pi$, and

$$W' = W + \frac{t}{\pi}(\ln\frac{2H}{t} + 1) \qquad (4.16b)$$

for $W/H \geq 1/2\pi$. Figure 4.4 shows plots of the normalized conductor attenuation constant versus W/H for several t/H values, calculated using Eq. 4.15.

To calculate the dielectric attenuation constant α_d, Eq. 4.13 can be shown to equal to

$$\alpha_d = \frac{\sigma \iint E^2\, ds}{2V^2/Z_o} \qquad (4.17)$$

92. Dell-Imagine, R. A., "A Parallel Coupled Microstrip Filter Design Procedure," G-MTT 1970 Int. Microwave Symp. Digest, pp. 29-32.

93. Childs, W. H., "Design Techniques for Bandpass Filters Using Edge-Coupled Microstrip Lines on Fused Silica," G-MTT 1976 Int. Microwave Symp. Digest, pp. 194-196.

94. Microwave Engineers' Handbook and Buyers' Guide, Horizon House, Dedham, Mass., 1974.

95. Cisco, T. C., Design of Microstrip Components by Computer, Tech. Report NASA-CR-1982, March 1972.

96. Kaupe, A. F., Jr., "Algorithm 178: Direct Search," Commun. ACM, Vol. 6, pp. 313-314, June 1963.

97. Bell, M., and Pike, M. C., "Remark on 'Algorithm 178: Direct Search,'" Commun. ACM, Vol. 9, pp. 684-685, September 1966.

98. Emery, F. E., and O'Hagen, M., "Optimal Design of Matching Networks for Microwave Transistor Amplifiers," IEEE Trans. on Microwave Theory and Techniques, Vol. MTT-14, pp. 696-698, December 1966.

99. Bandler, J. W., and Macdonald, P. A., "Optimization of Microwave Networks by Razor Search," IEEE Trans. on Microwave Theory and Techniques, Vol. MTT-17, pp. 552-562, August 1969.

100. Denlinger, E. J., et al., "Microstrip Varactor-Tuned Millimeter-Wave IMPATT Diode Oscillators," IEEE Trans. on Microwave Theory and Techniques, Vol. MTT-23, pp. 953-958, December 1975.

101. Wu, Y. S., and Rosenbaum, F. J., "Wide-Band Operation of Microstrip Circulators," IEEE Trans. on Microwave Theory and Techniques, Vol. MTT-22, pp. 849-856, October 1974.

102. Branner, G. R., and Chan, S.-P., "A New Technique for Synthesis of Broad-Band Parametric Amplifiers," IEEE Trans. on Microwave Theory and Techniques, Vol. MTT-21, pp. 437-444, July 1973.

103. Getsinger, W. J., "Coupled Rectangular Bars Between Parallel Plates," IRE Trans. on Microwave Theory and Techniques, Vol. MTT-10, pp. 65-72, January 1962.

C-3

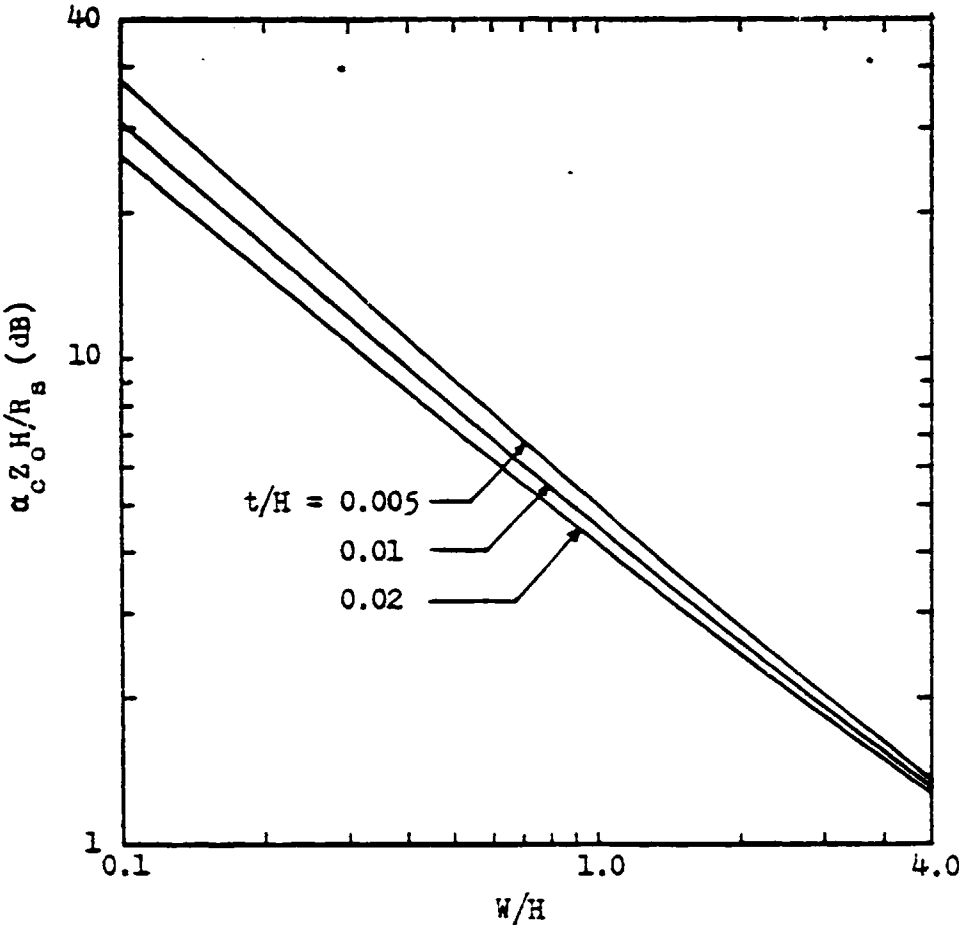

Fig. 4.4 Microstrip Conductor Attenuation Factor as a Function of W/H.

where σ is the conductivity of the dielectric substrate, E is the electric field intensity at any point inside the substrate, and V is the voltage across the center conductor and the ground plane. The double integral is defined over the cross section of the substrate. Simpson and Tseng [73] have developed an efficient numerical algorithm for evaluating Eq. 4.17. The calculated results are in excellent agreement with the experimental data of Hyltin [74]. Table 4.1 gives the normalized dielectric attenuation constant, α_d/σ, for several dielectric constants.

Based on the concept of a "filling factor" defined by Poole [75], Schneider has derived an approximate equation for dielectric attenuation constant [76],

$$\alpha_d \approx 27.3 \frac{q \tan\delta}{\lambda_g} \tag{4.18}$$

where $\tan\delta = \sigma/2\pi f\epsilon_r\epsilon_o$ is the loss tangent of the substrate, and α_d is in dB per unit length. The filling factor q is given by

$$q = \frac{1}{1 + \frac{F - 1}{\epsilon_r(F + 1)}} \tag{4.19}$$

with

$$F = (1 + 10H/W)^{1/2} \tag{4.20}$$

Numerical results calculated from Eq. 4.18 are also given in Table 4.1.

4.3 Discontinuity Effects in Microstrip Lines

4.3.1 Microstrip Open Circuits. In construction of microstrip cir-

Table 4.1 Normalized Dielectric Attenuation Constants

W/H	$\epsilon_r = 2.22$		$\epsilon_r = 3.82$		$\epsilon_r = 9.0$	
	α_{dn}^{*}	α_{dn}^{**}	α_{dn}^{*}	α_{dn}^{**}	α_{dn}^{*}	α_{dn}^{**}
0.4	743.8	743.9	594.6	596.9	405.0	406.8
0.6	760.2	764.3	606.0	611.1	411.9	415.1
0.8	774.7	780.9	616.2	622.6	418.0	421.7
1.0	787.9	794.9	625.5	632.3	423.4	427.4
2.0	836.8	844.9	659.5	666.7	443.3	447.3
3.0	871.2	877.8	683.6	689.2	457.5	460.3
4.0	896.4	902.1	700.8	705.8	467.3	469.8
5.0	916.4	921.1	714.3	718.6	475.1	477.2
6.0	931.1	936.5	724.7	729.0	481.1	483.2

* Results obtained by numerical integration [73].
** Results obtained by approximate equation [76].

cuits, an open circuit is usually realized by simply cutting the strip off square as illustrated in Fig. 4.5(a). The end region of an open circuit formed in this way will store considerably more charge per unit length than the remaining portion of the line. Thus, the end effect can be represented by an equivalent capacitance, C_{oc}, as shown in Fig. 4.5(b). This capacitance can be calculated from

$$C_{oc} = \lim_{\ell \to \infty} \frac{1}{2}[\, C(\ell) - \ell C_o] \tag{4.21}$$

where $C(\ell)$ is the total capacitance of the section of length ℓ and width W as shown in Fig. 4.5(a), C_o is the capacitance per unit length of a uniform line of the same width. In actual calculation, ℓ is not infinite, instead, it is equal to some large value beyond which the change in $C(\ell) - \ell C_o$ is negligible.

Alternatively, the end effect can be represented by a length of transmission line that corresponds to the capacitance C_{oc}, as shown in Fig. 4.5(c). The length $\Delta\ell$ may be calculated from

$$\Delta\ell = \frac{C_{oc}}{C_o} \tag{4.22}$$

Many researchers have studied this discontinuity [77][78][79][80][81], and good agreements are usually observed between results calculated from different techniques, and between calculated and measured results. For design purposes, two empirical equations will now be given.

Silvester and Benedek [78] have, in addition to the graphical plots,

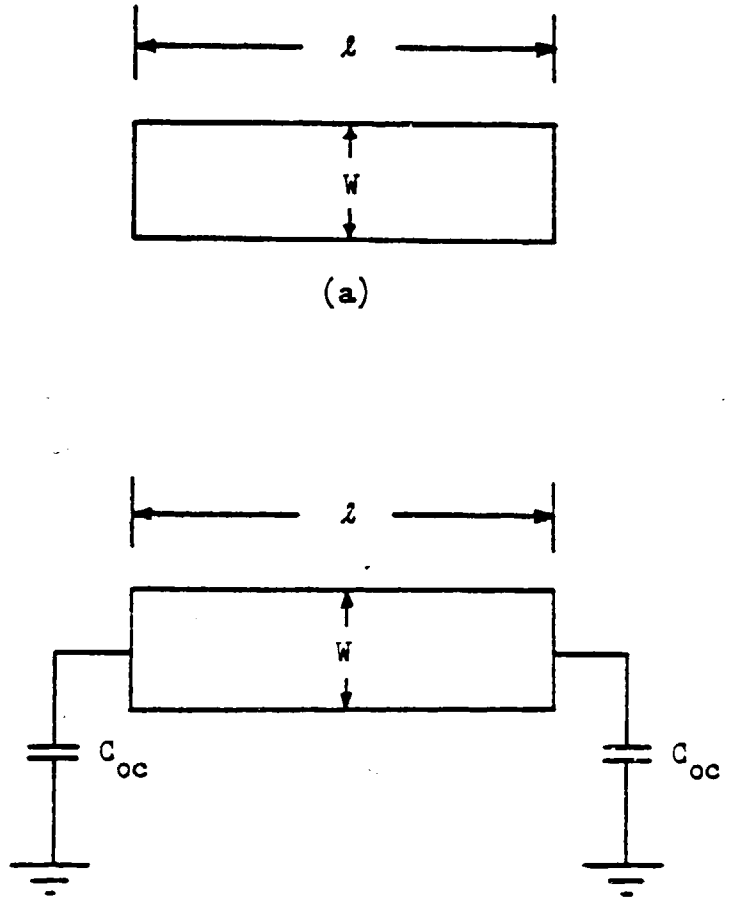

Fig. 4.5 Microstrip Open Circuit Representation.

presented their calculated data for open circuit capacitance by an empirical expression

$$C_{oc} = \exp[2.303 \sum_{k=1}^{5} c_k(\epsilon_r)(\ln\frac{W}{H})^{k-1}] \qquad (4.23)$$

where the coefficients c_k for six different values of ϵ_r are tabulated in Table 4.2.

Hammerstad [69] has found that it is possible to reduce these equations to one valid for all values of ϵ_r by expressing the capacitance in terms of an equivalent line extension $\Delta\ell$,

$$\frac{\Delta\ell}{H} = 0.412 \frac{\epsilon_{eff} + 0.300}{\epsilon_{eff} - 0.258} \frac{W/H + 0.262}{W/H + 0.813} \qquad (4.24)$$

Table 4.2 Coefficients c_k for Equation 4.23

k	$\epsilon_r = 1.0$	$\epsilon_r = 2.5$	$\epsilon_r = 4.2$	$\epsilon_r = 9.6$	$\epsilon_r = 16$	$\epsilon_r = 51$
1	1.110	1.295	1.443	1.738	1.938	2.403
2	-0.2892	-0.2817	-0.2535	-0.2538	-0.2233	-0.2220
3	0.1815	0.1367	0.1062	0.1308	0.1317	0.2170
4	-0.0033	-0.0133	-0.0260	-0.0087	-0.0267	-0.0240
5	-0.0540	-0.0267	-0.0073	-0.0113	-0.0147	-0.0840

4.3.2 Microstrip T-junctions. The microstrip T-junction, as shown in Fig. 4.6(a), is incorporated in a wide variety of microwave circuits. The characterization of the tee by a direct junction is inadequate since it ignores the equivalent reactances associated with the energy stored in the neighborhood of the junction. Two different models are usually used to represent this discontinuity. In the model shown in Fig. 4.6(b), the T-junction is represented by three series inductances and one shunt capacitance. These equivalent inductances have been investigated by Thomson and Gopinath [82], and the capacitance can be calculated from a numerical technique developed by Silvester and Benedek [83]. However, these computations are extremely time consuming, and thus are not suitable for computer-aided designs.

The second model as depicted in Fig. 4.6(c) was originally developed for stripline T-junction by Franco and Oliner [84], with extensions by Leighton and Milnes [85], Vogel [86], and Hammerstad [69]. The microstrip T-junction is redrawn in Fig. 4.7 to identify the requisite parameters.

In this model, the most important parameter is the stub arm reference displacement, i. e., Δd as indicated in Fig. 4.7. As is evident from the figure, Δd may be calculated from

$$\Delta d = D_1/2 - W_1/2 - d_2' \tag{4.25}$$

where W_1 is the linewidth of the main line, and D_1, d_2' are given by

$$D_1 = \eta_o H/\sqrt{\epsilon_{eff1}}\, Z_1 \tag{4.26}$$

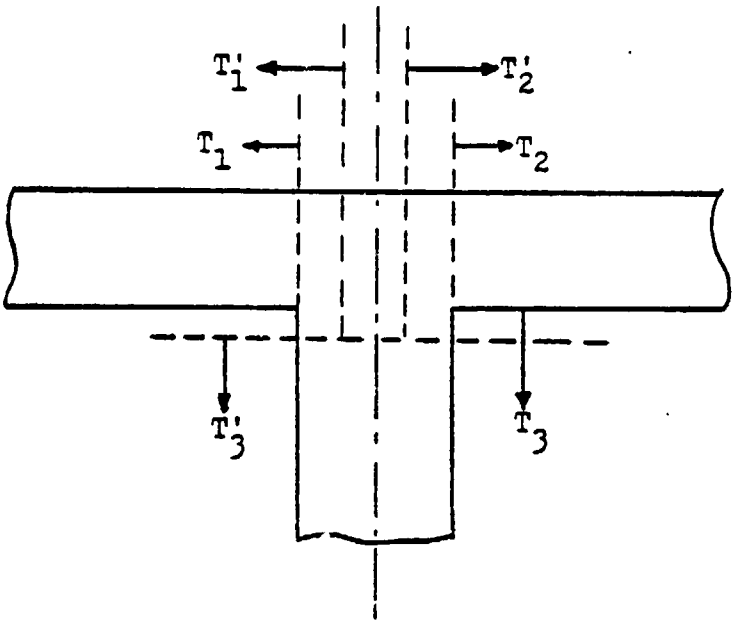

(a)

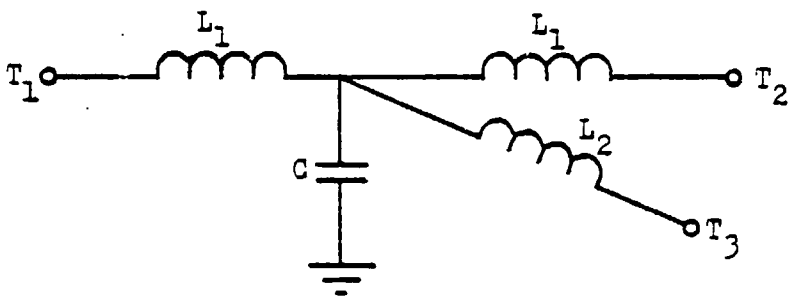

(b)

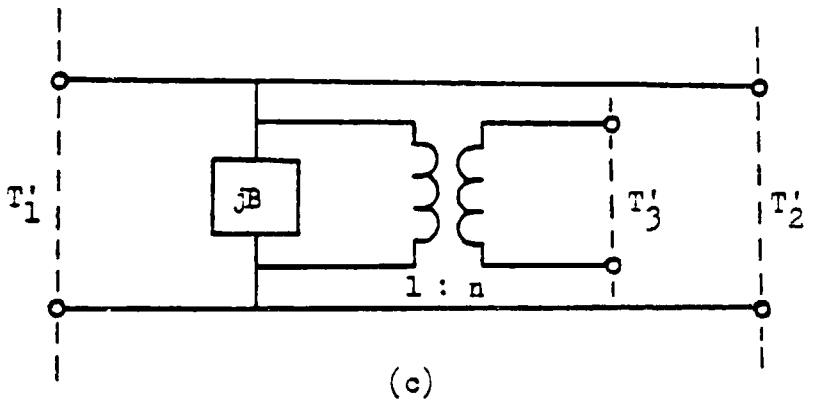

(c)

Fig. 4.6 Microstrip T-Junction Representation.

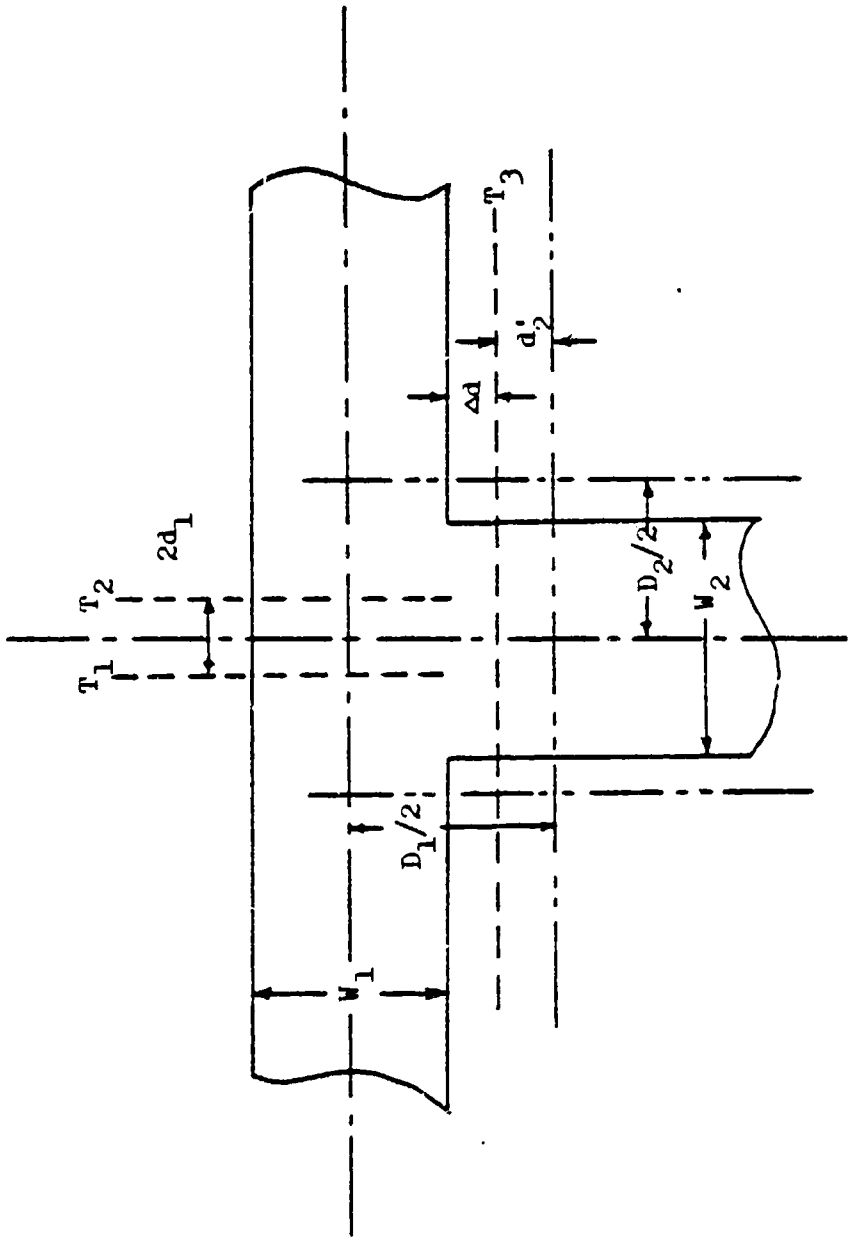

Fig. 4.7 Microstrip T-Junction.

$$d_2' = D_1\left[0.076 + 0.2\left(\frac{2D_1}{\lambda_{g1}}\right)^2 + 0.663\exp\left(\frac{-1.71Z_1}{Z_2}\right) - 0.172\,\ell n\left(\frac{Z_1}{Z_2}\right)\right]\frac{Z_1}{Z_2} \tag{4.27}$$

where Z_1 and Z_2 denote the characteristic impedance of the main line and the stub, respectively, and ϵ_{eff1} the effective dielectric constant, λ_{g1} the wavelength, of the main line. The displacement of the main line reference plane is generally very small, and is given as

$$d_1 = 0.05\, n^2\, D_2\, Z_1/Z_2 \tag{4.28}$$

where

$$D_2 = \eta_o\, H/\sqrt{\epsilon_{eff2}}\, Z_2 \tag{4.29}$$

$$n^2 = \left[\frac{\sin\left(\frac{\pi}{2}\,\frac{2D_1}{\lambda_{g1}}\,\frac{Z_1}{Z_2}\right)}{\frac{\pi}{2}\,\frac{2D_1}{\lambda_{g1}}\,\frac{Z_1}{Z_2}}\right]\cdot\left[1 - \left(\pi\frac{2d_2'}{\lambda_{g1}}\right)^2\right] \tag{4.30}$$

The shunt susceptance, B, can be calculated from

$$B = 2\pi\left(\frac{D_1}{\lambda_{g1}}\right)(2d_1/D_2 - d_2'/D_1)/Z_2 \tag{4.31}$$

this model has been observed to be in fair agreement with experimental results [69].

In a recent paper by Menzel and Wolff [87], the scattering parameters of the T-junction are calculated using a mode-matching procedure. The dynamic effects are included in this model. The discussion on the feasibility of using this model in computer-aided design will be deferred until

Chapter VI.

4.4 Microstrip Parallel-Coupled Band-Pass Filters

Parallel-coupled microstrip lines have been used extensively in the realizations of microwave band-pass filters and directional couplers. This structure, as shown in Fig. 4.8, can simultaneously support two different modes of propagation, namely, even- and odd-modes. In the even-mode propagation, waves in the two strips propagate in the same direction; while in the odd-mode propagation, waves propagate in the opposite directions. Thus, there are four parameters associated with this structure, namely, the even- and odd-mode characteristic impedances, and the even- and odd-mode effective dielectric constants. These parameters will be denoted by Z_{oe}, Z_{oo}, ϵ_{effe}, and ϵ_{effo}, respectively, and can be calculated by the analytical techniques developed by Bryant and Weiss [88].

A microstrip parallel-coupled band-pass filter consists of a number of resonators each with a length of approximately half-wavelength. Figure 4.9 shows the typical layout of a three-resonator band-pass filter. The analytical techniques and design procedure of this type of filters will now be given.

4.4.1 Analysis of Parallel-Coupled Band-Pass Filters. To facilitate analysis, a single section of parallel-coupled microstrip line is redrawn in Fig. 4.10(a), in which port 1 is connected to the previous section, port 3 is connected to the following section, and ports 2 and 4 are open-

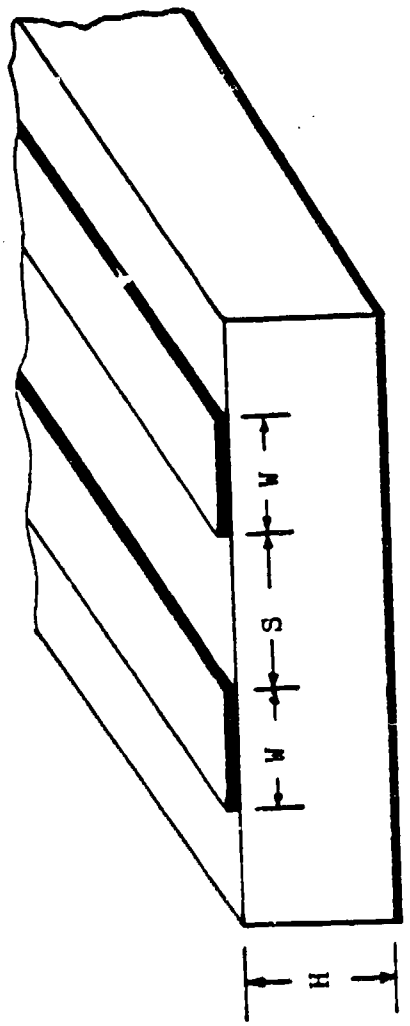

Fig. 4.8 Parallel-Coupled Microstrip Line

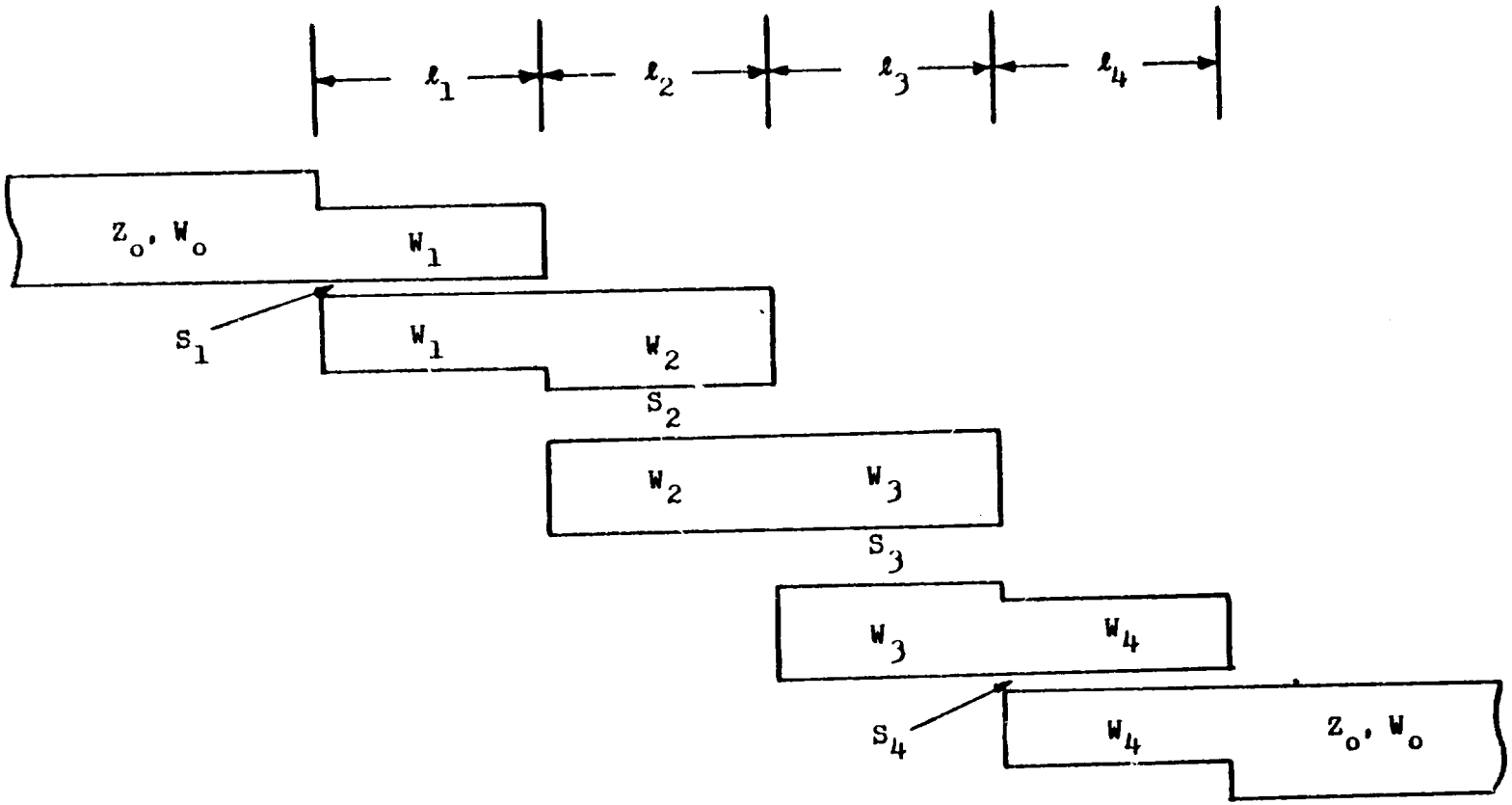

Fig. 4.9 Layout of a Three-Resonator Microstrip Band-Pass Filter

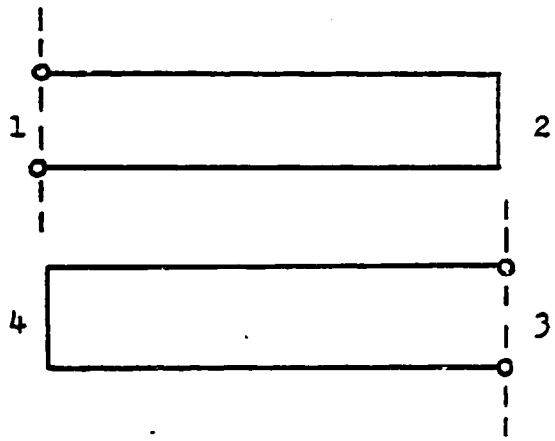

(a)

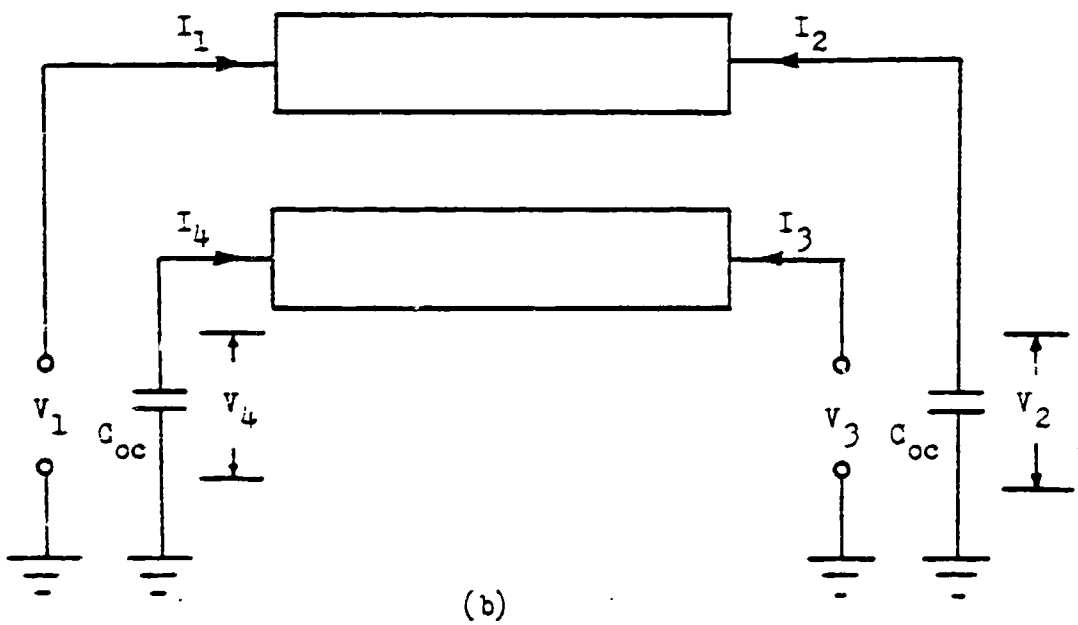

(b)

Fig. 4.10 Circuit for Parallel-Coupled Microstrip line Analysis

circuited. Figure 4.10(b) shows the current and voltage associated with each port together with the open circuit capacitances of ports 2 and 4. The current-voltage relationship of this circuit can be expressed in terms of an impedance matrix,

$$\begin{bmatrix} V_1 \\ V_2 \\ V_3 \\ V_4 \end{bmatrix} = \begin{bmatrix} Z_{11} & Z_{12} & Z_{13} & Z_{14} \\ Z_{21} & Z_{22} & Z_{23} & Z_{24} \\ Z_{31} & Z_{32} & Z_{33} & Z_{34} \\ Z_{41} & Z_{42} & Z_{43} & Z_{44} \end{bmatrix} \begin{bmatrix} I_1 \\ I_2 \\ I_3 \\ I_4 \end{bmatrix} \tag{4.32}$$

where the matrix elements as derived by Zysman and Johnson [89] are given by

$$Z_{11} = Z_{22} = Z_{33} = Z_{44} = Z_1 = \frac{1}{2}\left[\frac{Z_{oe}}{\tanh(\gamma_e \ell)} + \frac{Z_{oo}}{\tanh(\gamma_o \ell)}\right] \tag{4.33a}$$

$$Z_{12} = Z_{21} = Z_{34} = Z_{43} = Z_2 = \frac{1}{2}\left[\frac{Z_{oe}}{\tanh(\gamma_e \ell)} - \frac{Z_{oo}}{\tanh(\gamma_o \ell)}\right] \tag{4.33b}$$

$$Z_{13} = Z_{31} = Z_{24} = Z_{42} = Z_3 = \frac{1}{2}\left[\frac{Z_{oe}}{\sinh(\gamma_e \ell)} - \frac{Z_{oo}}{\sinh(\gamma_o \ell)}\right] \tag{4.33c}$$

$$Z_{14} = Z_{41} = Z_{23} = Z_{32} = Z_4 = \frac{1}{2}\left[\frac{Z_{oe}}{\sinh(\gamma_e \ell)} + \frac{Z_{oo}}{\sinh(\gamma_o \ell)}\right] \tag{4.33d}$$

and γ_e, γ_o are the even- and odd-mode propagation constants, and are given as

$$\gamma_{e(o)} = \alpha_{e(o)} + j\beta_{e(o)} \tag{4.34}$$

The even- and odd-mode attenuation constants, α_e and α_o, can be calculated from Eqs. 4.15 and 4.17 with Z_o replaced by Z_{oe} and Z_{oo}, respectively. The even- and odd-mode phase constants, β_e and β_o, are given by

$$\beta_{e(o)} = \frac{2\pi}{\lambda_{ge(o)}} \tag{4.35}$$

where λ_{ge} and λ_{go} are the even- and odd-mode wavelengths.

The current and voltage relations at ports 2 and 4 are

$$I_2 = -j\omega C_{oc} V_2 \tag{4.36a}$$

$$I_4 = -j\omega C_{oc} V_4 \tag{4.36b}$$

Substitution of Eq. 4.35 into Eq. 4.32 yields (after some lengthy algebraic manipulation),

$$\begin{bmatrix} V_1 \\ V_3 \end{bmatrix} = \begin{bmatrix} Z'_{11} & Z'_{13} \\ Z'_{31} & Z'_{33} \end{bmatrix} \cdot \begin{bmatrix} I_1 \\ I_3 \end{bmatrix} \tag{4.37}$$

where

$$Z'_{11} = Z'_{33} = Z_1 + \frac{(Z_2^2 + Z_4^2)(Z_1 + \frac{1}{j\omega C_{oc}}) - 2Z_2Z_3Z_4}{Z_3^2 - (Z_1 + \frac{1}{j\omega C_{oc}})^2} \tag{4.38a}$$

$$Z'_{13} = Z'_{31} = Z_3 + \frac{2Z_2Z_4(Z_1 + \frac{1}{j\omega C_{oc}}) - Z_3(Z_2^2 + Z_4^2)}{Z_3^2 - (Z_1 + \frac{1}{j\omega C_{oc}})^2} \tag{4.38b}$$

For computer-aided analysis, the impedance matrix is then transformed to an ABCD matrix (see Appendix A),

$$\begin{bmatrix} V_1 \\ I_1 \end{bmatrix} = \begin{bmatrix} A & B \\ C & D \end{bmatrix} \begin{bmatrix} V_3 \\ -I_3 \end{bmatrix} \tag{4.39}$$

where $$A = D = Z'_{11}/Z'_{13} \tag{4.40a}$$

$$B = C = \frac{(Z'_{11})^2 - (Z'_{13})^2}{Z'_{13}} \tag{4.40b}$$

The over-all ABCD matrix for the filter can be readily obtained from the individual matrices. Then the input VSWR, insertion loss, and phase shift can be calculated as follows: Assuming both the source impedance Z_s, and load impedance Z_ℓ are real and positive, the input impedance is given by

$$Z_{IN} = \frac{AZ_\ell + B}{CZ_\ell + D} \tag{4.41}$$

The reflection coefficient is

$$\Gamma = \frac{Z_{IN} - Z_s}{Z_{IN} + Z_s} \tag{4.42}$$

and the input VSWR is

$$S = \frac{1 + |\Gamma|}{1 - |\Gamma|} \tag{4.43}$$

The voltage transmission coefficient is defined as [90],

$$T = T_r + jT_i$$

$$= A + B/Z_\ell + CZ_s + DZ_s/Z_\ell \qquad (4.44)$$

and the insertion loss and phase shift, in terms of T, are

$$L_i = 10 \log(|T|^2 Z_\ell/4Z_s) \qquad (4.45)$$

$$\theta = \arctan(T_i/T_r) \qquad (4.46)$$

where L_i, the insertion loss, is in dB, and θ, the phase shift, is in radian.

4.4.2 Synthesis of Parallel-Coupled Band-Pass Filters. The design procedure was originally developed by Cohn [91] for stripline, and later extended by Dell-Imagine [92] to include microstrip. Cohn has shown that each parallel-coupled section with a length of quarter-wavelength is equivalent to an ideal impedance inverter with quarter-wavelength of line on either side. From this equivalent circuit, the even- and odd-mode characteristic impedances are derived as [91],

$$\frac{Z_{oe}}{Z_o} = 1 + \frac{Z_o}{K} + (\frac{Z_o}{K})^2 \qquad (4.47a)$$

$$\frac{Z_{oo}}{Z_o} = 1 - \frac{Z_o}{K} + (\frac{Z_o}{K})^2 \qquad (4.47b)$$

where Z_o is the terminating impedance (see Fig. 4.9), and K is the impedance of the ideal impedance inverter, and can be calculated from low-pass

prototype elements [91].

The length of each section is given by [92],

$$\ell = \frac{\lambda_o}{4} \frac{Z_{oe} + Z_{oo}}{\sqrt{\epsilon_{effe}}\, Z_{oe} + \sqrt{\epsilon_{effo}}\, Z_{oo}} \qquad (4.48)$$

This procedure usually results, even for filters with moderate bandwidth, in very high Z_{oe} and very low Z_{oo} for the first and the last sections. In terms of physical parameters, this means extremely narrow gaps between strips for these sections, and thus requires a high degree of accuracy in photolithographic techniques. However, it has been determined that more workable parameters can be obtained by slightly perturbing, using computer-aided optimization techniques, the parameters calculated from this design procedure [93].

Using this technique, a four-section Butterworth (maximally-flat) band-pass filter with 8% bandwidth for operation at 5.5 GHz was designed for a Duroid 5880 substrate (H = 0.508 mm). The even- and odd-mode characteristic impedances for each section were first calculated from Cohn's equations. A computer program* was then used to optimize these impedances. The initial and the optimized values are listed in Table 4.3.

---

* This program consists of three subroutines similar to "EPFILT", "DIRECT", and "EXPLOR in Appendix C. See descriptions of these subroutines in Chapter 7.

The width of the first and the last gaps (S_1 and S_4 in Fig. 4.9) is increased from 0.07 mm to 0.11 mm, thus considerably lessening the tolerance requirements imposed on the photolithographic process. The physical dimensions are given in Table 4.4. Calculated and actual responses are plotted in Fig. 4.11. The passband insertion loss was measured to be 0.5 dB at 5.5 GHz as compared to the calculated value of 0.38 dB at the same frequency. The measured 1-dB bandwidth is 430 MHz (5.30-5.73 GHz) as compared to the calculated bandwidth of 460 MHz (5.27-5.73 GHz).

Table 4.4 also gives the dimensions of a 11 GHz band-pass filter with 8% bandwidth. Calculated and measured responses of this filter were also in excellent agreement. The passband insertion loss was approximately 0.7 dB.

Table 4.3 Even- and Odd-Mode Characteristic Impedances for a Butterworth Band-Pass Filter with 8% Bandwidth

Section	Initial Impedances		Optimized Impedances	
	Z_{oe}	Z_{oo}	Z_{oe}	Z_{oo}
1,4	74.01	38.56	70.15	40.84
2,3	54.84	45.95	55.79	46.08

(All impedances in ohms)

Table 4.4 Dimensions of Parallel-Coupled Band-pass Filters

Section	W(mm)	S(mm)	ℓ(mm)*	ℓ(mm)**
1,4	1.23	0.11	9.76	4.77
2,3	1.51	0.64	9.70	4.74

* f_o = 5.5 GHz

** f_o = 11 GHz

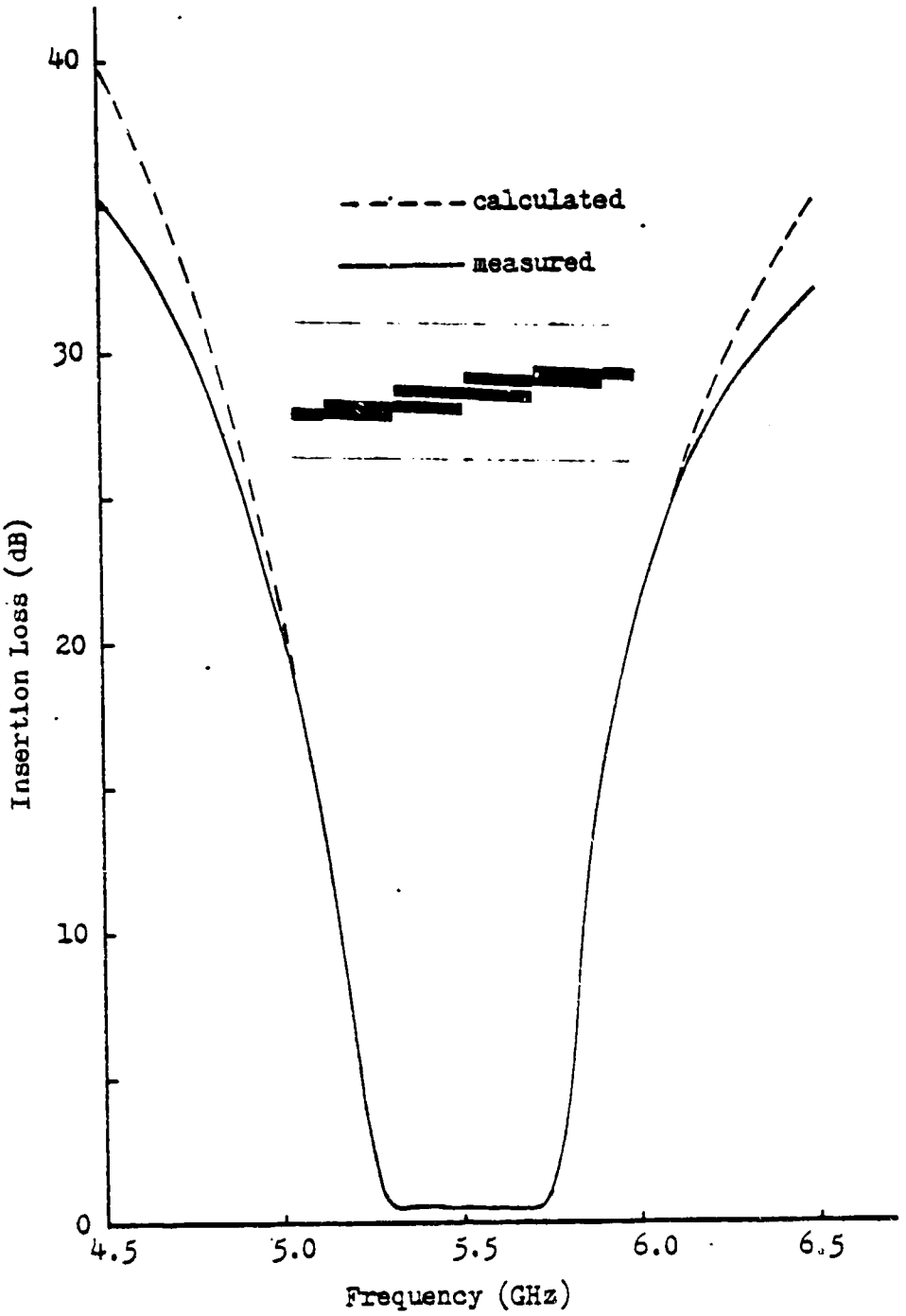

Fig. 4.11 A 5.5 GHz Band-Pass Filter Characteristics

CHAPTER V DESIGN AND REALIZATION OF MIC DEGENERATE AMPLIFIERS

5.1 Description of computer program CADDAC

In recent years, a number of computer-aided design programs have been made available to microwave engineers on time-sharing systems [94]. Large microwave firms have also developed their own package programs that are only available to their design engineers. These programs usually require large computer memory, and are very costly. Moreover, they are general purpose programs which handle mostly passive networks with some including a transistor, and others including a diode as the sole active device.

The computer program CADDAC (Computer-Aided Design of Degenerate Amplifier Circuits) developed in this report is intended primarily for the design of degenerate parametric amplifiers, though it is also useful for certain types of passive networks. It can be readily extended to include nondegenerate amplifiers. Furthermore, with a few minor changes, the program can be run on a mini-computer since it requires very little memory. The source listing of CADDAC, written in FORTRAN language, is given in Appendix C, together with circuit element identification codes and input data card requirements. Similar to that of Cisco[95] in structure, the program consists of the followings:

Main program

Subroutine RESPON

Subroitine BPFILT

Subroutine DIRECT

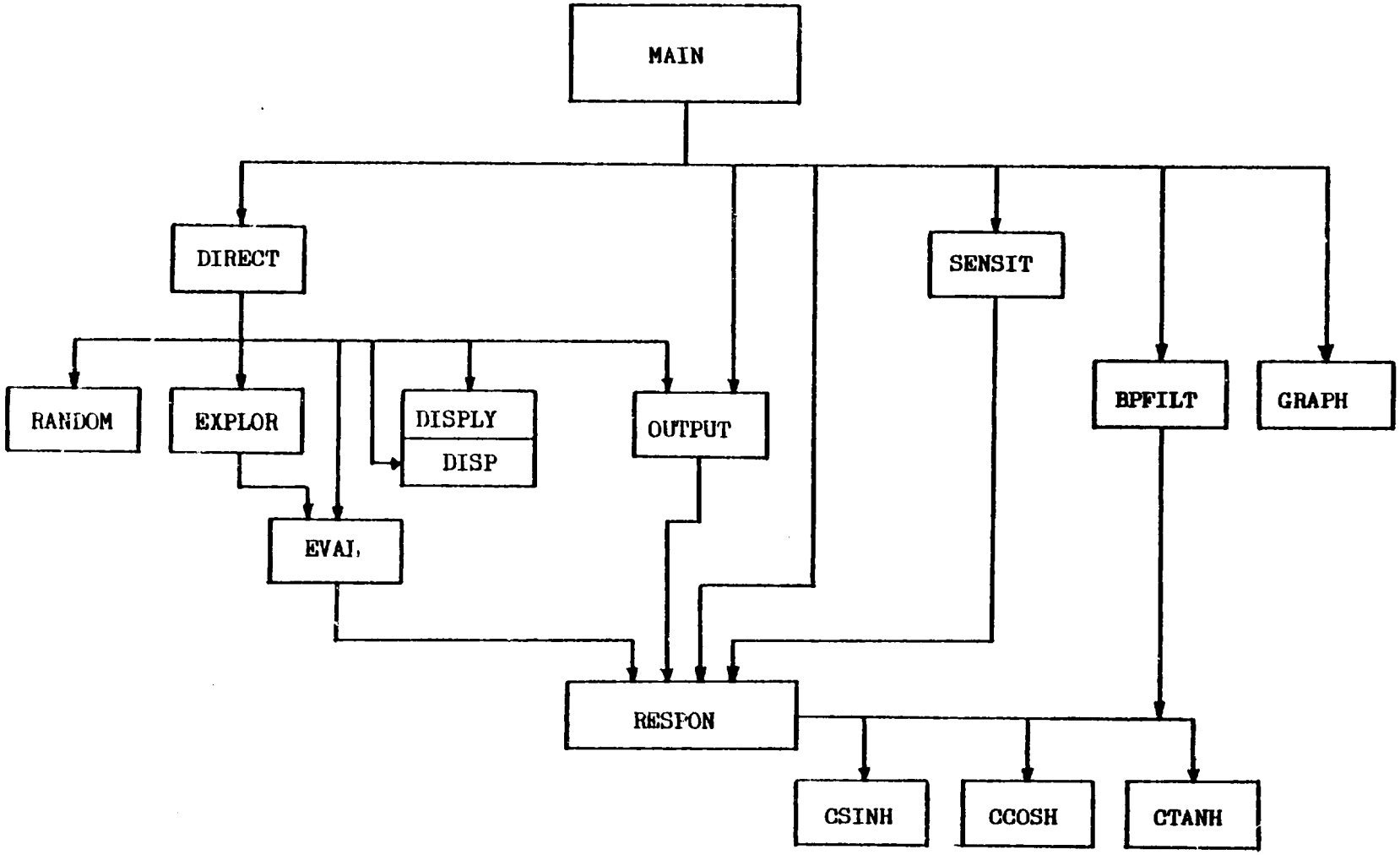

Fig. 5.1 Flow Chart of Program CADDAC

Subroutine EXPLOR

Subroutine RANDOM

Subroutine EVAL

Subroutine GRAPH

Subroutine DISPLY (with entry DISP)

Subroutine OUTPUT

Subroutine SENSIT

Functions CSINH, CCOSH, and CTANH.

The interrelations between these individual programs are illustrated in the flow chart in Fig. 5.1. The arrows are understood to be directed from the calling programs toward the called programs.

Before these programs are explained, a brief review on the basic structure of a computer-aided design program is perhaps in order. Figure 5.2 shows a simplified flow chart of such a program.

The computer reads the circuit topology and initial parameter values, and proceeds to calculate the actual response. Next, a comparison is made between the actual response and the objective function (desired response) from which an error function is generated under certain criteria. At this point, the error is tested to see if it exceeds some prescribed value. If it does, the program goes to the optimization subroutine. The optimization subroutine generates a set of incremental parameter values, which, when added to the previous parameter values, will yield a smaller error. This procedure is iterated until the program is stopped when one of the following conditions occurs:

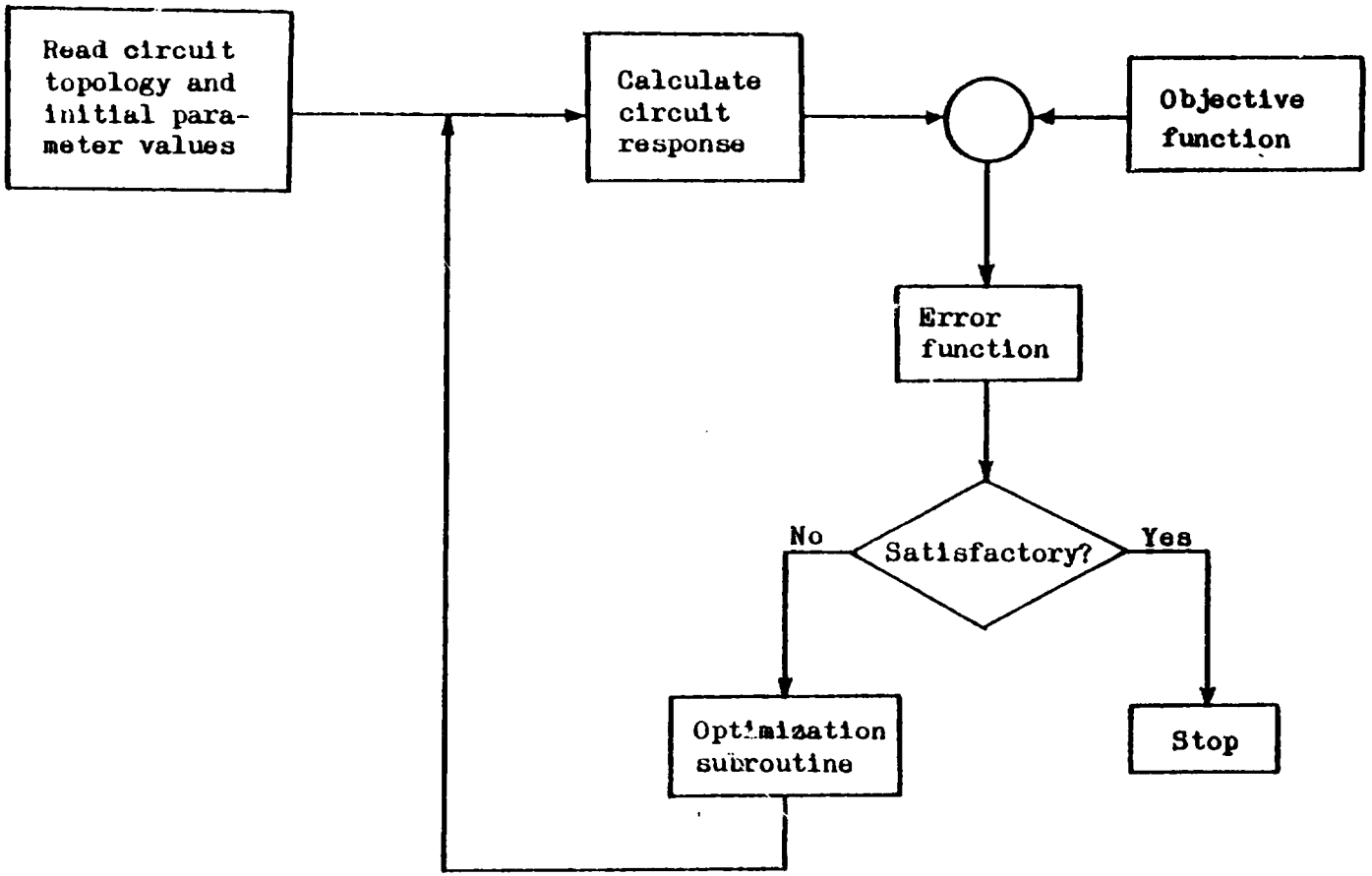

Fig. 5.2 Simplified Flow Chart of a Computer-Aided Design Program

(1) that the error is less than a prescribed value,

(2) that a specified number of iterations is exceeded, or

(3) that an allotted computing time is exceeded.

Returning to program CADDAC, each subprogram will be now described.

5.1.1 Main program. The main program reads all input data which include objective function, frequencies of interest, circuit topology, circuit parameter values, and values of various parameters associated with the optimization procedure. It also decides whether the circuit is to be analyzed or optimized, whether a graph of gain versus frequency is to be plotted, and whether sensitivity analysis is to be performed.

5.1.2 Subroutines RESPON, BPFILT, and functions CSINH, CCOSH, and CTANH. This group of subprograms calculate the circuit response. The three functions calculate values of hyperbolic sine, cosine, and tangent functions with complex arguments.

Subroutine BPFILT calculates the ABCD matrices of the parallel-coupled microstrip band-pass filter at all frequencies of interest according to the equations derived in Section 4.4.1. To avoid repetitive computations, this subroutine is only called by the main program when the existence of a band-pass filter in the circuit is detected. Once the ABCD matrices are calculated, they are stored and made available to subroutine RESPON via a COMMON statement.

Subroutine RESPON calculates transducer power gain according to the equations derived in Section 3.4.1. Algorithm for noise figure calculations is not included. However, with the equations derived in Section

3.4.2, the implementation should be a straightforward matter.

5.1.3 Subroutines RANDOM, EVAL, DIRECT, and EXPLOR. This group of subroutines performs the optimization procedure and thus can be considered as the backbone of this program.

Subroutine RANDOM is a random number generator.

Subroutine EVAL evaluates the error between the objective function and the calculated response. In CADDAC, the error is defined as

$$\text{ERROR} = (E)^{1/2}/(\text{NFP}) \tag{5.1}$$

where NFP is the number of frequency points, and E is calculated from

$$E = \sum_{k=1}^{\text{NFP}} \left[G_t(f_k)_{\text{cal.}} - G_t(f_k)_{\text{obj.}} \right]^2 \tag{5.2}$$

Subroutines DIRECT and EXPLOR employ an improved "direct search" method to perform circuit optimization. Algorithms [96][97] for the original direct search method developed by Hooke and Jeeves [34] are available, and modified methods such as "spider search" [98], "razor search" [99] have also been published. The algorithm used in CADDAC, when compared with others, has been observed to reduce the computing time considerably.

Basically, the direct search consists of two major moves, namely, the exploratory move and the pattern move. At the beginning, initial values are assigned to N circuit parameters which are to be optimized,

and error is evaluated at this set of parameter values (called "basepoint" in direct search). Next an exploratory move is made. The exploratory move varies the value of each parameter by some small amount (called "step size"), and observes the effect of each of these variations on the error function. Those that reduce the error are retained. After the exploratory move is completed, certain parameters are increased, others decreased, and still others remain unchanged.

A "vector" in the N-dimensional hyperspace can be defined as the difference between the new and the initial set of parameter values. A move in the direction of this vector is then attempted. This move is called a pattern move. If the pattern move is successful in reducing the error, a move in the same direction with larger step size is taken. and so on, until failure occurs. Upon the failure of a pattern move, the last "good" point is established as the new basepoint from which another exploratory move is conducted to determine the new direction for pattern moves. If this exploratory move also fails, the step size is reduced, and the whole process is repeated. The optimization process is terminated when the step size is smaller than a prescribed minimum step size. The flow charts in Fige. 5.3 and 5.4 outline subroutines DIRECT and EXPLOR, respectively.

A number of features that are not shown in the flow charts will now be described:

(1) Both the exploratory and the pattern moves are restricted within a certain range imposed by parameter constraints. This is necessary for,

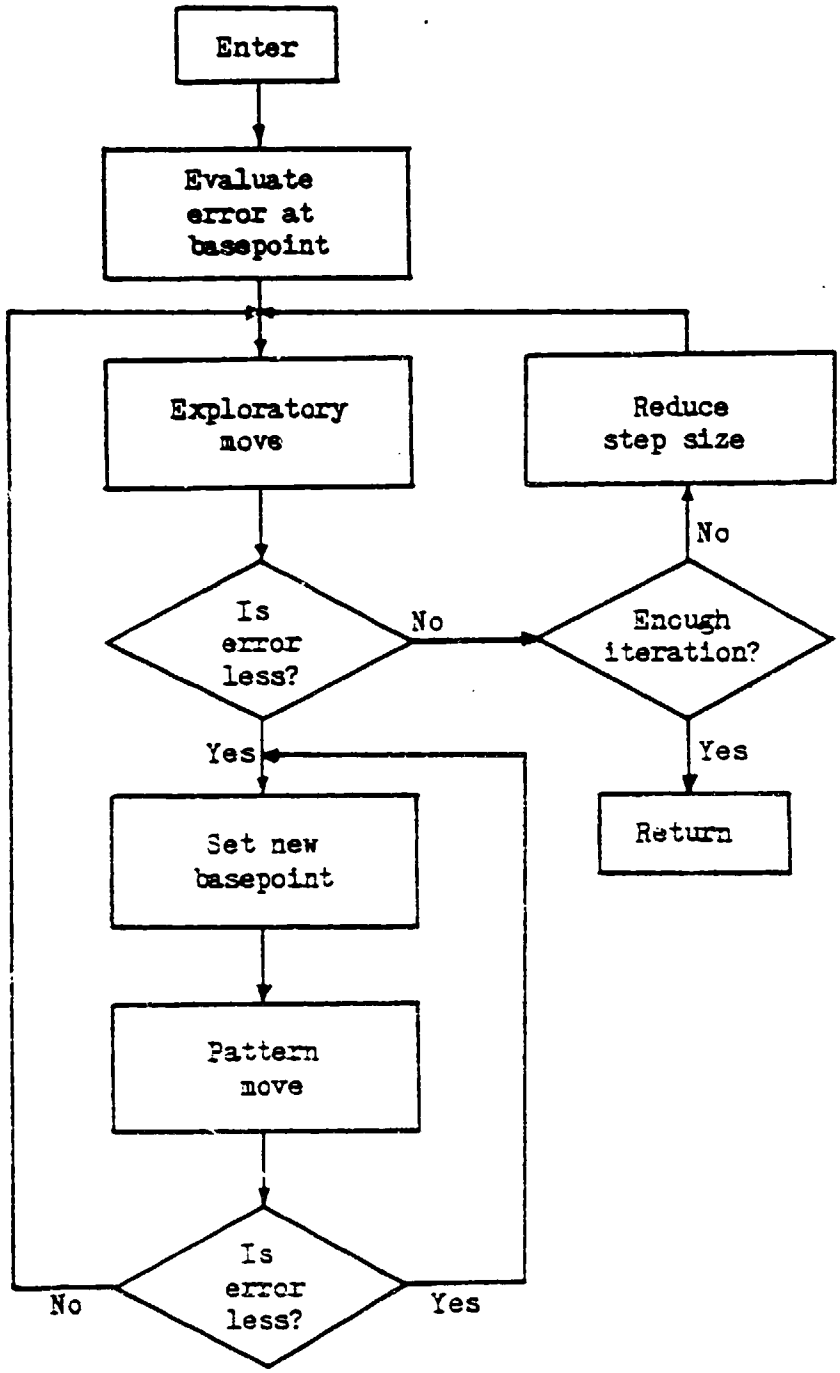

Fig. 5.3 Flow Chart of Subroutine DIRECT

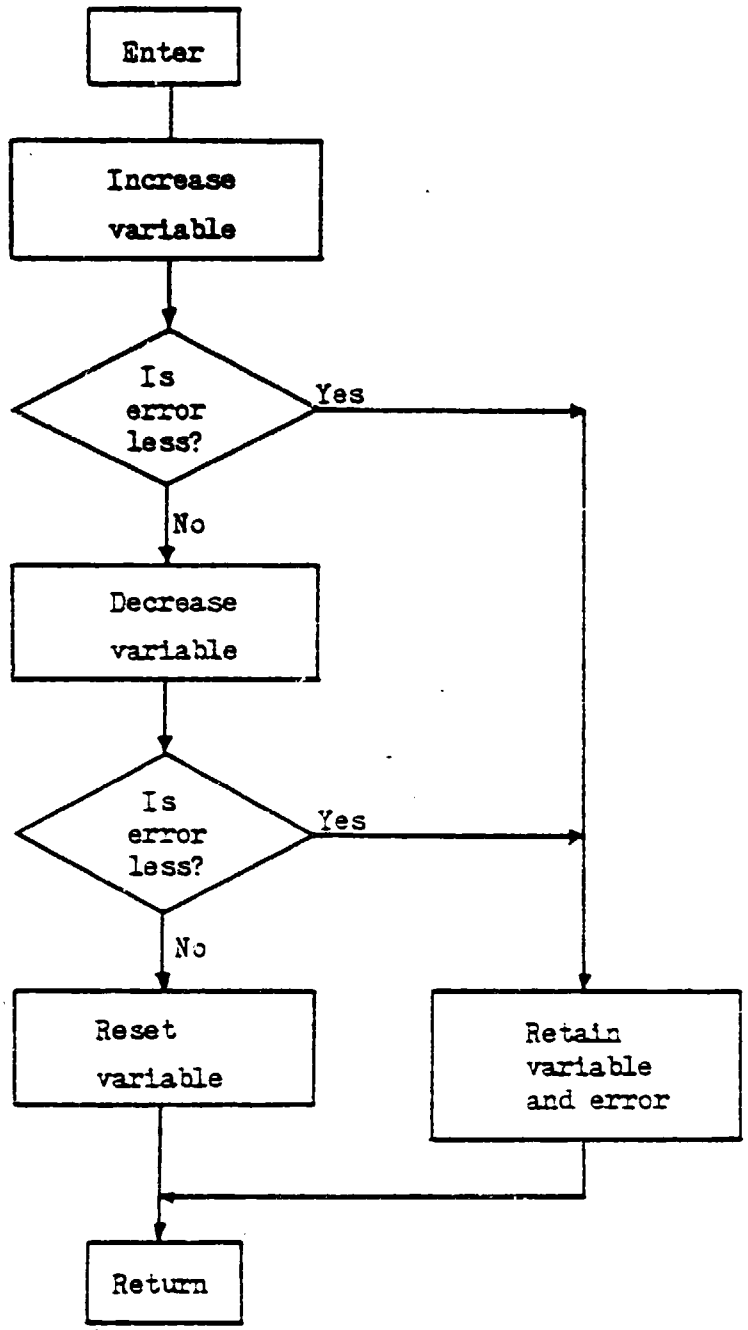

Fig. 5.4 Flow Chart of Subroutine EXPLOR

otherwise, certain parameters may acquire values that are physically meaningless, such as negative lengths, or values that are physically meaningful, but are difficult to be realized in practice.

(2) An accelerating factor is included in making the pattern moves, i. e., each new move is always larger than the previous move in step size.

(3) In subroutine DIRECT, after an optimization process is terminated when the step size smaller than a prescribed minimum value, it can be restarted from a new basepoint generated randomly by subroutine RANDOM. This can be repeated as many times as the user wishes.

(4) The flow chart in Fig. 5.4 only indicates the exploratory move for one parameter. Actually, each time subroutine EXPLOR is called, all N parameters are explored at once. This is easily accomplished by a DO-loop.

5.1.4 Subroutine SENSIT. The effect on transducer power gain by the variation of a parameter X is called the gain sensitivity with respect to parameter X, $S_X^{G_t}$, and is given by

$$S_X^{G_t} = \lim_{\Delta x \to 0} \frac{\Delta G_t / G_t}{\Delta x / x} = \frac{x}{G_t} \cdot \frac{\partial G_t}{\partial x} \qquad (5.3)$$

where x is the nominal value of parameter X. In subroutine SENSIT, which performs sensitivity analysis, the partial differentiation is carried out numerically by

$$\frac{\partial G_t}{\partial x} = \frac{G_t\big|_x - G_t\big|_{x + \Delta x}}{\Delta x} \qquad (5.4a)$$

or

$$\frac{\partial G_t}{\partial x} = \frac{G_t\big|_x - G_t\big|_{x - \Delta x}}{\Delta x} \qquad (5.4b)$$

...ere Δx is taken to be 2% of the nominal parameter value. The calculated sensitivities are expressed in terms of percentage gain variation with respect to one per cent variation in nominal parameter value.

5.1.5 Subroutines GRAPH, DISPLY, and OUTPUT. This group of subroutines does most of the printouts.

Subroutine GRAPH plots the gain versus frequency. response

Subroutine DISPLY prints out optimized parameter values, number of iterations, number of functions evaluated, and error. Entry DISP prints out new basepoint.

Subroutine OUTPUT tabulates the gain versus frequency response.

5.2 Design Examples

Figure 5.5 shows the basic circuit topology chosen for degenerate amplifiers to be designed by CADDAC. Quarter-wavelength open-circuited transmission lines are placed in shunt one quarter-wavelength behind the diode at both the pump and the signal frequencies. These lines are intended to block pump frequency power from reaching the signal output port, and the signal frequency power from reaching the pump port. The combined insertion losses of these lines together with the respective band-pass filters were measured to be nearly 45 dB at the signal output port for pump frequency power, and in excess of 50 dB at pump port for

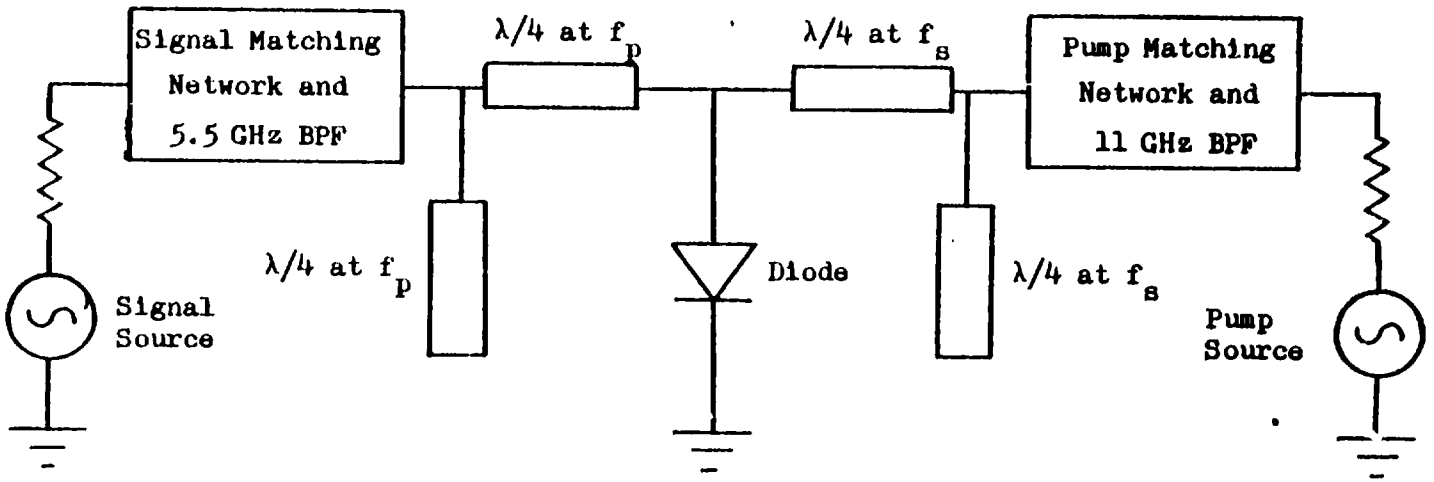

Fig. 5.5 Basic Circuit Topology for MIC Degenerate Amplifiers

signal frequency power. They also provide a very high impedance in parallel with the diode at the respective frequencies so that circuit elements behind the diode need not be considered in designing the matching networks. This means the signal matching network and the pump matching network can be designed independently. The pump matching network design can be readily accomplished with a Smith Chart, or by experimental techniques [41]. It will not be covered here.

For signal matching network design, program CADDAC is used. Although, the program was also used successfully in designing amplifiers operated at 1.4 GHz using a Motorola MV 1863D varactor, the discussion in this section will be limited to only the 5.5 GHz amplifiers which employ the MA 48509E varactors listed in Tables 2.1 and 2.2. In the design examples to be given below, varactor #2 was used. Parameters of this varactor at 1.5 volts bias and 95% pumping (a = 0.95) are:

$$C_j = 0.374 \quad pF$$
$$R_s = 0.82 \quad \Omega$$
$$L_s = 0.324 \quad nH$$
$$C_{p1} = 0.251 \quad pF$$
$$C_{p2} = 0.046 \quad pF$$
$$C_0 = 0.530 \quad pF$$
$$\gamma_1 = 0.367$$

The parameter constraints were set as follows:

Impedance	$15\ \Omega \leq Z_o \leq 100\ \Omega$
Length	$0.1\ \lambda \leq \ell \leq 0.5\ \lambda$

where λ is referred to a frequency at the center of the signal frequency band.

5.2.1 Example 1. In the first example, a simple circuit containing two series sections of transmission lines and a parallel tuning stub as shown in Fig. 5.6 is chosen as the signal matching network.

The desired response is 15 dB power gain in the frequency range of 5.4 GHz to 5.6 GHz. Arbitrary initial parameter values of 60 ohms and 0.3 wavelength were assigned to each element. Table 5.1 shows the initial and the optimized parameter values. The calculated frequency response is plotted in Fig. 5.7. Power gain of this amplifier fluctuates between 14.3 dB and 15.1 dB.

In calculating the frequency response, the condition of short-circuited harmonics was assumed for the pumped diode. Using the optimized parameter values, an analysis was made, assuming the condition of open-circuited harmonics, which yielded a lower gain and a narrower bandwidth. The frequency response is also plotted in Fig. 5.7.

Table 5.1 Initial and Optimized Parameter Values of the Signal Matching Network in Fig. 5.6

Parameters	Initial Values	Optimized Values
Z_1, ℓ_1	60 Ω, 0.3 λ	25.0 Ω, 0.2115 λ
Z_2, ℓ_2	60 Ω, 0.3 λ	68.1 Ω, 0.2787 λ
Z_3, ℓ_3	60 Ω, 0.3 λ	25.0 Ω, 0.4102 λ

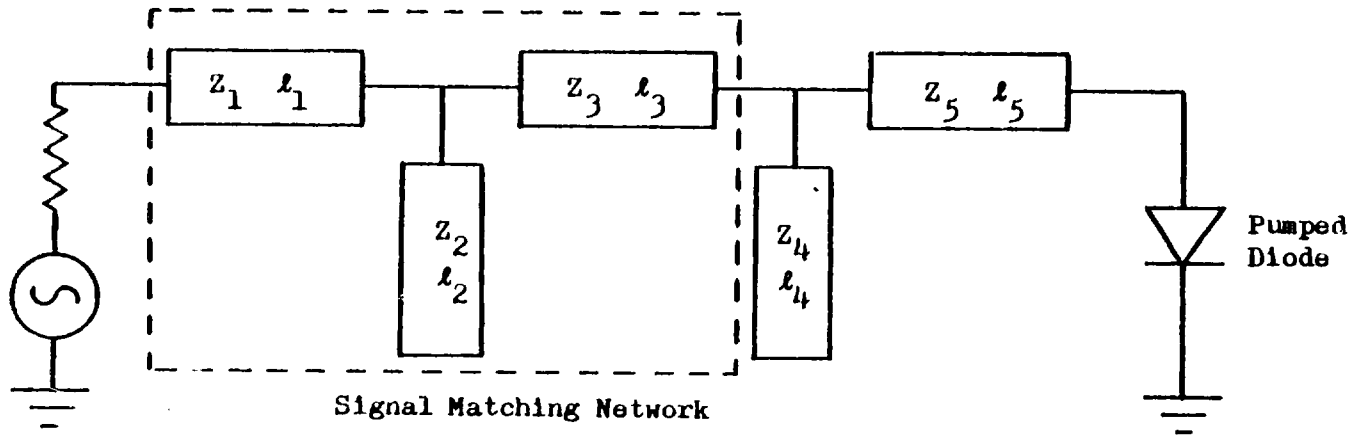

Fig. 5.6 Circuit Used in the First Design Example in Section 5.2

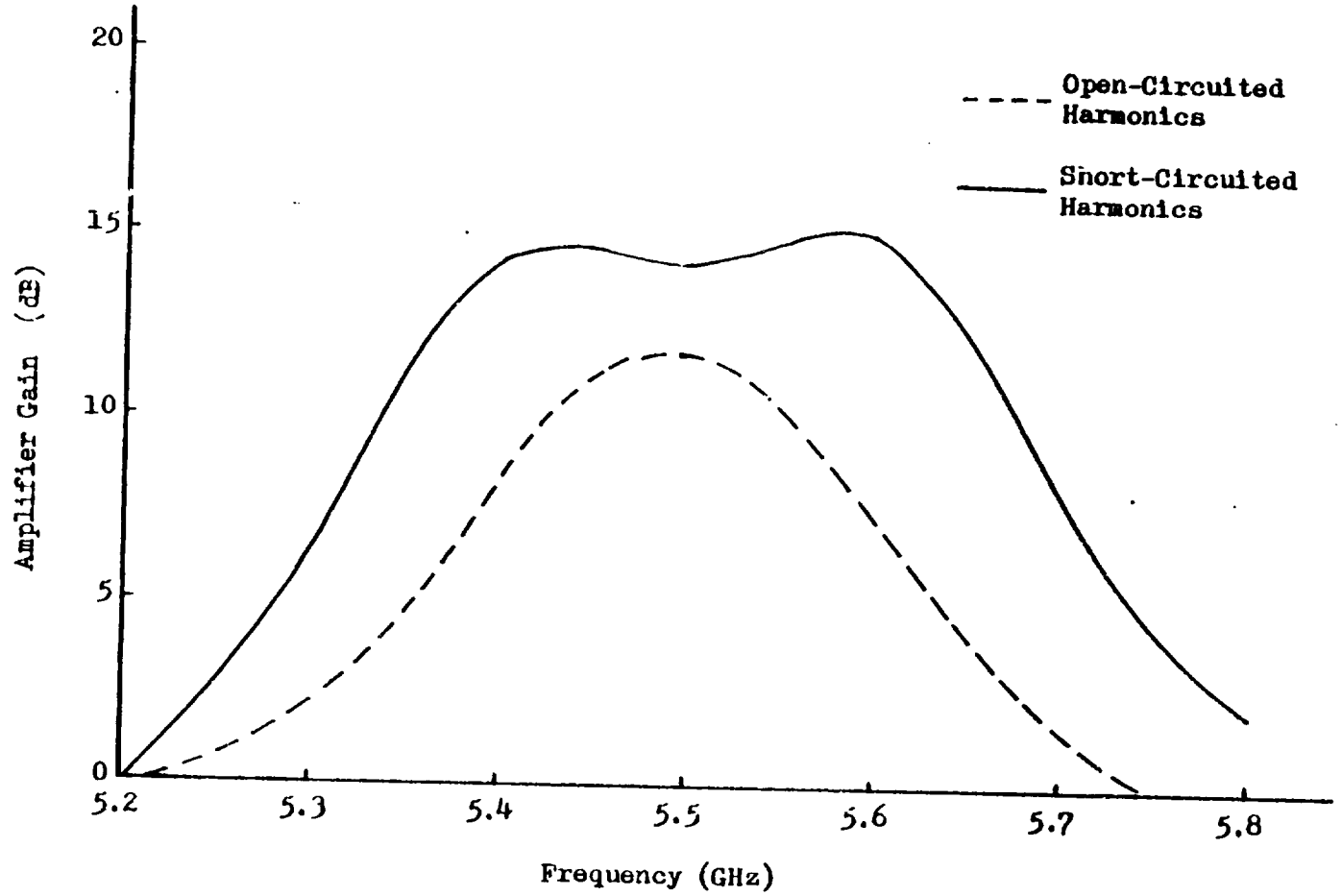

Fig. 5.7 Gain Characteristics of the Amplifier in the First Design Example

5.2.2 Example 2. In this example, the signal matching network contains two more elements than the previous case, i. e., three series transmission line sections and two parallel tuning stubs, as shown in Fig. 5.8. The objective function is 18 dB power gain in the frequency range of 5.4 GHz to 5.6 GHz. The initial and the optimized parameter values are given in Table 5.2, and calculated frequency response is plotted in Fig. 5.9. In the frequency range of interest, gain fluctuates between 17 dB and 19.1 dB.

Table 5.2 Initial and Optimized Parameter Values of the Signal Matching Network in Fig. 5.8

Parameters	Initial Values	Optimized Values
z_1, ℓ_1	55 Ω, 0.3 λ	52.36 Ω, 0.304 λ
z_2, ℓ_2	55 Ω, 0.3 λ	36.63 Ω, 0.346 λ
z_3, ℓ_3	55 Ω, 0.3 λ	52.48 Ω, 0.441 λ
z_4, ℓ_4	55 Ω, 0.3 λ	20.11 Ω, 0.168 λ
z_5, ℓ_5	55 Ω, 0.3 λ	53.34 Ω, 0.488 λ

In this example, the sensitivity analysis has been performed. Figure 5.10 shows the gain sensitivity with respect to the matching network elements, while Fig. 5.11 shows the gain sensitivities with

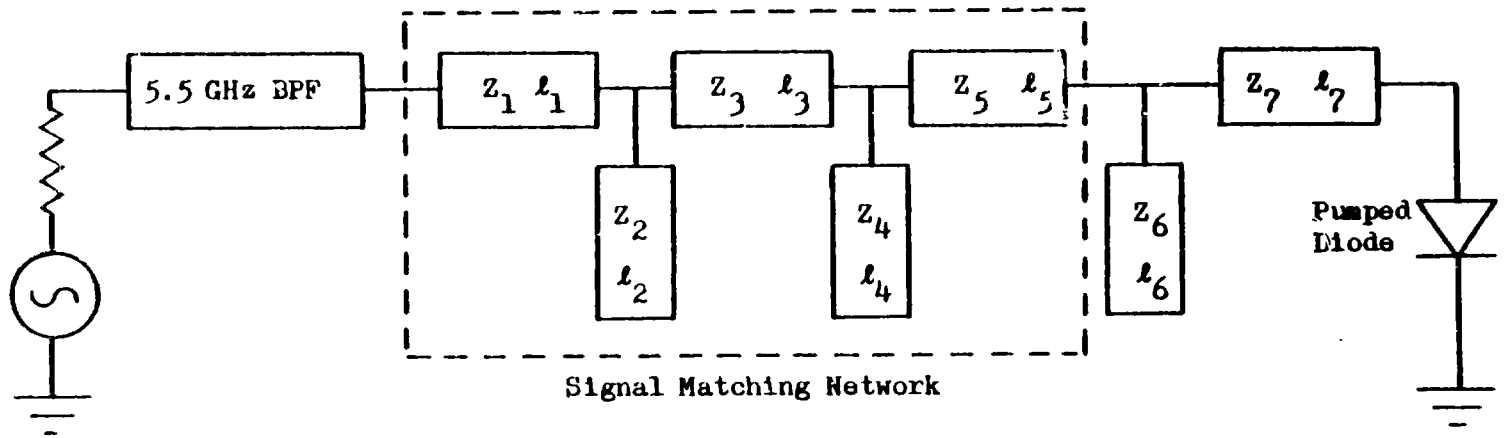

Fig. 5.8 Circuit Used in the Second Design Example in Section 5.2

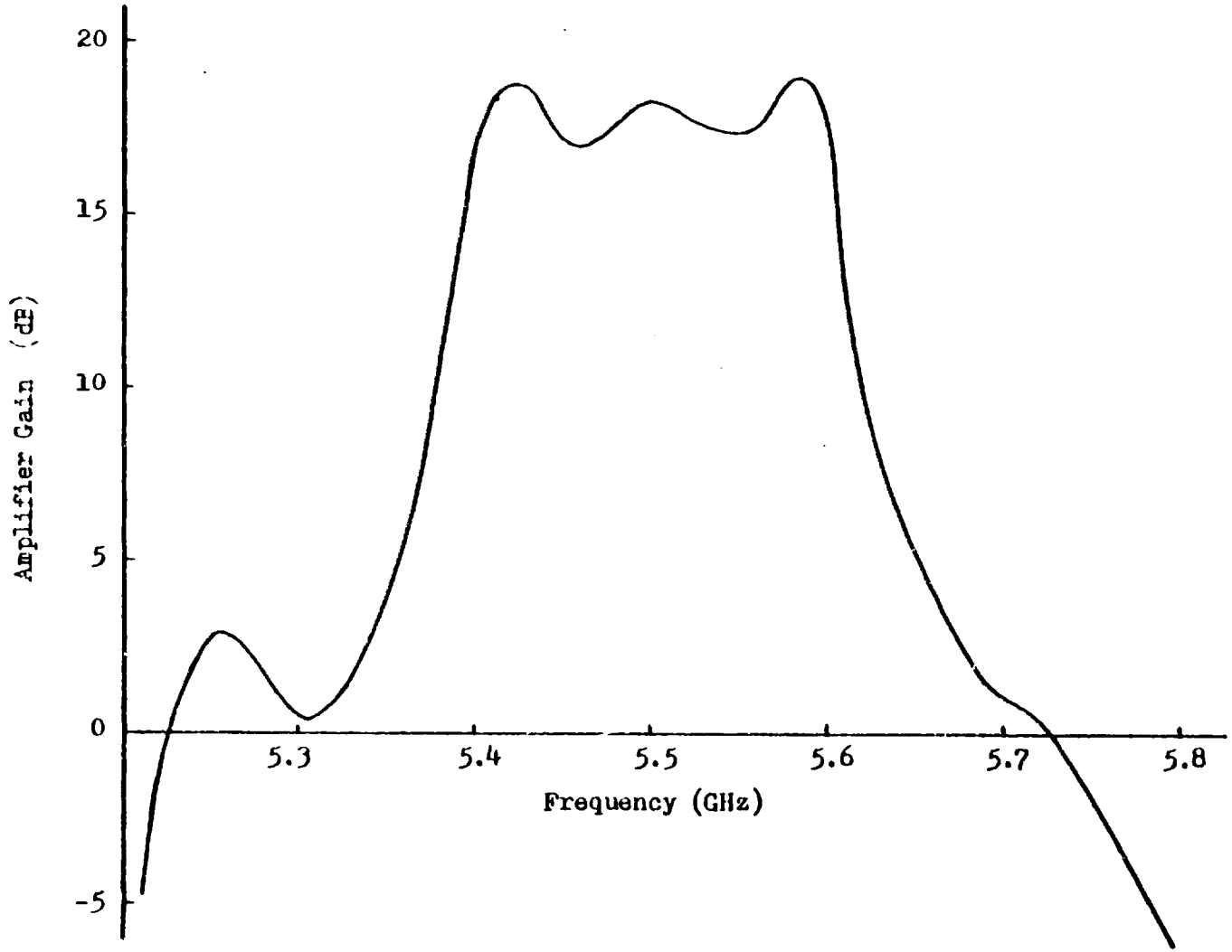

Fig. 5.9 Gain Characteristics of the Amplifier in the Second Design Example

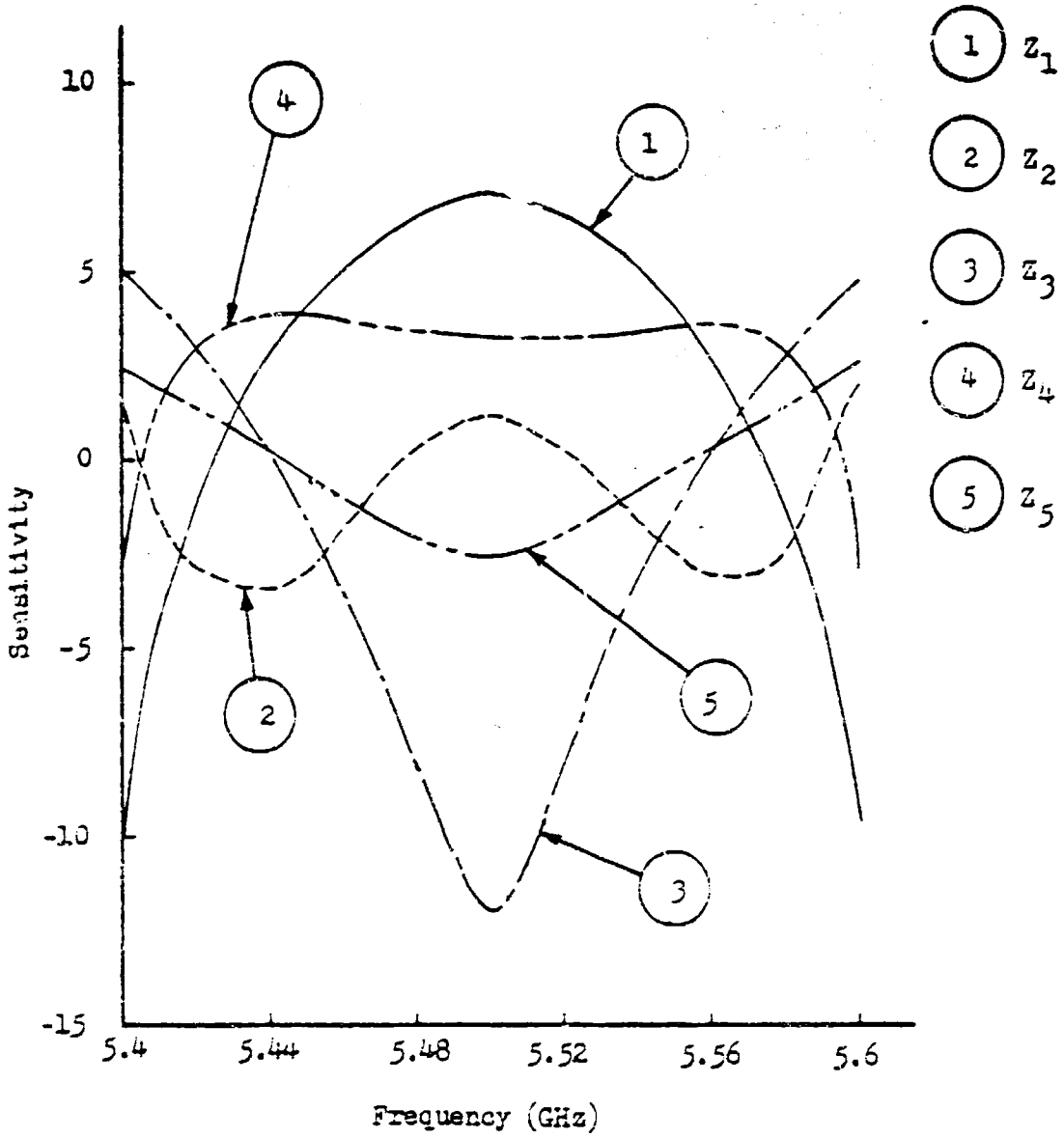

(a)

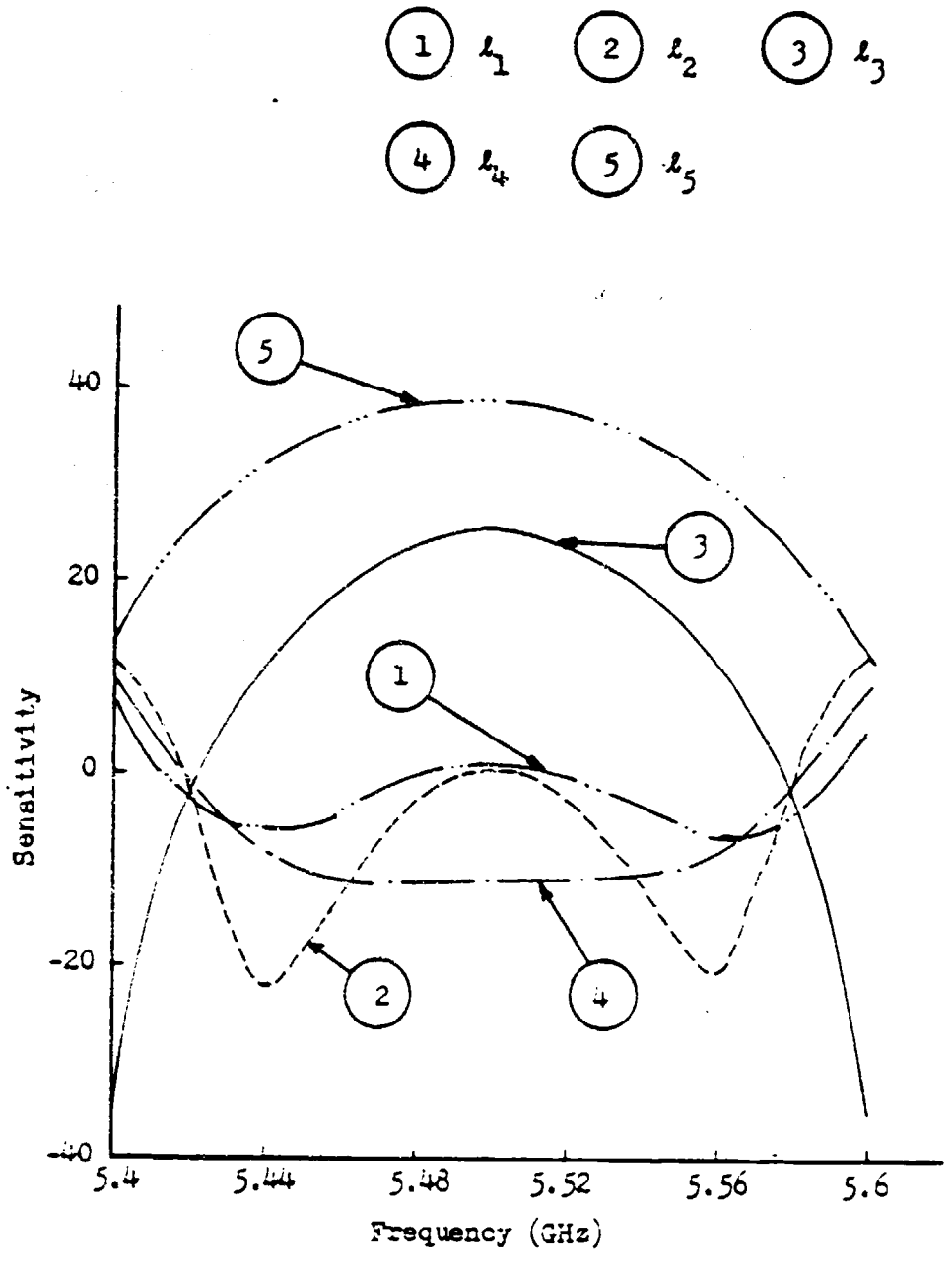

Fig. 5.10 Gain Sensitivities with Respect to Matching Network Parameters

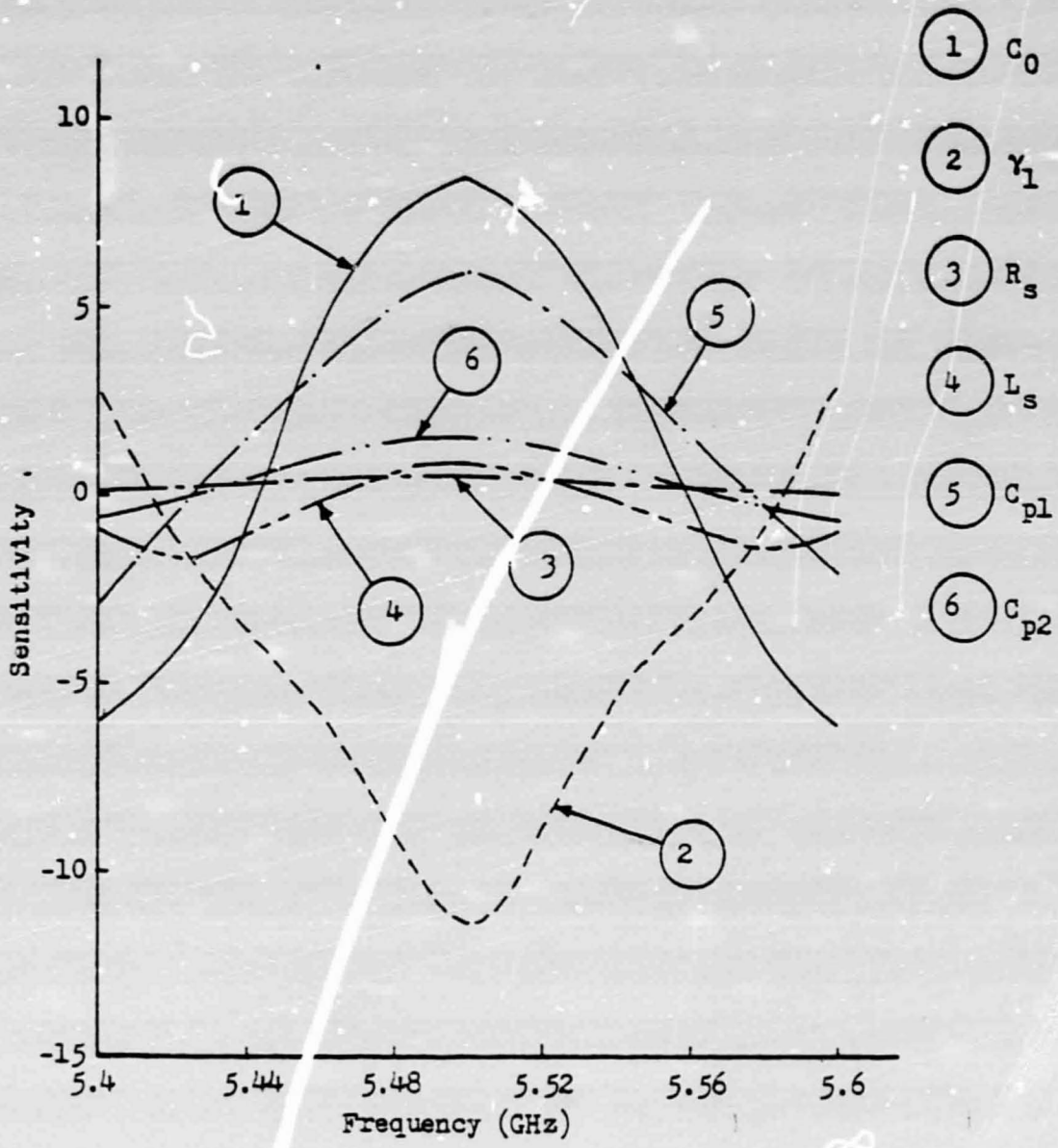

Fig. 5.11 Gai. Sensitivities with Respect to Diode Parameters

respect to the diode parameters.

In view of these figures, one obvious conclusion can be immediately drawn; a degenerate amplifier is indeed a very sensitive device. The power gain is sensitive to both the circuit and the diode parameters. This is not limited to this particular circuit. For the numerous amplifier circuitsdesigned in this study, all with different topologies and different objective functions, the gain sensitivities with respect to one or more parameters invariably possess some values in excess of 15. Therefore, not only must the diode parameters be precisely measured, but also extreme care must be exercised in the realization of amplifier circuits. This point can be easily demonstrated by considering, for example, curve #5 in Fig. 5.10(b).

The gain sensitivity with respect to the length of element #5 (see Fig. 5.8) is approximately 38 at 5.5 GHz where the amplifier has a nominal gain of 18.34 dB. The nominal length of element #5 is 0.488λ at 5.5 GHz which corresponds to an actual length (on a Duroid substrate with ϵ_{eff}= 1.88 for Z_o = 53.34 Ω) of approximately 1.94 cm. Thus, the power gain of this amplifier would decrease from 18.34 dB to 11.37 dB if the length of element #5 is increased by 1% of 1.94 cm, or 0.194 mm. This should serve the purposes of illustrating the importance of precisely determining the microstrip discontinuity effects.

The computing time for the first example in which six parameters were optimized, ranged from 20 to 30 seconds with an IBM 360/75 computer. For the second example, in which ten parameters were optimized, it usually

took 70 to 100 seconds.

5.3 Experimental Results of an MIC Degenerate Amplifier

Throughout this study, several dielectric materials with dielectric constants in the low to medium range were investigated and compared. Specifically, they were quartz ($\epsilon_r = 3.82$), polyolefin ($\epsilon_r = 2.32$), and Duroid ($\epsilon_r = 2.22$). Materials with high dielectric constants, such as alumina ($\epsilon_r = 9.0 - 10.0$), were not considered because of their more profound dispersive characteristics and tighter tolerance requirements. Of the three substrate materials considered, Duroid has the advantage over quartz in that the dielectric constant is lower, it is much easier to machine and fabricate, and the cost is much lower. However, the lower loss of quartz may make it more attractive at higher frequencies. The polyolefin material was found to be less stable mechanically than the Duroid, and variations in substrate thickness were considerably in excess of specified tolerances.

The amplifier described in Section 5.2.1 was realized on a Duroid substrate with a thickness of 0.508 mm. A photograph of this amplifier, housed in a 10 cm by 10 cm aluminum casing, is shown in Fig. 5.12. Bias voltage was applied through a high impedance line ($Z_o = 120\ \Omega$) connected to the pump circuit. Quarter-wavelength open-circuited transmission lines, serving as RF chokes, were placed on the bias line one quarter-wavelength away from the main line at both the signal and the pump frequencies. The measured insertion losses, from signal port to bias port at 5.5 GHz, and

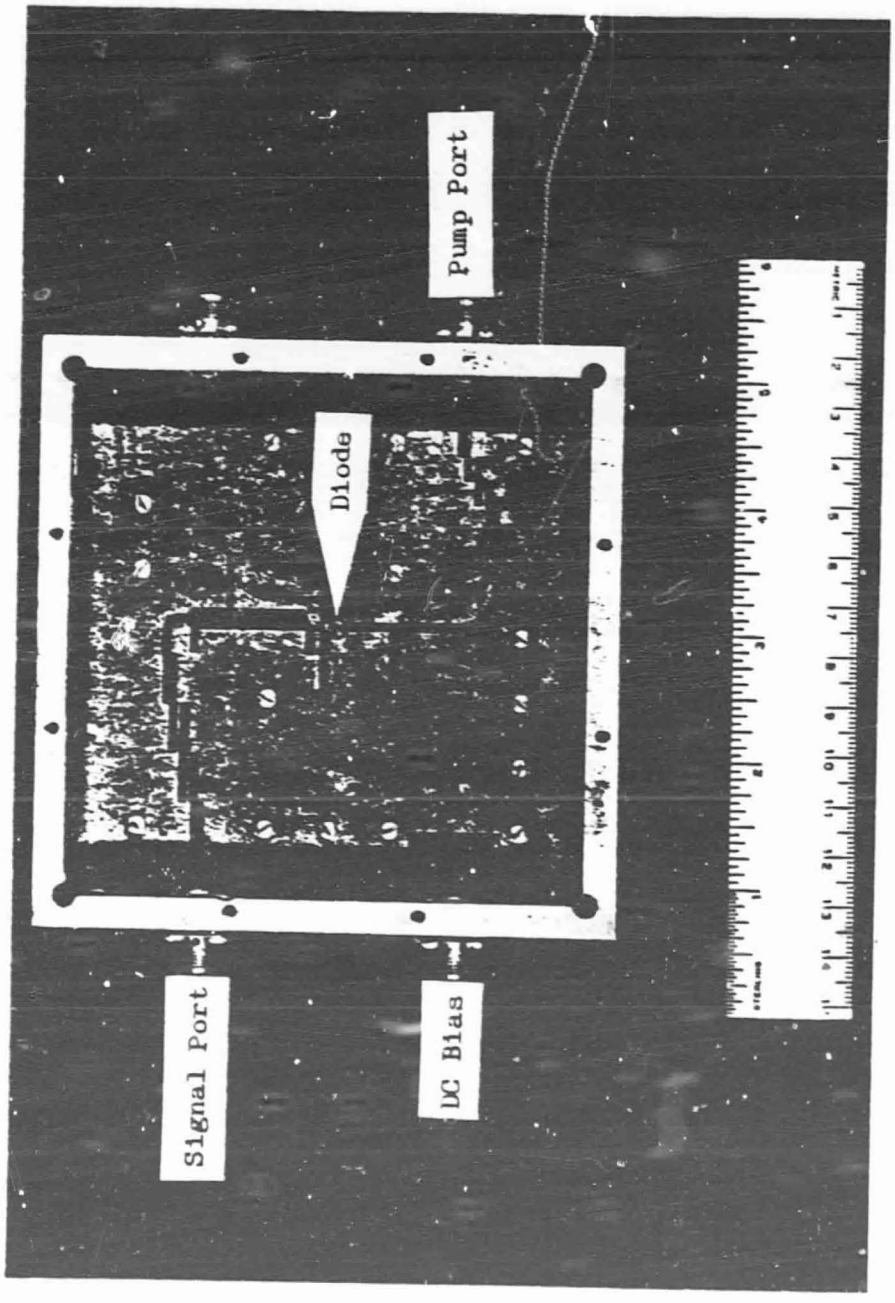

Fig. 5.12 Photograph of a 5.5 GHz MIC Degenerate Amplifier on Duroid Substrate

from pump port to bias port at 11 GHz, are both in excess of 30 dB. The pump source employed a Varian X-13 klystron which can deliver an output power of 300 mW at 11 GHz. The signal port was connected to a Melabs XH-421 circulator with an insertion loss of 0.3 dB from 4.5 GHz to 6.5 GHz, and an isolation ranging between 20 dB and 33 dB over the same frequency range. Isolation was 24 dB at 5.5 GHz. The characteristics of the amplifier were measured with a Hewlett-Packard Swept Amplitude Analyzer (HP 8755A).

The amplifier frequency response curve reproduced in Fig. 5.13 was the result of operation with a bias of 1.5 volts and a pump power level of approximately 32 mW at a frequency of 10.995 GHz. Amplifier gain was observed to be 17 dB $\pm$ 1 dB over a frequency range of approximately 70 MHz. By increasing the pump power level to 38 mW, amplifier gain was raised to 19.5 dB $\pm$ 1 dB over a frequency of 50 MHz before oscillation occurred. The frequency agility was demonstrated by successfully operating the amplifier over a pump frequency range of 10.7 GHz to 11.14 GHz with bias voltage ranging from 0.05 to 3.07 volts, and with a minimum gain of 10 dB.

The amplifier gain characteristics in Fig. 5.13 were recorded at a signal power level of -18 dBm (0.016 mW). It was observed that below the signal power level of -15 dBm, amplifier gain changed insignificantly with respect to the variations in signal power level, while above -15 dBm, amplifier gain was decreasing noticeably with increasing signal power, and when the signal power was above approximately -9 dBm, amplifier gain ceased to exist.

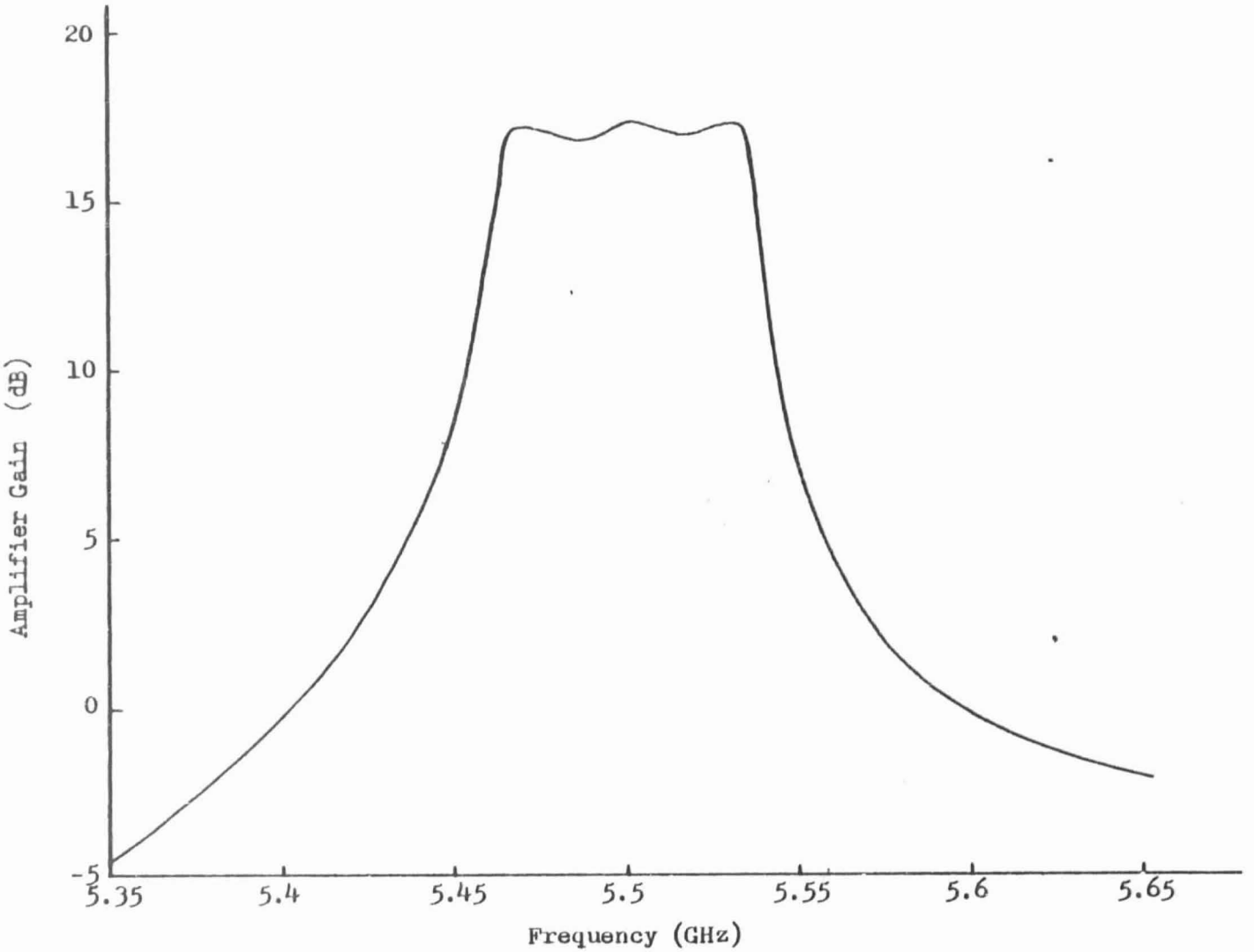

Fig. 5.13 Gain Characteristics of the Degenerate Amplifier in Fig. 5.12

The single-sideband noise figure for the amplifier was calculated, for the operating conditions under which the gain curve in Fig. 5.13 was recorded, at a diode temperature of 305 ^{o}K with a resulting figure of 3.3 dB. This calculation, however, did not include the transmission loss in the signal filter (about 0.5 dB), matching network loss (about 1 dB), and circulator loss (about 0.3 dB). Due to the lack of noise source in the frequency range of interest, a noise figure measurement was made using the simple and crude "signal generator" method [37] with a resulting figure of 5.7 dB. This method requires that the noise output of the amplifier be measured with zero power input and that the power input to double the output be measured. The output determinations in the presence of noise were difficult to accomplished accurately, and hence the accuracy of this measurement was estimated to be $\pm$ 1 dB.

Certain discrepancies between the actual and the calculated responses were observed. When the amplifier was first constructed using parameter values from Table 5.1, amplifier gain was observed to be only 7 dB at 5.5 GHz over a frequency range of about 22 MHz. Additional elements were needed to adjust the gain to that shown in Fig. 5.13. These elements (the short stub behind the 5.5 GHz band-pass filter, and the long stub next to the diode as shown in the photograph in Fig. 5.12) were arrived at experimentally. This discrepancy may be caused by the non-ideal characteristics of the circulator and the microstrip to SMA connector transition. The asymmetrical T-junction near the diode is another possible source of trouble.

Another discrepancy exists in the bandwidths, namely, the actual bandwidth was only one-third of that predicted. This may be partially attributed to the fact that the simple structure used to separate the pump circuit from the signal circuit is only functional over a rather narrow frequency range centered at 5.5 GHz, outside this frequency range, the loading effect of the pump circuit on the signal circuit becomes significant, and thus can not be ignored outright. These discrepancies will be examined in more detail in Chapter VI together with possible remedies.

CHAPTER VI SUMMSRY, CONCLUSIONS AND RECOMMENDATIONS FOR FURTHER STUDY

6.1 Summary and Conclusions

The purpose of this study has been to investigate the feasibility of designing microwave parametric amplifiers by computer-aided optimization techniques, with special emphasis placed upon amplifiers in microwave integrated circuit form. That such an approach is feasible has been demonstrated. The salient features of this study can be summarized as follows:

(1) A precision measurement technique has been developed for varactor characterization. In implementing this technique, a diode test mount which can accommodate various types of diode packages, has been designed, and the test mount equivalent circuit has been accurately determined. Measurements have been made of the driving-point impedances of several MA 48509E varactors over a wide frequency range.

(2) A number of lumped-element equivalent circuits for packaged varactors valid at various frequency ranges have been proposed. Circuit elements and diode parameters have been successfully determined from the measured impedance data by computer-aided optimization techniques.

(3) Expressions of power gain and noise figure for parametric amplifiers employing a more realistic equivalent circuit have been derived. These expressions have been presented in such a manner to facilitate computer programming.

(4) Electrical characteristics and discontinuity effects of microstrip

transmission lines have been investigated. Analysis and synthesis methods for parallel-coupled microstrip band-pass filters have been presented. It has been found that the synthesis method usually results in extremely high impedances which are difficult to realize in practice. This deficiency has been removed by employing computer-aided optimization techniques to perturb the impedances calculated from the synthesis method. Band-pass filters with moderate bandwidth have been successfully designed and fabricated at 5.5 GHz and 11 GHz. Actual and calculated responses have been observed to be in excellent agreement.

(5) A computer program, CADDAC, has been developed for degenerate parametric amplifier designs. It employs an improved "direct search" method to perform circuit optimization which has been observed to reduce the computing time considerably when compared with other algorithms. The program requires very little computer memory, and thus can be modified for a mini-computer.

(6) An MIC degenerate amplifier has been constructed on a Duroid substrate. The amplifier has a power gain of 17.5 dB $\pm$ 1 dB over a frequency range of 70 MHz. The single-sideband noise figure of this amplifier has been measured to be approximately 5.7 dB.

6.2 Recommendations for Further Study

For the degenerate amplifier constructed in this study, the pump source and the circulator have not been integrated into the same substrate on which the amplifier was fabricated. Since circuit miniaturization is

a major advantage of MIC technology, the integration is desirable, and it can be accomplished by using solid-state devices such as IMPATT diode oscillators [100], and microstrip Y-junction circulators [101]. Besides achieving circuit miniaturization, the integration also serves another purpose: it enables one to predict the amplifier response more accurately by including the circulator model, either analytical or experimental, in the computer program, and thus remove some of the discrepancies between the actual and the calculated responses as discussed in Section 5.3.

The microstrip T-junction model developed in Section 4.3 is only applicable to symmetrical junctions, i. e., the main line impedances are identical on both sides of the stub. For asymmetrical junctions, the model of Menzel and Wolff [87], in which the T-junction is characterized in terms of scattering parameters, seems to be adequate. However, for computer-aided design purposes, this model suffers from two major drawbacks: one, that the calculations of these parameters are relatively time consuming, and two, that these parameters are calculated from line widths instead of line impedances. This implies that should this model be directly implemented in a computer-aided design program, physical parameters, not electrical parameters from which circuit responses are calculated, would be optimized, and thus computing time would be increased drastically. A possible approach is to first optimize the electrical parameters by simply neglecting the junction effects, Next, optimized electrical parameters are converted to physical parameters, and scattering parameters for all junctions in the circuit are calculated at frequencies of interest.

Optimization process is then restarted, but this time only the length of each element is to be optimized so that the scattering parameters remain valid and need not be calculated over and over again during the optimization process. However, it is not certain that convergence to objective function is achievable.

Although the computer program can perform broadband amplifier designs, broadband amplifier realizations were not attempted in this study. As discussed in Section 5.3, the simple structure used to separate the pump circuit from the signal circuit is only functional over a rather narrow frequency range. For broadband amplifiers, different structures must be used. It is also worthwhile to point out that in the case of broadband amplifier design, the computing time can be reduced considerably if the initial parameter values are obtained from one of the conventional synthesis methods discussed in Chapter I [102].

Finally, on diode characterization, it is highly desirable to have the diode measured in situ. Intuitively, the lumped-element equivalent circuit derived from slotted-line measurement with the diode mounted in a coaxial test mount should remain valid when the diode is shunt mounted in a microstrip if the diameter of the diode package is much smaller than the microstrip linewidth. However, if the diameter of the diode package is comparable to, or even larger than the microstrip linewidth, the validity of the lumped-element equivalent circuit is doubtful. In order to measure the diode in situ, the launchers, i. e., the coaxial-to-microstrip transitions, must first be precisely characterized. To

this end, measurement by automatic network analyzer is preferred over slotted-line measurement.

APPENDIX A REPRESENTATION OF TWO-PORT NETWORKS BY ABCD PARAMETERS

The purpose of this appendix is to give a brief review on ABCD parameters (also referred as general circuit parameters), which are often used in two-port network representations.

In terms of Fig. A.1, the ABCD parameters are defined by the following equations

$$V_1 = AV_2 + BI_2 \tag{A.1}$$

$$I_1 = CV_2 + DI_2 \tag{A.2}$$

or in matrix notation

$$\begin{bmatrix} V_1 \\ I_1 \end{bmatrix} = \begin{bmatrix} A & B \\ C & D \end{bmatrix} \begin{bmatrix} V_2 \\ I_2 \end{bmatrix} \tag{A.3}$$

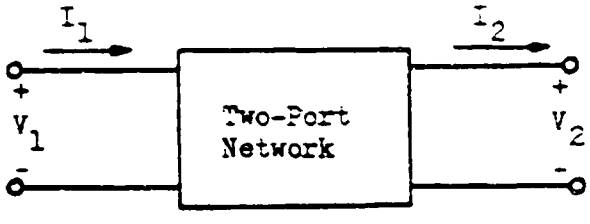

Fig. A.1 Definition of Voltages and Currents for Two-Port Networks

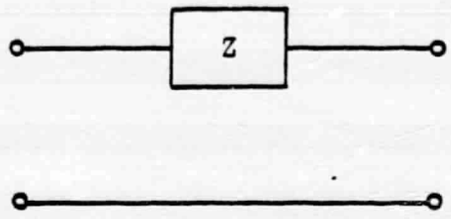

A = 1 B = Z

C = 0 D = 1

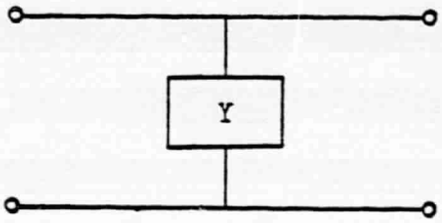

A = 1 B = 0

C = Y D = 1

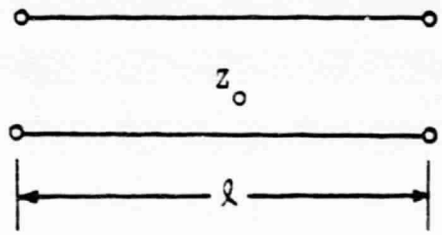

$A = D = \cosh(\gamma\ell)$

$B = Z_o \sinh(\gamma\ell)$

$C = \sinh(\gamma\ell)/Z_o$

γ = propagation constant

Z_o = characteristic impedance

Fig. A.2 ABCD Parameters of Some Common Structures

For certain types of networks, the ABCD parameters are interrelated in the following special ways: If the network is reciprocal

$$AD - BC = 1 \tag{A.4}$$

If the network is symmetrical

$$A = D \tag{A.5}$$

If the network is lossless, A and D are purely real. and B and C are purely imaginary. Figure A.2 gives the ABCD parameters for several common structures.

These parameters are particularly useful in relating the performance of cascaded networks to the performance of each network when operated individually. The ABCD parameters of N cascaded networks as shown in Fig. A.3 are given by

$$\begin{bmatrix} A & B \\ C & D \end{bmatrix} = \begin{bmatrix} A_1 & B_1 \\ C_1 & D_1 \end{bmatrix} \begin{bmatrix} A_2 & B_2 \\ C_2 & D_2 \end{bmatrix} \cdots\cdots \begin{bmatrix} A_N & B_N \\ C_N & D_N \end{bmatrix} \tag{A.6}$$

The input impedance Z_{IN1} defined in Fig. A.4 can be expressed in terms of the ABCD parameters and the termination Z_2,

$$Z_{IN1} = \frac{AZ_2 + B}{CZ_2 + D} \tag{A.7}$$

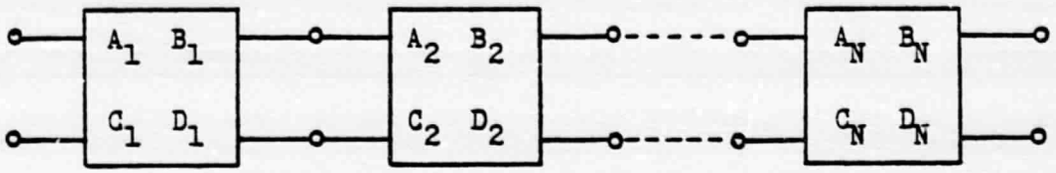

Fig. A.3 Cascaded Two-Port Networks

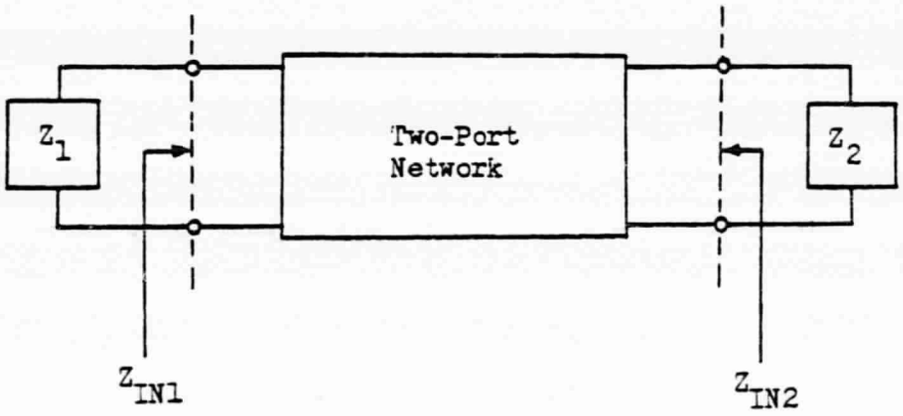

Fig. A.4 Two-Port Network with Terminations

Similarly, for the input impedance Z_{IN2} in Fig. A.4,

$$Z_{IN2} = \frac{AZ_2 + B}{CZ_2 + D} \tag{A.8}$$

and

$$\frac{t}{b} = 0.205$$

From Fig. 3 of Getsinger [103], C_{fe}/ϵ is found to be

$$\frac{C_{fe}}{\epsilon} = 0.32$$

hence

$$C_f = \pi\epsilon D_o(0.32) = 0.062 \text{ pF}$$

B.2 Evaluation of L_c

L_c is the coaxial inductance due to the magnetic field in the volume outside an imaginary continuation of the inner conductor over the length, h. If it is assumed that the fields are not affected by the actual configuration of the package, then L_c is

$$L_c = \frac{\mu h}{2\pi} \ln(D_o/D_i) \qquad (B.4)$$

where μ is the permeability in air and is equal to $4\pi \times 10^{-7}$ H/m. Substitution of numerical values into Eq. B.4 yields

$$L_c = 0.118 \text{ nH}$$

B.3 Evaluation of C_{r1}, C_{r2}, and L_r

The admittance parameters of a radial line pi-network are given by Marcuvitz [32]. Special linear combinations of Bessel function have been defined particularly for this problem, and numerical values are given graphically. However, if both h and D_i are small in terms of wavelengths,

the pi-network elements can be found from a simple coaxial line approximation [31],

$$L_r = \frac{\mu h}{2\pi} \ln(D_i/d) \tag{B.5}$$

$$C_{r1} + C_{r2} = C_r = \epsilon \frac{\pi(D_i^2 - d^2)}{4h} \tag{B.6}$$

Substitution of numerical values into Eqs. B.5 and B.6 yields

$$L_r = 0.0577 \text{ nH}$$

$$C_r = 0.050 \text{ pF}$$

The problem of dividing C_r into C_{r1} and C_{r2} is not a simple matter. However, in the present case, this problem may be avoided by observing that at the highest frequency of interest, i. e., 12 GHz,

$$\omega^2(C_r/2)L_r = 0.008 \ll 1$$

Thus the position of L_r and that of either C_{r1} or C_{r2} are interchangeable, as discussed previously in Scetion 2.3. It follows that no matter how C_r is divided between C_{r1} and C_{r2}, the error will always be negligibly small. Therefore, it is possible to arbitrarily set

$$C_{r1} = C_{r2} = 0.025 \text{ pF}$$

APPENDIX C CADDAC COMPUTER PROGRAM

C.1 Purpose

This program performs analysis and/or synthesis of lumped-element and/or distributed-element degenerate parametric amplifier circuits.

C.2 Structure

This program recognizes ten different structures. These structures are listed below together with their type identification numbers and required parameters. All impedances are in ohms, capacitances in picofarads, inductances in nanohenries, and lengths in fractional wavelengths referred to a center frequency in GHz. A negative value for any parameter indicates that this parameter is to be optimized. However, diode parameters, source impedance, and band-pass filter parameters may not be optimized. A type number of 0 (zero) indicates the end of network configuration.

(1) Series-parallel RLC

Type : 1

Data : R, L, C

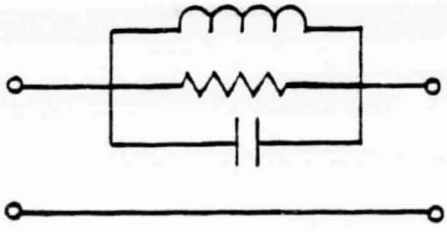

(2) Parallel-parallel RLC

Type : 2

Data : R, L, C

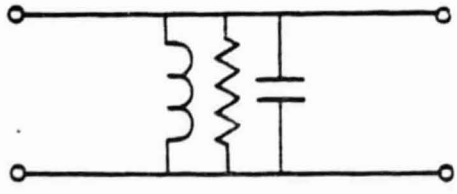

(3) Series-series RLC

Type : 3

Data : R, L, C

(4) Parallel-series RLC

Type : 4

Data : R, L, C

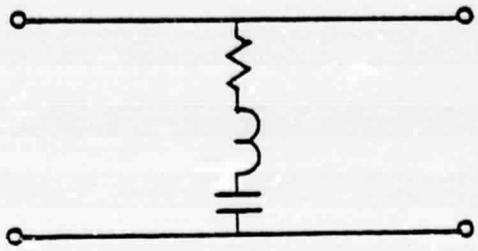

(5) Series transmission line

Type : 5

Data : Z_o, ℓ

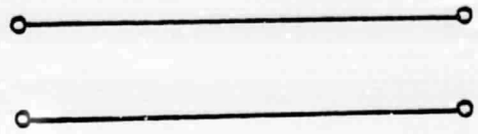

(6) Parallel open-circuited transmission line

Type : 6

Data : Z_o, ℓ

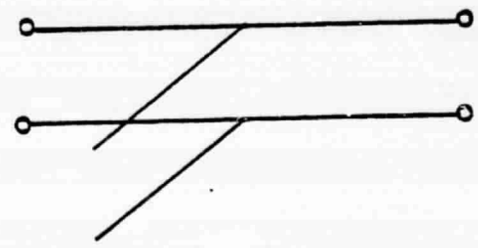

(7) Parallel short-circuited transmission line

Type : 7

Data : Z_o, ℓ

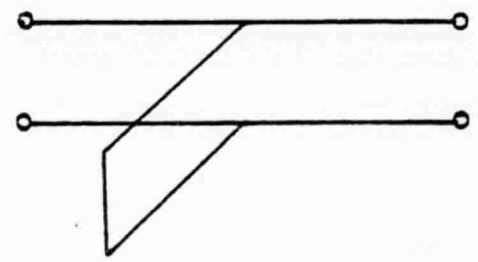

(8) Pumped varactor

Type : 8

Data : C_0, Y_1, R_s, L_s, C_{p1}, C_{p2}

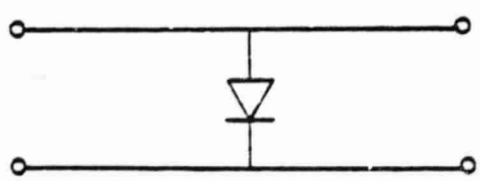

(9) Source impedance

Type : 9

Data : R_g

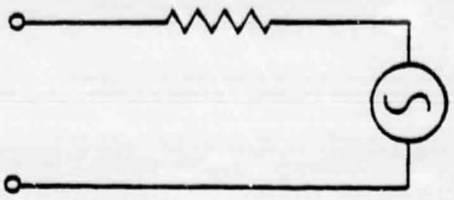

(10) Parallel-coupled band-pass filter

Type : 10

Data : See Section C.4

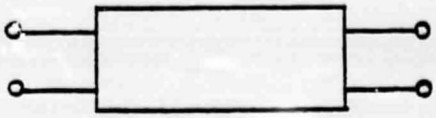

C.3 Limitations

(1) Number of total circuit parameters ≤ 100 .

(2) Number of circuit parameters to be optimized ≤ 50

(3) Number of sections ≤ 50

(4) Number of frequency points ≤ 101

C.4 Input Data Cards

Variable	Columns	Description
First card :		
FCENTR	1-10	Center frequency (GHz)
FSTART	11-20	Starting frequency (GHz)
FSTOP	21-30	Stopping frequency (GHz)
FDEL	31-40	Frequency increment (GHz)
FPUMP	41-50	Pump frequency (GHz)
Second card :		
ZHI	1-10	Upper limit of Z_o (ohms)

ZLO	11-20	Lower limit of Z_o (ohms)
BHI	21-30	Upper limit of length (λ)
BLO	31-40	Lower limit of length (λ)
ALPHA	41-50	Line loss (dB/λ)
GAINO	51-60	Desired power gain (dB)

Third card :

DELTA	1-10	Initial step size
DELMIN	11-20	Minimum step size
DRATIO	21-30	Step size reducing factor
TOL	31-40	Minimum error

Description of circuit topology starts from the fourth card which must be the source impedance card (type 9). Except for the band-pass filter, each section takes one card and all parameter values are in F10.0 format. The end of circuit topology description is indicated by a type 0 (zero) card.

For a band-pass filter, a type 10 card is placed in its normal position relative to the other sections. Following the type 0 card, the parameters of the band-pass are then given. For a filter with N sections, N+1 cards are required. The first card contains: the number of sections, the conductivity of center conductor (10^{-6}mho/cm), the conductivity of ground plane (10^{-6}mho/cm). The second card describes the first section, the third card describes the second section, and so on. Each card contains: even-mode impedance (ohms), odd-mode impedance (ohms), even-mode effective dielectric constant, odd-mode effective

dielectric constant, line width (cm), length (cm), gap width (mm), open-circuit equivalent capacitance (pF).

Following the filter cards, two more cards are required. The first card indicates whether a sensitivity analysis is desired. A letter Y on the first column indicates sensitivity analysis is desired, otherwise the card is left blank. The second card indicates whether a plot of frequency response (usually with smaller frequency increment and wider frequency range) is desired. Again, a letter Y on the first column indicates "yes", and blank otherwise. In the first case, FSTART, FSTOP, and FDEL must also be specified in F10.0 format starting from column 11.

A set of data cards used for the analysis of the amplifier described in Section 5.2.2 are given in Fig. C.1.

```
  5.5          5.4          5.6          C.C2         11.0
  100.         15.          0.49         C.15         0.113        18.0
  0.15         0.0005       C.2          0.1
  9.           50.
  10.
  5.           52.3569      C.3C39
6.             38.63C8      0.3457
  5.           52.4827       C.441
  6.           20.1125      C.1677
  5.           53.3374      C.4877
  6.           50.          C.125
  5.           50.          C.125
  8.           0.5298        C.3665       0.8          0.32         0.251        0.046
  0.
  4.0          0.5885       0.3571

 70.145       40.841       1.5648       1.7163       0.12313      0.98414      0.1119       0.01755
 55.792       46.08        1.5856       1.7929       0.15112      0.97015      0.6437       0.02076
 55.742       46.148       1.5854       1.7548       0.15112      0.97015      0.653        0.02076
 70.748       41.658       1.5632       1.7084       0.12127      0.98134      0.1213       0.01734
YES
YES           5.0          6.C          C.C1
```

Fig. C.1 Sample Data Cards for Program CADDAC

```
C
C
C
C
C
C     ***********************************************
C     ***********************************************
C     *****                                     *****
C     *****                                     *****
C     *****  DEGENERATE PARAMETRIC AMPLIFIERS   *****
C     *****                                     *****
C     *****                                     *****
C     ***********************************************
C     ***********************************************
C
C
C     PROGRAM FOR DESIGNING SIGNAL CIRCUIT OF DPA
C
C     SUBROUTINES REQUIRED:
C      1. RESPON
C      2. DIRECT
C      3. EXPLOR
C      4. RANDOM
C      5. EVAL
C      6. GRAPH
C      7. OUTPUT
C      8. DISPLY
C      9. SENSIT
C     10. BPFILT
C      ALSO THREE FUNCTIONS: CSINH, CCOSH, AND CTANH.
C
C
C     MAIN PROGRAM
C
      DIMENSION     PAR(50),ELMENT(10),G(101)
      DATA          RYES/1HY/
      COMMON        SIGN(50),PARMAX(50),PARMIN(50)
      COMMON        PARAM(100),ITYPE(50),LIST(50)
      COMMON        FPUMP,FCENTR,FSTART,FDEL,GAINO
      COMMON        NPARAM,NLIST,NUMSEC,NEVAL,NFREQ
      COMMON        DELTA,DELMIN,TOL,DRATIC,ALPHA
      COMPLEX       AF(101),BF(101),CF(101),DF(101)
      COMMON        AF,BF,CF,DF
      IR=5
      IW=6
    1 NUMSEC=0
      NPARAM=0
      NLIST=0
```

```
      KBPF=0
      READ(IR,500,END=999) FCENTR,FSTART,FSTOP,FDEL,FPUMP
      READ(IR,500) [illegible],ZLO,BHI,BLO,ALPHA,GAINO
      READ(IR,500) DELTA,DELMIN,DRATIO,TCL
  500 FORMAT(8F10.0)
      WRITE(IW,6100) FSTART,FSTOP,FPUMP
 6100 FORMAT(1H1,//,28H PARAMETRIC AMPLIFIER DESIGN,/,
     +       15H SIGNAL NETWORK,//,
     +       30H FREQUENCIES OF INTEREST .....,/,
     +       12H SIGNAL.....,F8.3,4H TO ,F8.3,4H GHZ,/,
     +       13H PUMPING.....,F8.3,4H GHZ,/)
      WRITE(IW,6200) GAINO,ALPHA,ZHI,ZLO,BHI,BLO
 6200 FORMAT(17H POWER GAIN .....,F8.2,3H DB,/,
     +       16H LINE LOSS .....,F7.4,1CH DB/LAMBDA,/,
     +       28H PARAMETER CONSTRAINTS .....,/,
     +       16H IMPEDANCE .....,/,
     +       20H   UPPER BOUND .....,F8.2,5H OHMS,/,
     +       20H   LOWER BOUND .....,F8.2,5H OHMS,/,
     +       13H LENGTH .....,/,
     +       20H   UPPER BOUND .....,F8.3,7H LAMBDA,/,
     +       20H   LOWER BOUND .....,F8.3,7H LAMBDA,//)
      ALPHA=ALPHA/8.686
      NFREQ=(FSTOP-FSTART)/FDEL+1.6
   10 READ(IR,500) TYPE,(ELMENT(I),I=1,6)
      INTYPE=TYPE+0.1
      IF(INTYPE) 30,110,20
   20 IF(INTYPE-10) 50,50,30
   30 WRITE(IW,600)
  600 FORMAT(///,19H INVALID CARD TYPE,/,I5,3F9.4,//)
      GOTO 998
   50 GOTO (60,60,60,60,70,70,70,90,80,95),INTYPE
C
C     LUMPED ELEMENT CARDS
C
   60 IF(ELMENT(1)) 62,61,62
   61 ELMENT(1)=1.E-6
   62 DO 64 I=1,3
      NPARAM=NPARAM+1
      IF(ELMENT(I)) 63,64,64
   63 NLIST=NLIST+1
      LIST(NLIST)=NPARAM
      PARMAX(NLIST)=1000.*ABS(ELMENT(I))
      PARMIN(NLIST)=0.001*ABS(ELMENT(I))
   64 PARAM(NPARAM)=ABS(ELMENT(I))
      N=3
      GOTO 100
C
C     TRANSMISSION LINE ELEMENT CARDS
```

```
C
 70   DO 76 I=1,2
      NPARAM=NPARAM+1
      IF(ELMENT(I)) 72,76,76
 72   NLIST=NLIST+1
      LIST(NLIST)=NPARAM
      IF(I .EQ. 1) GOTO 75
      PARMAX(NLIST)=BHI
      PARMIN(NLIST)=BLO
      GOTO 76
 75   PARMAX(NLIST)=ZHI
      PARMIN(NLIST)=ZLO
 76   PARAM(NPARAM)=ABS(ELMENT(I))
      N=2
      GOTO 100
C
C     SOURCE IMPEDANCE CARD
C
 80   IF(NUMSEC+NPARAM+NLIST) 81,82,81
 81   WRITE(IW,610)
 610  FORMAT(//,36H SOURCE CARD MUST BE THE FOURTH CARD)
      GOTO 998
 82   NPARAM=NPARAM+1
      PARAM(NPARAM)=ABS(ELMENT(1))
      N=1
      WRITE(IW,620)
 620  FORMAT(28H INPUT NETWORK CONFIGURATION,//,
     +       28H SECT TYPE          PARAMETERS,/)
      GOTO 100
C
C     DIODE CARD
 90   N=6
      DO 94 I=1,N
      NPARAM=NPARAM+1
 94   PARAM(NPARAM)=ABS(ELMENT(I))
      NUMSEC=NUMSEC+1
      ITYPE(NUMSEC)=INTYPE
      WRITE(IW,630) NUMSEC,INTYPE,(ELMENT(I),I=1,N)
 630  FORMAT(2I4,6F13.4)
      GOTO 10
C
C     COUPLED LINE BANDPASS FILTER
C
 95   NUMSEC=NUMSEC+1
      ITYPE(NUMSEC)=INTYPE
      KBPF=1
      WRITE(IW,635) NUMSEC,INTYPE
 635  FORMAT(2I4,21H       BANDPASS FILTER)
```

```
      GOTO 10
  100 NUMSEC=NUMSEC+1
      ITYPE(NUMSEC)=INTYPE
      WRITE(IW,630) NUMSEC,INTYPE,(ELMENT(I),I=1,N)
      GOTO 10
  110 IF(NUMSEC-50) 130,130,120
  120 WRITE(IW,640) NUMSEC
  640 FORMAT(//,29H TOO MANY SECTIONS IN NETWORK,I5,//)
      GOTO 998
  130 IF(NPARAM-100) 150,150,140
  140 WRITE(IW,650) NPARAM
  650 FORMAT(//,20H TOO MANY PARAMETERS,I5,//)
      GOTO 998
  150 IF(NLIST-50) 165,165,160
  160 WRITE(IW,660) NLIST
  660 FORMAT(//,19H TOO MANY VARIABLES,I5,//)
      GOTO 998
C
C     PRINT OUT BANDPASS FILTER CONFIGURETION
C     AND STORE ABCD MATRIX OF FILTER AT
C     FREQUENCY POINTS OF INTEREST.
C
  165 IF(KBPF .EQ. 0) GOTO 170
      KFILT=0
      CALL BPFILT(KFILT)
      KFILT=1
C
C     RUN A FREQUENCY RESPONSE
C
  170 CALL OUTPUT
      IF(NLIST .NE. 0) GOTO 180
      WRITE(IW,670)
  670 FORMAT(///,16H END OF ANALYSIS,//)
      GOTO 225
C
C     SYNTHESIS REQUIRED
C
  180 DO 190 I=1,NLIST
      J=LIST(I)
  190 PAR(I)=PARAM(J)
      CALL DIRECT(PAR,FMERIT)
      IF(FMERIT-TOL) 200,200,210
  200 WRITE(IW,680)
  680 FORMAT(///,18H SEARCH SUCCESSFUL)
      GOTO 220
  210 WRITE(IW,690)
  690 FORMAT(///,22H ERROR ABOVE TOLERANCE)
  220 CONTINUE
```

```
C
C       WANT A SENSITIVITY ANALYSIS? INDICATE YES OR NO.
C
 225    READ(IR,510) CHECK
        IF(CHECK-RYES) 240,230,240
 230    CALL SENSIT
C
C       WANT A FREQUENCY RESPONSE WITH FINER INCREMENT PLOTTED
C       INDICATE YES OR NO.
C       IF YES, SPECIFY FSTART,FSTOP,AND FDEL.
C
 240    READ(IR,510) CHECK,FSTART,FSTOP,FDEL
 510    FORMAT(A1,9X,7F10.0)
        IF(CHECK-RYES) 270,250,270
C
 250    NFREQ=(FSTOP-FSTART)/FDEL+1.6
        IF ( KBPF .EQ. 0 ) GOTO 255
        CALL BPFILT(KFILT)
 255    FREQ=FSTART
        DO 260 I=1,NFREQ
        II=I
        CALL RESPON(G(I),FREQ,II)
 260    FREQ=FREQ+FDEL
        NF=NFREQ
        CALL GRAPH(FSTART,FDEL,G,NF)
 270    CONTINUE
        GOTO 1
 998    WRITE(IW,700)
 700    FORMAT(//,29H ROUTINE TERMINATED BY ERRORS,//)
        GOTO 1
 999    STOP
        END
        SUBROUTINE RESPON(GAIN,FREQ,KSF)
C
C       THIS SUBROUTINE CALCULATES GAIN CHARACTERISTICS
C       OF DEGENERATE PARAMETRIC AMPLIFIERS
C
        DIMENSION       BETA(2)
        COMMON          SIGN(50),PARMAX(50),PARMIN(50)
        COMMON          PARAM(100),ITYPE(50),LIST(50)
        COMMON          FPUMP,FCENTR,FSTART,FDEL,GAINO
        COMMON          NPARAM,NLIST,NUMSEC,NEVAL,NFREQ
        COMMON          DELTA,DELMIN,TOL,ORATIO,ALPHA
        COMPLEX         Z11,Z12,Z21,Z22,ZIP,ZEQ,ZIN,ZID,RHO
        COMPLEX         GAMMA,CSINH,CCOSH,CTANH,CMPLX,CONJG,CJ
        COMPLEX         A(2),B(2),C(2),D(2),A2(2),C2(2),Z(2),Y(2)
        COMPLEX         A1(2),B1(2),C1(2),D1(2),SJ(2),SJ1(2)
        COMPLEX         AF(101),BF(101),CF(101),DF(101)
```

```
      COMMON        AF,BF,CF,DF
C
C
C
      CJ=(0.,1.)
      FIDLER=FPUMP-FREQ
      PI=3.141592654
      OMEGAS=2.*PI*FREQ
      OMEGAI=2.*PI*FIDLER
      BETA(1)=OMEGAS/FCENTR
      BETA(2)=OMEGAI/FCENTR
      SJ(1)=CJ*OMEGAS
      SJ(2)=CJ*OMEGAI
      SJ1(1)=SJ(1)*1.E-3
      SJ1(2)=SJ(2)*1.E-3
      DO 2 I=1,2
      A1(I)=1.
      B1(I)=0.
      C1(I)=0.
 2    D1(I)=1.
      IPOINT=1
      NMAX=NUMSEC-1
      IF(NMAX-1) 200,200,5
 5    DO 180 J=2,NMAX
      JTYPE=ITYPE(J)
      GOTO (10,20,30,40,50,60,70,180,180,80), JTYPE
C
C     LUMPED ... SERIES PARALLEL
C
 10   DO 15 I=1,2
      Z(I)=1./PARAM(IPOINT+1)+1./(SJ(I)*PARAM(IPOINT+2))
 15   Z(I)=1./(Z(I)+SJ1(I)*PARAM(IPOINT+3))
      IPOINT=IPOINT+3
      GOTO 150
C
C     LUMPED ... PARALLEL PARALLEL
C
 20   DO 25 I=1,2
      Y(I)=1./PARAM(IPOINT+1)+1./(SJ(I)*PARAM(IPOINT+2))
 25   Y(I)=Y(I)+SJ1(I)*PARAM(IPOINT+3)
      IPOINT=IPOINT+3
      GOTO 160
C
C     LUMPED ... SERIES SERIES
C
 30   DO 35 I=1,2
      Z(I)=PARAM(IPOINT+1)+SJ(I)*PARAM(IPOINT+2)
 35   Z(I)=Z(I)+1./(SJ1(I)*PARAM(IPOINT+3))
```

```
      IPOINT=IPOINT+3
      GOTO 150
C
C     LUMPED ... PARALLEL SERIES
C
 40   DO 45 I=1,2
      Y(I)=PARAM(IPOINT+1)+SJ(I)*PARAM(IPCINT+2)
 45   Y(I)=1./(Y(I)+1./(SJ1(I)*PARAM(IPCINT+3)))
      IPOINT=IPOINT+3
      GOTO 160
C
C     TRANSMISSION LINE ... SERIES SECTION
C
 50   DO 55 I=1,2
      ALPHAL=ALPHA*PARAM(IPCINT+2)
      BETAL=BETA(I)*PARAM(IPCINT+2)
      GAMMA=CMPLX(ALPHAL,BETAL)
      A(I)=CCOSH(GAMMA)
      D(I)=A(I)
      B(I)=CSINH(GAMMA)
      C(I)=B(I)/PARAM(IPCINT+1)
 55   B(I)=B(I)*PARAM(IPCINT+1)
      IPOINT=IPOINT+2
      GOTO 170
C
C     TRANSMISSION LINE ... SHUNT OPEN
C
 60   DO 65 I=1,2
      ALPHAL=ALPHA*PARAM(IPCINT+2)
      BETAL=BETA(I)*PARAM(IPCINT+2)
      GAMMA=CMPLX(ALPHAL,BETAL)
 65   Y(I)=CTANH(GAMMA)/PARAM(IPCINT+1)
      IPOINT=IPOINT+2
      GOTO 160
C
C     TRANSMISSION LINE ... SHUNT SHORTED
C
 70   DO 75 I=1,2
      ALPHAL=ALPHA*PARAM(IPCINT+2)
      BETAL=BETA(I)*PARAM(IPCINT+2)
      GAMMA=CMPLX(ALPHAL,BETAL)
 75   Y(I)=1./(CTANH(GAMMA)*PARAM(IPCINT+1))
      IPOINT=IPOINT+2
      GOTO 160
C
C     COUPLED LINE BANDPASS FILTER.
C
 80   ISF=KSF
```

```
      DO 85 I=1,2
      A(I)=AF(ISF)
      B(I)=BF(ISF)
      C(I)=CF(ISF)
      D(I)=DF(ISF)
 85   ISF=NFREQ-KSF+1
      GOTO 170
C
C     ABCD MATRIX OF SERIES SECTION
C
 150  DO 155 I=1,2
      A(I)=1.
      B(I)=Z(I)
      C(I)=0.
 155  D(I)=1.
      GOTO 170
C
C     ABCD MATRIX OF PARALLEL SECTION
C
 160  DO 165 I=1,2
      A(I)=1.
      B(I)=0.
      C(I)=Y(I)
 165  D(I)=1.
C
C     MATRIX MULTIPLICATION ... NETWORKS IN CASCADE
C
 170  DO 175 I=1,2
      A2(I)=A1(I)*A(I)+B1(I)*C(I)
      B1(I)=A1(I)*B(I)+B1(I)*D(I)
      A1(I)=A2(I)
      C2(I)=C1(I)*A(I)+D1(I)*C(I)
      D1(I)=C1(I)*B(I)+D1(I)*D(I)
 175  C1(I)=C2(I)
 180  CONTINUE
      RG=PARAM(1)
      RL=RG
      ZID=(D1(2)*RL+B1(2))/(C1(2)*RL+A1(2))
      ZID=1./ZID+SJ1(2)*PARAM(IPCINT+5)
      ZID=1./ZID+SJ(2)*PARAM(IPCINT+4)
      ZID=1./ZID+SJ1(2)*PARAM(IPCINT+6)
      ZID=1./ZID+PARAM(IPCINT+3)
      ZIP=CONJG(ZID)
      AUX=1.-PARAM(IPCINT+2)*PARAM(IPCINT+2)
      Z11=1./(SJ1(1)*PARAM(IPCINT+1)*AUX)
      Z12=PARAM(IPCINT+2)/(SJ1(2)*PARAM(IPCINT+1)*AUX)
      Z21=-Z11*PARAM(IPCINT+2)
      Z22=-Z12/PARAM(IPCINT+2)
```

```
      ZEQ=Z11-Z12*Z21/(ZIP+Z22)
      ZEQ=ZEQ+PARAM(IPCINT+3)
      ZEQ=1./ZEQ+SJ1(1)*PARAM(IPCINT+6)
      ZEQ=1./ZEQ+SJ(1)*PARAM(IPCINT+4)
      ZEQ=1./ZEQ+SJ1(1)*PARAM(IPCINT+5)
      ZEQ=1./ZEQ
      ZIN=(A1(1)*ZEQ+B1(1))/(C1(1)*ZEQ+D1(1))
      RHO=(ZIN-RG)/(ZIN+RG)
      ARHO=CABS(RHO)
      GAIN=ARHO*ARHO
      GAIN=10.*ALOG10(GAIN)
  200 RETURN
      END
      SUBROUTINE BPFILT(K)
C
C     THIS SUBROUTINE CALCULATES ABCD PARAMETERS OF A
C     COUPLED LINE BANDPASS FILTER AT ALL FREQUENCY POINTS.
C
      DIMENSION     ZEVEN(10),ZODD(10),WIDTH(10),GAP(20)
      REAL          KEVEN(10),KODD(10),LENGTH(10),COP(10)
      COMPLEX       Z1,Z2,Z3,Z4,Z1P,Z2P,Z3P,Z4P,X,Y,Z
      COMPLEX       A,B,C,D,A1,C1,CJ,ZTEMP,CMPLX
      COMPLEX       CSINH,CTANH,GAMMAO,GAMMAE
      COMMON        SIGN(50),PARMAX(50),PARMIN(50)
      COMMON        PARAM(100),ITYPE(50),LIST(50)
      COMMON        FPUMP,FCENTR,FSTART,FDEL,GAINO
      COMMON        NPARAM,NLIST,NUMSEC,NEVAL,NFREQ
      COMMON        DELTA,DELMIN,TOL,DRATIO,ALPHA
      COMPLEX       AF(101),BF(101),CF(101),DF(101)
      COMMON        AF,BF,CF,DF
      IR=5
      IW=6
      VC=29.97925
      PI2=6.283185
      CJ=(0.,1.)
      IF( K .NE. 0 ) GOTO 15
      READ(IR,51) RN,SIGO,SIGG
      N=RN+0.1
      FACTOR=0.001*PI2*(SQRT(1./SIGO)+SQRT(1./SIGG))
      WRITE(IW,61)
   61 FORMAT(///,20X,20HFILTER CONFIGURETION,//,
     +       41H SECT    ZEVEN      ZODD     KEVEN      KODD,
     +       30H      WIDTH     LENGTH        GAP,/,10X,3HOHM,
     +       6X,3HOHM,26X,2HCM,7X,2HCM,10X,2HMM,//)
      DO 10  I=1,N
      READ(IR,51) ZEVEN(I),ZODD(I),KEVEN(I),KODD(I),
     +            WIDTH(I),LENGTH(I),GAP(I),COP(I)
   51 FORMAT(8F10.0)
```

```
      WRITE(IW,62) I,ZEVEN(I),ZODD(I),KEVEN(I),KODD(I),
     +                    WIDTH(I),LENGTH(I),GAP(I)
62    FORMAT(I5,2F9.3,2F9.4,F10.4,F10.3,F10.4)
10    COP(I)=0.001*COP(I)
15    FREQ=FSTART
      DO 30 I=1,NFREQ
      AF(I)=1.
      BF(I)=0.
      CF(I)=0.
      DF(I)=1.
      OMEGA=PI2*FREQ
      RS=FACTOR*SQRT(FREQ)
      DO 20 J=1,N
      ALPHAE=0.5*RS/(WIDTH(J)*ZEVEN(J))*LENGTH(J)
      ALPHAC=ALPHAE*ZEVEN(J)/ZODD(J)
      AUX=SQRT(KEVEN(J))
      BETAE=OMEGA*AUX*LENGTH(J)/VC
      BETAO=BETAE*SQRT(KODD(J))/AUX
      GAMMAE=CMPLX(ALPHAE,BETAE)
      GAMMAO=CMPLX(ALPHAC,BETAC)
      Z1P=ZEVEN(J)/CTANH(GAMMAE)
      Z2P= ZODD(J)/CTANH(GAMMAO)
      Z3P=ZEVEN(J)/CSINH(GAMMAE)
      Z4P= ZODD(J)/CSINH(GAMMAO)
      Z1=0.5*(Z1P+Z2P)
      Z2=0.5*(Z1P-Z2P)
      Z3=0.5*(Z3P-Z4P)
      Z4=0.5*(Z3P+Z4P)
      ZTEMP=Z1+1./(CJ*OMEGA*COP(J))
      Z=Z3*Z3/ZTEMP-ZTEMP
      X=Z2-Z3*Z4/ZTEMP
      Y=Z4-Z2*Z3/ZTEMP
      Z1P=Z1+(Z2*X+Z4*Y)/Z
      Z2P=Z3+(Z2*Y+Z4*X)/Z
      A=Z1P/Z2P
      C=A
      B=(Z1P*Z1P-Z2P*Z2P)/Z2P
      C=1./Z2P
      A1=AF(I)*A+BF(I)*C
      BF(I)=AF(I)*B+BF(I)*D
      AF(I)=A1
      C1=CF(I)*A+DF(I)*C
      DF(I)=CF(I)*B+DF(I)*D
      CF(I)=C1
20    CONTINUE
      FREQ=FREQ+FDEL
30    CONTINUE
      RETURN
```

```
      END
      COMPLEX FUNCTION CSINH(Z)
C
C     HYPERBOLIC SINE FUNCTION WITH COMPLEX ARGUMENT.
C
      COMPLEX       Z,CEXP
      CSINH=(CEXP(Z)-CEXP(-Z))/2.
      RETURN
      END
      COMPLEX FUNCTION CCOSH(Z)
C
C     HYPERBOLIC COSINE FUNCTION WITH COMPLEX ARGUMENT.
C
      COMPLEX       Z,CEXP
      CCOSH=(CEXP(Z)+CEXP(-Z))/2.
      RETURN
      END
      COMPLEX FUNCTION CTANH(Z)
C
C     HYPERBOLIC TANGENT FUNCTION WITH COMPLEX ARGUMENT.
C
      COMPLEX       Z,CMPLX
      X=REAL(Z)
      Y=AIMAG(Z)
      IF((Y.GT. 4.7123) .AND. (Y .LT. 4.7124)) Y=4.7123
      IF((Y .GT. 1.5707) .AND. (Y .LT. 1.5709)) Y=1.5707
      CTANH=CMPLX(TANH(X),TAN(Y))/CMPLX(1.,TANH(X)*TAN(Y))
      RETURN
      END
      SUBROUTINE DIRECT(PARP,FMP)
C
C
C     OPTIMIZATION SUBROUTINE -- DIRECT SEARCH
C
C
C     THIS SUBROUTINE PERFORMS CIRCUIT OPTIMIZATION
C     BY USING DIRECT SEARCH METHOD.  IF THE SEARCH
C     FROM THE ORIGINAL BASEPOINT REACHES AN
C     UNSATISFACTORY RESULT, THIS SUBROUTINE WILL
C     GENERATE A NEW BASEPOINT RANDOMLY AND RESTART
C     THE SEARCH ROUTINE.  THIS WILL BE REPEATED
C     MRANDU TIMES.
C
C
      DIMENSION     PARP(50),PARN(50),PARB(50)
      COMMON        SIGN(50),PARMAX(50),PARMIN(50)
      COMMON        PARAM(100),ITYPE(50),LIST(50)
      COMMON        FPUMP,FCENTR,FSTART,FDEL,GAINC
```

```
      COMMON          NPARAM,NLIST,NLMSEC,NEVAL,NFREQ
      COMMON          DELTA,DELMIN,TOL,DRATIC,ALPHA
      COMPLEX         AF(101),BF(101),CF(101),DF(101)
      COMMON          AF,BF,CF,DF
      IW=6
C
C     INITIATION
C
      MRANDU=4
      WRITE(IW,10)
   10 FORMAT(1H1,////,
     +        37H OPTIMIZATION FROM ORIGINAL BASEPOINT,//)
      IX=77777
      CALL RANDOM(IX,IY,RNC)
      IX=IY
      KRANDU=0
      DELINT=DELTA
      NEVAL=0
      DO 20 I=1,NLIST
   20 PARB(I)=PARP(I)
      CALL EVAL(FMB,PARB)
      NEVAL=NEVAL+1
      NIT=1
   40 DO 50 I=1,NLIST
      SIGN(I)=1.
   50 PARN(I)=PARP(I)
      CALL EVAL(FMN,PARN)
      NEVAL=NEVAL+1
      IF(FMN-TOL) 900,900,80
   80 FMP=FMN
      CALL EXPLOR(FMN,PARN)
      IF(FMP-FMN) 450,450,150
  150 IF(FMN-TOL) 850,850,160
  160 FACTOR=1.2
  170 FMP=FMN
C
C     PATTERN MOVE
C
      DO 300 I=1,NLIST
      TEMP=PARP(I)
      PARP(I)=PARN(I)
      DELPAR=PARN(I)-TEMP
      PARN(I)=PARN(I)+DELPAR*FACTOR
C
C     CHECK FOR PARAMETER'S CONSTRAINTS
C
      IF(PARN(I)-PARMAX(I)) 200,200,180
  180 PARN(I)=PARMAX(I)
```

```
      GOTO 300
  200 IF(PARN(I)-PARMIN(I)) 250,300,300
  250 PARN(I)=PARMIN(I)
  300 CONTINUE
      CALL EVAL(FMN,PARN)
      NEVAL=NEVAL+1
      IF(FMN-TOL) 850,850,305
  305 IF(FMN-FMP) 310,320,320
  310 FACTOR=FACTOR+0.2
      IF(FACTOR .GT. 3.) FACTOR=3.
      GOTO 170
C
C     IF THE PATTERN MOVE FAILS, BACK UP ONE STEP
C     AND MAKE ANOTHER EXPLORATORY MOVE
C
  320 FMN=FMP
      DO 400 I=1,NLIST
  400 PARN(I)=PARP(I)
      CALL EXPLOR(FMN,PARN)
      IF(FMN-TOL) 850,850,420
  420 IF(FMP-FMN) 450,450,160
C
C     REDUCE STEP SIZE
C
  450 DELTA=DELTA*DRATIO
C
C     IS STEP SIZE SMALL ENOUGH?
C
      IF(DELTA-DELMIN) 600,600,500
  500 CONTINUE
      NIT=NIT+1
      GOTO 80
C
C     PRINT OUT INTERMEDIATE RESULTS
C
  600 DO 604 I=1,NLIST
      L=LIST(I)
  604 PARAM(L)=PARP(I)
      CALL DISPLY(FMP,NIT)
      CALL OUTPUT
C
C     SEARCH FROM PREVIOUS SET OF BASEPOINTS HAS FAILED,
C     GENERATE A NEW SET OF BASEPOINTS RANDOMLY AND
C     RE-START THE SEARCH ROUTINE
C
      IF(FMB-FMP) 609,609,605
  605 FMB=FMP
      DO 606 I=1,NLIST
```

```
606   PARB(I)=PARP(I)
609   KRANDU=KRANDU+1
      IF(KRANDU-MRANDU) 610,610,900
610   WRITE(IW,930) KRANDU
930   FORMAT(1H1,
     +       ////,33H GENERATE A NEW SET OF BASEPOINTS,/,
     +             18H   *** ATTEMPT NO.,I2,4H ***,//)
      DO 650 I=1,NLIST
      CALL RANDOM(IX,IY,RNO)
      IX=IY
      PARP(I)=0.5*(PARMAX(I)+PARMIN(I))+PARP(I)*(RNO-0.5)
      IF(PARP(I)-PARMAX(I)) 620,615,615
615   PARP(I)=PARMAX(I)
      GOTO 6
620   IF(PARP(I)-PARMIN(I)) 625,625,650
625   PARP(I)=PARMIN(I)
650   CONTINUE
      DELTA=DELI
      DO 660 I=1,NLIST
      L=LIST(I)
660   PARAM(L)=PARP(I)
      WRITE(IW,940)
940   FORMAT(//,17H     NEW BASEPOINT,//,
     +       23H SECT TYPE        PARAMETERS,//)
      CALL DISP
      GOTO 40
850   DO 860 I=1,NLIST
860   PARP(I)=PARN(I)
      FMP=FMN
      DO 870 I=1,NLIST
      L=LIST(I)
870   PARAM(L)=PARP(I)
      GOTO 990
900   DO 910 I=1,NLIST
      PARP(I)=PARB(I)
      L=LIST(I)
910   PARAM(L)=PARP(I)
      WRITE(IW,920)
920   FORMAT(1H1,//,17H *** BEST BET ***,//)
      FMP=FMB
990   CONTINUE
      CALL DISPLY(FMP,NIT)
      CALL OUTPUT
      RETURN
      END
      SUBROUTINE EXPLOR(FMP,PARN)
C
C
```

```
C       THIS SUBROUTINE MAKES EXPLORATORY MOVES
C       TO DECIDE THE DIRECTION FOR PATTERN MOVES.
C
C
        DIMENSION       PARN(50)
        COMMON          SIGN(50),PARMAX(50),PARMIN(50)
        COMMON          PARAM(100),ITYPE(50),LIST(50)
        COMMON          FPUMP,FCENTR,FSTART,FDEL,GAINO
        COMMON          NPARAM,NLIST,NUMSEC,NEVAL,NFREQ
        COMMON          DELTA,DELMIN,TOL,DRATIO,ALPHA
        COMPLEX         AF(101),BF(101),CF(101),DF(101)
        COMMON          AF,BF,CF,DF
C
        DO 100 I=1,NLIST
        TEMP=PARN(I)
C
        PARN(I)=TEMP*(1.+SIGN(I)*DELTA)
        IF(PARN(I)-PARMAX(I))15,10,10
  10    PARN(I)=PARMAX(I)
        GOTO 25
  15    IF(PARN(I)-PARMIN(I)) 20,20,25
  20    PARN(I)=PARMIN(I)
  25    CALL EVAL(FMN,PARN)
        NEVAL=NEVAL+1
        IF(FMN-FMP) 30,40,40
  30    FMP=FMN
        GOTO 100
C
  40    SIGN(I)=-SIGN(I)
        PARN(I)=TEMP*(1.+SIGN(I)*DELTA)
        IF(PARN(I)-PARMAX(I)) 60,50,50
  50    PARN(I)=PARMAX(I)
        GOTO 70
  60    IF(PARN(I)-PARMIN(I)) 65,70,70
  65    PARN(I)=PARMIN(I)
  70    CALL EVAL(FMN,PARN)
        NEVAL=NEVAL+1
        IF(FMN-FMP) 80,90,90
  80    FMP=FMN
        GOTO 100
  90    PARN(I)=TEMP
 100    CONTINUE
        RETURN
        END
        SUBROUTINE RANDOM(IX,IY,RNO)
C
C       RANDOM NUMBER GENERATOR
C
```

```
      COMMON          SIGN(50),PARMAX(50),PARMIN(50)
      COMMON          PARAM(100),ITYPE(50),LIST(50)
      COMMON          FPUMP,FCENTR,FSTART,FDEL,GAINO
      COMMON          NPARAM,NLIST,NUMSEC,NEVAL,NFREQ
      COMMON          DELTA,DELMIN,TOL,DRATIC,ALPHA
      COMPLEX         AF(101),BF(101),CF(101),DF(101)
      COMMON          AF,BF,CF,DF
      IY=IX*65539
      IF(IY) 10,20,20
   10 IY=IY+2147483647+1
   20 RNO=IY
      RNO=RNO*.4656613E-9
      RETURN
      END
      SUBROUTINE EVAL(FM,PAR)
C
C     THIS SUBROUTINE EVALUATES FIGURE OF MERIT.
C
      DIMENSION       PAR(50)
      COMMON          SIGN(50),PARMAX(50),PARMIN(50)
      COMMON          PARAM(100),ITYPE(50),LIST(50)
      COMMON          FPUMP,FCENTR,FSTART,FDEL,GAINO
      COMMON          NPARAM,NLIST,NUMSEC,NEVAL,NFREQ
      COMMON          DELTA,DELMIN,TOL,DRATIC,ALPHA
      COMPLEX         AF(101),BF(101),CF(101),DF(101)
      COMMON          AF,BF,CF,DF
      DO 5 I=1,NLIST
      L=LIST(I)
    5 PARAM(L)=PAR(I)
      FM=0.
      FREQ=FSTART
      DO 10 I=1,NFREQ
      II=I
      CALL RESPON(GAIN,FREQ,II)
      TEMP=GAIN-GAINO
      FM=FM+TEMP*TEMP
   10 FREQ=FREQ+FDEL
      FM=SQRT(FM/NFREQ)
      RETURN
      END
      SUBROUTINE GRAPH(X,DX,Y,NP)
C
C     THIS SUBROUTINE PLOTS FREQUENCY RESPONSE.
C
      DIMENSION       Y(101)
      INTEGER         TEMP,TEMPZ,VERT/1H|/,STAR/1H*/
      INTEGER         LINE(91)/1H.,89*1H ,1H./
      COMMON          SIGN(50),PARMAX(50),PARMIN(50)
```

```
      COMMON          PARAM(100),ITYPE(50),LIST(50)
      COMMON          FPUMP,FCENTR,FSTART,FDEL,GAINC
      COMMON          NPARAM,NLIST,NUMSEC,NEVAL,NFREQ
      COMMON          DELTA,DELMIN,TOL,ORATIO,ALPHA
      COMPLEX         AF(101),BF(101),CF(101),DF(101)
      COMMON          AF,BF,CF,DF
      IW=6
      WRITE(IW,666)
  666 FORMAT(1H1)
      YMAX=Y(1)
      YMIN=YMAX
      DO 10 I=2,NP
      IF (Y(I).GT.YMAX) YMAX=Y(I)
   10 IF (Y(I).LT.YMIN) YMIN=Y(I)
      DIFF=YMAX-YMIN
      IF (DIFF.NE.0) GOTO 20
      WRITE(IW,300) YMAX
  300 FORMAT(1X,'FOR ALL VALUES OF X, Y EQUALS ',1PE12.5)
      GOTO 80
   20 WRITE(IW,100)
  100 FORMAT (1H-///29X,91('.'))
      IF(YMAX.LT.0.OR.YMIN.GT.0) GOTO 50
      IZ=90.0*(-YMIN)/DIFF+1.5
      TEMPZ=LINE(IZ)
      LINE(IZ)=VERT
   50 DO 60 I=1,NP
      IY=90.0*(Y(I)-YMIN)/DIFF+1.5
      TEMP=LINE(IY)
      LINE(IY)=STAR
      XX=X+(I-1)*DX
      WRITE(IW,200) XX,Y(I),LINE
  200 FORMAT (1X, 2G12.5,4X,91A1)
   60 LINE(IY)=TEMP
      WRITE(IW,400)
  400 FORMAT (29X,91('.'))
      IF (YMAX.GE.0.AND.YMIN.LE.0) LINE(IZ)=TEMPZ
   80 RETURN
      END
      SUBROUTINE OUTPUT
C
C     THIS SUBROUTINE PRINTS OUT FREQUENCY RESPONSE.
C
      COMMON          SIGN(50),PARMAX(50),PARMIN(50)
      COMMON          PARAM(100),ITYPE(50),LIST(50)
      COMMON          FPUMP,FCENTR,FSTART,FDEL,GAINC
      COMMON          NPARAM,NLIST,NUMSEC,NEVAL,NFREQ
      COMMON          DELTA,DELMIN,TOL,ORATIO,ALPHA
      COMPLEX         AF(101),BF(101),CF(101),DF(101)
```

```
      COMMON        AF,BF,CF,DF
      IW=6
      WRITE(IW,600)
  600 FORMAT(////,1X,18HFREQUENCY RESPONSE,//,
     +       19H FREQUENCY      GAIN,/,
     +       19H  (GHZ)         (DB),//)
      FREQ=FSTART
      DO 200 I=1,NFREQ
      II=I
      CALL RESPON(GAIN,FREQ,II)
      WRITE(IW,610) FREQ,GAIN
  610 FORMAT(2F10.3)
  200 FREQ=FREQ+FDEL
      RETURN
      END
      SUBROUTINE DISPLY(FMP,NIT)
C
C     THIS SUBROUTINE DISPLAYS OPTIMIZED PARAMETERS.
C
      DIMENSION     BUFFER(10)
      COMMON        SIGN(50),PARMAX(50),PARMIN(50)
      COMMON        PARAM(100),ITYPE(50),LIST(50)
      COMMON        FPLMP,FCENTR,FSTART,FDEL,GAINO
      COMMON        NPARAM,NLIST,NUMSEC,NEVAL,NFREQ
      COMMON        DELTA,DELMIN,TOL,ORATIO,ALPHA
      COMPLEX       AF(101),BF(101),CF(101),DF(101)
      COMMON        AF,BF,CF,DF
      IW=6
      WRITE(IW,600) NIT,NEVAL,FMP
  600 FORMAT(///,23H    NO. OF ITERATION = ,I5,/,
     +           23H FUNCTIONS EVALUATED = ,I5,/,
     +           23H                ERROR = ,E13.6)
      WRITE(IW,610)
  610 FORMAT(////,21H OPTIMIZED PARAMETERS,//,
     +          28H SECT TYPE        PARAMETERS,//)
C
C
C     ENTRY POINT
C
C
      ENTRY DISP
      JLIST=1
      ITEMP=0
      DO 400 I=1,NUMSEC
      IF(JLIST-NLIST) 300,300,410
  300 J=ITYPE(I)
      GOTO (310,310,310,310,320,320,320,330,340,400),J
  310 N=3
```

```
      GOTO 350
  320 N=2
      GOTO 350
  330 N=5
      GOTO 350
  340 N=1
  350 NMAX=ITEMP+N
      JFLAG=0
C     WAS THIS ELEMENT VARIABLE
  355 IF(LIST(JLIST)-NMAX) 360,360,370
  360 JLIST=JLIST+1
      JFLAG=1
      IF(JLIST-NLIST) 355,355,370
C
C     WAS FLAG SET DURING THE SEARCH
C
  370 ITEMP=NMAX
      IF(JFLAG) 400,400,380
  380 ITEMP=ITEMP-N
      DO 390 K=1,N
      ITEMP=ITEMP+1
  390 BUFFER(K)=PARAM(ITEMP)
      WRITE(IW,640) I,J,(BUFFER(L),L=1,N)
  640 FORMAT(I4,I4,5E10.4)
  400 CONTINUE
  410 RETURN
      END
      SUBROUTINE SENSIT
C
C
C     THIS SUBROUTINE PERFORMS SENSITIVITY ANALYSIS.
C
C.
      COMMON        SIGN(50),PARMAX(50),PARMIN(50)
      COMMON        PARAM(100),ITYPE(50),LIST(50)
      COMMON        FPUMP,FCENTR,FSTART,FDEL,GAIND
      COMMON        NPARAM,NLIST,NUMSEC,NEVAL,NFREQ
      COMMON        DELTA,DELMIN,TOL,DRATIO,ALPHA
      COMPLEX       AF(101),BF(101),CF(101),DF(101)
      COMMON        AF,BF,CF,DF
      IW=6
      WRITE(Iw,600)
  600 FORMAT(1H1,///,28(1H*),/,
     +       28H*** SENSITIVITY ANALYSIS ***,/,28(1H*))
      DO 500 I=1,NPARAM
      WRITE(IW,610) I,PARAM(I)
  610 FORMAT(///,19H *** PARAMETER NO. ,I2,
     +       12H    VALUE = ,F9.4,4H ***,//,
```

```
     +        38H FREQUENCY    GAIN    GAIN-P    GAIN-M,
     +        24H     SENSIT-P     SENSIT-M,/,
     +        3X,5H(GHZ),6X,4H(DB),4X,4H(DB),6X,4H(DB),
     +        5X,10H(PER CENT),2X,10H(PER CENT),//)
      FREQ=FSTART
      DO 400 J=1,NFREQ
      JJ=J
      TEMP=PARAM(I)
      CALL RESPON(OBJ,FREQ,JJ)
      PARAM(I)=1.02*TEMP
      CALL RESPON(OBJP,FREQ,JJ)
      PARAM(I)=0.98*TEMP
      CALL RESPON(OBJM,FREQ,JJ)
      SENTYP=50.*(OBJ-OBJP)/OBJ
      SENTYM=50.*(OBJ-OBJM)/OBJ
      WRITE(IW,620) FREQ,OBJ,OBJP,OBJM,SENTYP,SENTYM
620   FORMAT(F10.3,F8.3,2F10.3,2F12.2)
      PARAM(I)=TEMP
      FREQ=FREQ+FDEL
400   CONTINUE
500   CONTINUE
      RETURN
      END
```

REFERENCES

1. Van der Ziel, A., "On the Mixing Properties of Non-Linear Condensers," J. Applied Phys., Vol. 19, pp. 999-1006, November 1948.

2. Faraday, M., "On a Peculiar Class of Acoustical Figures; and Certain Forms Assumed by a Group of Particles Upon Vibrating Elastic Surfaces," Phil. Trans. Roy. Soc., London, Vol. 121, pp. 299-318, May 1831.

3. Strutt, J. W., Lord Raleigh, "On the Crispations of Fluid Resting Upon a Vibrating Support," Phil. Mag., Vol. 16, pp. 50-53, July 1883.

4. Hartley, R. V. L., "Oscillations in Systems with Nonlinear Reactances," Bell System Tech. J., Vol. 15, pp. 424-440, July 1936.

5. Weiss, M. T., "A Solid-State Microwave Amplifier and Oscillator Using Ferrites," Phys. Rev., Vol. 107, p. 317, July 1957.

6. Suhl, H., "Proposal for a Ferromagnetic Amplifier in the Microwave Range," Phys. Rev., Vol. 106, pp. 384-385, April 1957.

7. Seidel, H., and Herrmann, G., "Circuit Aspects of Parametric Amplifiers," IRE WESCON Convention Record, Part 2, pp. 83-90, 1959.

8. Matthaei, G. L., "A Study of the Optimum Design of Wide Band Parametric Amplifiers and Up-Converters," IRE Trans. on Microwave Theory and Techniques, Vol. MTT-9, pp. 23-30, January 1961.

9. Kuh, E. S., and Fukada, M., "Optimum Synthesis of Wide-Band Parametric Amplifiers and Converters," IRE Trans. on Circuit Theory, Vol. CT-8, pp. 410-415, December 1961.

10. Ku, W., "A Broad-Banding Theory for Varactor Parametric Amplifiers-Part I," IEEE Trans. on Circuit Theory, Vol. CT-11, pp. 50-59, March 1964.

11. DeJager, J. T., "Maximum Bandwidth Performance of a Nondegenerate Parametric Amplifier with Single-tuned Idler Circuit," IEEE Trans. on Microwave Theory and Techniques, Vol. MTT-12, pp. 459-467, July 1964.

12. Egami, S., "A Design Theory for Wide-Band Parametric Amplifiers," IEEE Trans. on Microwave Theory and Techniques, Vol. MTT-22, pp. 119-125, February 1974.

13. Connors, W. P., "Maximally Flat Bandwidth of a Nondegenerate Parametric Amplifier with Double Tuned Signal Circuit," IEEE Trans. on Microwave Theory and Techniques, Vol. MTT-13, pp.251-252, March 1965.

14. Porra, V., and Somervuo, P., "Broadband Matching of a Parametric Amplifier by Using Fano's Method," IEEE Trans. on Microwave Theory and Techniques, Vol. MTT-16, pp. 880-882, October 1968.

15. Snell, W. W., Jr., "Low-Loss Microstrip Filters Developed by Frequency Scaling," Bell System Tech. J., Vol. 50, pp. 1919-1931, July-August 1971.

16. Watson, H. A. (Ed.), Microwave Semiconductor Devices and Their Circuit Applications, McGraw-Hill, New York, 1969.

17. Lawrence, H., and Warner, R. M., "Diffused Junction Depletion Layer Calculations," Bell System Tech. J., Vol. 39, pp. 389-403, March 1960.

18. Terman, F. E., Radio Engineers' Handbook, McGraw-Hill, New York, 1969.

19. Caulton, M., Knight, S. P., and Daly, D. A., "Hybrid Integrated Lumped-Element Microwave Amplifiers," IEEE Trans. on Microwave Theory and Techniques, Vol. MTT-16, pp. 397-404, July 1968.

20. Pence, I. W., and Khan, P. J., "Broad-Band Equivalent-Circuit Determination of Gunn Diodes," IEEE Trans. on Microwave Theory and Techniques, Vol. MTT-18, pp. 784-790, November 1970.

21. Mortenson, K. E., Variable Capacitance Diodes, Artech House, Dedham, Mass., 1974.

22. DeLoach, B. C., "A New Microwave Measurement Technique to Characterize Diodes and an 800-Gc Cutoff Frequency Varactor at Zero Volts Bias," IEEE Trans. on Microwave Theory and Technique, Vol. MTT-12, pp. 15-20, January 1964.

23. Roberts, D. A. E., and Wilson, K., "Evaluation of High Quality Varactor Diodes," Radio and Electronic Engr., Vol. 31, pp. 277-285, May 1966.

24. Houlding, N., "Measurement of Varactor Quality," Microwave J., Vol. 3, pp. 40-45, January 1960.

25. Harrison, R. I., "Parametric Diode Q Measurements," Microwave J., Vol. 3, pp. 43-46, May 1960.

26. Sard, E. W., "A New Procedure for Calculating Varactor Q from Impedance Versus Bias Measurements," IEEE Trans. on Microwave Theory and Techniques, Vol. MTT-16, pp. 849-860, October 1968.

27. Bandler, J. W., "Precision Microwave Measurement of the Internal Parasitics of Tunnel-Diodes," IEEE Trans. on Electron Devices, Vol. ED-15, pp. 275-282, May 1968.

28. Sucher, M., and Fox, J. (Ed.), Handbook of Microwave Measurements, Vol. 1, John Wiley, New York, 1963.

29. King, D. D., Measurements at Centimeter Wavelength, D. Van Nostrand, New York, 1952.

30. Harvey, A. F., Microwave Engineering, Academic Press, New York, 1963.

31. Getsinger, W. J., "The Packaged and Mounted Diode as a Microwave Circuit," IEEE Trans. on Microwave Theory and Techniques, Vol. MTT-14, pp. 58-69, February 1966.

32. Marcuvitz, N., Waveguide Handbook, Radiation Lab. Series, Vol. 10, McGraw-Hill, New York, 1951.

33. Hildebrand, F. B., Introduction to Numerical Analysis, McGraw-Hill, New York, 1956.

34. Hooke, R., and Jeeves, T. A., " 'Direct Search' Solution of Numerical and Statistical Problems," J. Assoc. Comp. Mach., Vol. 8, pp. 212-229, April 1961.

35. Manley, J. M., and Rowe, H. E., "Some General Properties of Nonlinear Elements-Part I, General Energy Relations," Proc. IRE, Vol. 44, pp. 904-913, July 1956.

36. Engelbrecht, R. S., "Parametric Energy Conversion by Non-Linear Admittances," Proc. IRE, Vol. 50, pp. 312-321, March 1962.

37. Blackwell, L. A., and Kotzbue, K. L., Semiconductor-Diode Parametric Amplifiers, Prentice-Hall, Englewood Cliffs, N. J., 1961.

38. Penfield, P., Jr., and Rafuse, R. P., Varactor Applications, MIT Press, Cambridge, Mass., 1962.

39. Chang, K. K. N., Parametric and Tunnel Diodes, Prentice-Hall, Englewood Cliffs, N. J., 1964.

40. Howson, D. P., and Smith R. B., Parametric Amplifiers, McGraw-Hill, London, 1970.

41. Decroly, J. C., et al., Parametric Amplifiers, Macmillan, London, 1973.

42. Mumford, W. W., "Some Notes on the History of Parametric Transducers," Proc. IRE, Vol. 48, pp. 848-853, May 1960.

43. Mount, E., and Begg, B., "Parametric Devices and Masers: An Annotated Bibliography," IRE Trans. on Microwave Theory and Techniques, Vol. MTT-8, pp. 222-243, March 1960.

44. Sensiper, S., and Weglein, R. D., "Capacitance and Charge Coefficients for Parametric Diode Devices," Proc. IRE, Vol. 48, pp. 1482-1483, August 1960.

45. Penfield, P., Jr., "Fourier Coefficients of Power-Law Devices," J. Franklin Inst., Vol. 273, pp. 107-122, February 1962.

46. Heffner, H., and Wade, G., "Gain, Bandwidth, and Noise Characteristics of a Variable-Parameter Amplifier," J. Applied Phys., Vol. 29, pp. 1321-1331, September 1958.

47. Kurokawa, K., and Uenohara, M., "Minimum Noise Figure of the Variable-Capacitance Amplifier," Bell System Tech. J., Vol. 40, pp. 695-722, May 1961.

48. Nyguist, H., "Thermal Agitation of Electrical Charge in Conductors," Phys. Rev., Vol. 32, pp. 110-113, July 1928.

49. Assadourian, F., and Rimai, E., "Simplified Theory of Microstrip Transmission Systems," Proc. IRE, Vol. 40, pp. 1651-1657, December 1952.

50. Hyltin, T. M., "Microwave Integrated Electronics for Rader and Communication Systems," Microwave J., Vol. 11, pp. 51-55, February 1968.

51. Daly, D. A., et al., "Lumped Elements in Microwave Integrated Circuits," IEEE Trans. on Microwave Theory and Techniques, Vol. MTT-15, pp. 713-721, December 1967.

52. Aitchison, C. S., et al., "Lumped-Circuit Elements at Microwave Frequencies," IEEE Trans. on Microwave Theory and Techniques, Vol. MTT-19, pp. 928-937, December 1971.

53. Peters, R. W., et al., Handbook of Tri-Plate Microwave Components, Sanders Associates, Nashua, New Hampshire, 1956.

54. Cohn, S. B., "Slot Line on a Dielectric Substrate," IEEE Trans. on Microwave Theory and Techniques, Vol. MTT-17, pp. 768-778, December 1969.

55. Mariani, E. A., et al., "Slot Line Characteristics," IEEE Trans. on Microwave Theory and Techniques, Vol. MTT-17, pp. 1091-1096, December 1969.

56. Wen, C. P., "Coplanar Waveguide: A Surface Strip Transmission Line Suitable for Nonreciprocal Gyromagnetic Device Applications," IEEE Trans. on Microwave Theory and Techniques, Vol. MTT-17, pp. 1087-1090, December 1969.

57. Maissel, L. I., and Glang, M. M., Handbook of Thin Film Technology, McGraw-Hill, New York, 1970.

58. Young, L., and Sobol, H. (Ed.), Advances in Microwaves, Vol. 8, Academic Press, New York, 1974.

59. Howe, H., Jr., Stripline Circuit Design, Artech House, Dedham, Mass., 1974.

60. Collin, R. E., Field Theory of Guided Waves, McGraw-Hill, New York, 1960.

61. Wheeler, H. A., "Transmission Line Properties of Parallel Strips Separated by a Dielectric Sheet," IEEE Trans. on Microwave Theory and Techniques, Vol. MTT-13, pp. 172-185, March 1965.

62. Stinehelfer, H. E., Sr., "An Accurate Calculation of Uniform Microstrip Transmission Lines," IEEE Trans. on Microwave Theory and Techniques, Vol. MTT-16, pp. 439-444, July 1968.

63. Farrar, A., and Adams, A. T., "Characteristic Impedance of Microstrip by the Mehtod of Moment," IEEE Trans. on Microwave Theory and Techniques, Vol. MTT-18, pp. 65-66, January 1970.

64. Yamashita, E., and Mittra, R., "Variational Method for the Analysis of Microstrip Lines," IEEE Trans. on Microwave Theory and Techniques, Vol. MTT-16, pp. 251-256, April 1968.

65. Hornsby, J. S., and Gopinath, A., "Numerical Analysis of a Dielectric-Loaded Waveguide with a Microstrip Line - Finite-Difference Method," IEEE Trans. on Microwave Theory and Techniques, Vol. MTT-17, pp. 684-690, September 1969.

66. Denlinger, E. J., "A Frequency Dependent Solution for Microstrip Transmission Lines," IEEE Trans. on Microwave Theory and Techniques, Vol. MTT-19, pp. 30-39, January 1971.

67. Mittra, R., and Itoh, T., "A New Technique for the Analysis of the Dispersion Characteristics of Microstrip Lines," IEEE Trans. on Microwave Theory and Techniques, Vol. MTT-19, pp. 47-56, January 1971.

68. Schneider, M. V., "Microstrip Lines for Microwave Integrated Circuits," Bell System Tech. J., Vol. 48, pp. 1421-1444, May-June 1969.

69. Hammerstad, E. O., "Equations for Microstrip Circuit Design," Proceedings of Fifth European Microwave Conference, Hamburg, Germany, pp. 268-272, September 1975.

70. Schneider, M. V., "Microstrip Dispersion," Proc. IEEE, Vol. 60, pp. 144-146, January 1972.

71. Wheeler, H. A., "Formulas for the Skin Effect," Proc. IRE, Vol. 30, pp. 412-424, September 1942.

72. Pucel, R. A., Masse, D. J., and Hartwig, C. P., "Losses in Microstrip," IEEE Trans. on Microwave Theory and Techniques, Vol. MTT-16, pp. 342-350, June 1968. Also "Correction to 'Losses in Microstrip'," ibid., p. 1064, December 1968.

73. Simpson, T. L., and Tseng, B., "Dielectric Loss in Microstrip Lines," IEEE Trans. on Microwave Theory and Techniques, Vol. MTT-24, pp. 106-108, February 1976.

74. Hyltin, T. M., "Microstrip Transmission on Semiconductor Dielectric," IEEE Trans. on Microwave Theory and Techniques, Vol. MTT-13, pp. 777-781, November 1965.

75. Poole, C. P., Electron Spin Resonance, Interscience Publishers, New York, 1967.

76. Schneider, M. V., "Dielectric Loss in Integrated Microwave Circuits," Bell System Tech. J., Vol. 48, pp. 2325-2332, September 1969.

77. James, D. S., and Tse, S. H., "Microstrip End Effects," Electron. Lett., Vol. 8, pp. 46-47, January 1972.

78. Silvester, P., and Benedek, P., "Equivalent Capacitances of Microstrip Open Circuits," IEEE Trans. on Microwave Theory and Techniques, Vol. MTT-20, pp. 511-516, August 1972.

79. Itoh, T., Mittra, R., and Ward, R. D., "A Method for Computing Edge Capacitance of Finite and Semi-Infinite Microstrip Lines," IEEE Trans. on Microwave Theory and Techniques, Vol. MTT-20, pp. 847-849, December 1972.

80. Stinehelfer, H. E., Sr., Microstrip Circuit Design, Tech. Report AFAL-TR-69-10, February 1969.

81. Troughton, R., "Design of Complex Microstrip Circuits by Measurements and Computer Modeling," Proc. IEE, Vol. 118, pp. 469-474, March/April 1971.

82. Thomson, A. F., and Gopinath, A., "Calculation of Microstrip Discontinuity Inductances," IEEE Trans. on Microwave Theory and Techniques, Vol. MTT-23, pp. 648-655, August 1975.

83. Silvester, P., and Benedek, P., "Microstrip Discontinuity Capacitances for Right-Angle Bends, T Junctions, and Crossings," IEEE Trans. on Microwave Theory and Techniques, Vol. MTT-21, pp. 341-346, May 1973.

84. Franco, A. G., and Oliner, A. A., "Symmetric Strip Transmission Line Tee Junction," IRE Trans. on Microwave Theory and Techniques, Vol. MTT-10, pp. 118-124, March 1962.

85. Leighton, W. H., Jr., and Milnes, A. G., "Junction Reactance and Dimensional Tolerance Effects on X-Band 3-dB Directional Couplers," IEEE Trans. on Microwave Theory and Techniques, Vol. MTT-19, pp. 818-824, October 1971.

86. Vogel, R. W., "Effects of the T-Junction Discontinuity on the Design of Microstrip Directional Couplers," Vol. MTT-21, pp. 145-146, March 1973.

87. Menzel, W., and Wolff, I., "A Method for Calculating the Frequency-Dependent Properties of Microstrip Discontinuities," IEEE Trans. on Microwave Theory and Techniques, Vol. MTT-25, pp. 107-112, February 1977.

88. Bryant, T. G., and Weiss, J. A., "Parameters of Microstrip Transmission Lines and of Coupled Pairs of Microstrip Lines," IEEE Trans. on Microwave Theory and Techniques, Vol. MTT-16, pp. 1021-1027, December 1968.

89. Zysman, G. I., and Johnson, A. K., "Coupled Transmission Line Networks in an Inhomogeneous Dielectric Medium," IEEE Trans. on Microwave Theory and Techniques, Vol. MTT-17, pp. 753-759, October 1969.

90. Ghose, R. N., Microwave Circuit Theory and Analysis, McGraw-Hill, New York, 1963.

91. Cohn, S. B., "Parallel-Coupled Transmission-Line-Resonator Filters," IRE Trans. on Microwave Theory and Techniques, Vol. MTT-6, pp. 223-231, April 1958.

C-3

APPENDIX B APPROXIMATE EVALUATION OF DIODE TEST MOUNT EQUIVALENT CIRCUIT ELEMENTS

Numerical values for the diode test mount equivalent circuit elements in Fig. 2.11(b) will be evaluated here. The physical dimensions in Fig. 2.11(a) are as follows:

$$d = 2.03 \text{ mm}$$

$$h = 0.71 \text{ mm}$$

$$D_i = 3.04 \text{ mm}$$

$$D_o = 7.00 \text{ mm}$$

B.1 Evaluation of C_f

The fringing capacitance, C_f, is given by Getsinger [103] as

$$C_f = \pi \epsilon D_o \left[\frac{C_{fe}}{\epsilon} \left(\frac{s}{b}, \frac{t}{b} \right) \right] \tag{B.1}$$

For the structure in Fig. 2.11(a),

$$\frac{s}{b} = \frac{2h}{D_o - d} \tag{B.2}$$

$$\frac{t}{b} = \frac{D_i - d}{D_o - d} \tag{B.3}$$

Substitution of numerical values into Eqs. B.2 and B.3 yields

$$\frac{s}{b} = 0.287$$

92. Dell-Imagine, R. A., "A Parallel Coupled Microstrip Filter Design Procedure," G-MTT 1970 Int. Microwave Symp. Digest, pp. 29-32.

93. Childs, W. H.. "Design Techniques for Bandpass Filters Using Edge-Coupled Microstrip Lines on Fused Silica," G-MTT 1976 Int. Microwave Symp. Digest, pp. 194-196.

94. Microwave Engineers' Handbook and Buyers' Guide, Horizon House, Dedham, Mass., 1974.

95. Cisco, T. C., Design of Microstrip Components by Computer, Tech. Report NASA-CR-1982, March 1972.

96. Kaupe, A. F., Jr., "Algorithm 178: Direct Search," Commun. ACM, Vol. 6, pp. 313-314, June 1963.

97. Bell, M., and Pike, M. C., "Remark on 'Algorithm 178: Direct Search,'" Commun. ACM, Vol. 9, pp. 684-685, September 1966.

98. Emery, F. E., and O'Hagen, M., "Optimal Design of Matching Networks for Microwave Transistor Amplifiers," IEEE Trans. on Microwave Theory and Techniques, Vol. MTT-14, pp. 696-698, December 1966.

99. Bandler, J. W., and Macdonald, P. A., "Optimization of Microwave Networks by Razor Search," IEEE Trans. on Microwave Theory and Techniques, Vol. MTT-17, pp. 552-562, August 1969.

100. Denlinger, E. J., et al., "Microstrip Varactor-Tuned Millimeter-Wave IMPATT Diode Oscillators," IEEE Trans. on Microwave Theory and Techniques, Vol. MTT-23, pp. 953-958, December 1975.

101. Wu, Y. S., and Rosenbaum, F. J., "Wide-Band Operation of Microstrip Circulators," IEEE Trans. on Microwave Theory and Techniques, Vol. MTT-22, pp. 849-856, October 1974.

102. Branner, G. R., and Chan, S.-P., "A New Technique for Synthesis of Broad-Band Parametric Amplifiers," IEEE Trans. on Microwave Theory and Techniques, Vol. MTT-21, pp. 437-444, July 1973.

103. Getsinger, W. J., "Coupled Rectangular Bars Between Parallel Plates," IRE Trans. on Microwave Theory and Techniques, Vol. MTT-10, pp. 65-72, January 1962.

C-3